Simulation Studies of Laser-compression of Matter

By

N.A. Tahir, M.Sc., DIC.

A thesis submitted for the degree of Doctor of Philosophy in The University of Glasgow.

Department of Natural Philosophy,

The University,

Glasgow, G12 8QQ.

September, 1978.

CONTENTS

			Page No.
Acknowledgments.			
Preface.			
Chapter 1		A Review of Laser-Fusion	1
	1.1	Introduction.	1
	1.2	Principles of Laser-Fusion.	2
		(1.2a): Laser-plasma interaction	3
		(1.2b): Energy transport (Electron thermal conduction, fast electrons and radiative transfer)	4
		(1.2c): Compression	10
Chapter 2		Description of Computer programme MEDUSA.	15
	2.1	Physical Model of the code.	15
	2.2	System of Equations.	16
	2.3	Geometry of the target, initial and boundary conditions of the problem.	19
	2.4	Mesh and Numerical Scheme.	20
	2.5	Solution of The System of Equations.	21
	2.6	Limitations of the code.	26
		(a) No atomic physics.	
		(b) No fast electrons and radiative transfer.	
		(c) Does not allow shells and layered targets.	
Chapter 3		Atomic Physics	29
	3.1	Rate Equations Governing Atomic Physics Processes.	29
	3.2	Rate Coefficients used in the Rate Equations.	31
	3.3	Some Well Known Atomic Physics Models	32
		(3.3a) Steady State Models, including LTE model, Corona model, TRIP (4).	32

		(3.3b) Time-dependent models, including time-dependent Corona model and TRIP (2).	39
	3.4	Incorporation of Atomic Physics into MEDUSA and formation of MEDUSAT.	43
Chapter 4		Radiative Transfer.	47
	4.1	A Brief Review of the Theory of Radiative Transport.	47
	4.2	Incorporation of Transport of Continuum Radiation (free-free+free-bound) into MEDUSAT.	60
Chapter 5		Results: Atomic Physics.	72
	5.1	Solid Micro-spheres.	72
	5.2	Gas Filled Micro-balloons.	81
	5.4	Layered Targets.	87
Chapter 6		Results: Radiative Pre-heat Effects.	98
	6.1	Solid Micro-spheres.	98
	6.2	Gas filled Micro-balloons.	110
	6.3	Conclusions	116
	6.4	Future Work	117

APPENDICES

		Page No.
A.1	Calculation of γ for a partially ionized gas in coronal equilibrium.	119
A.2	Derivation of the energy equation for a gas with internal energy a function of density and temperature.	120
A.3	Source terms for the electron and ion energy equations in MEDUSA.	121
A.4	Modifications in MEDUSA to handle layered targets.	123
A.5	Evaluation of electron-radiation collision frequency.	125
A.6	Evaluation of thermal conduction rate in the plasma.	127
A.7	Evaluation of energy exchange rates in a 3-component (electrons, ions and radiation) plasma.	128
A.8	Evaluation of the coefficients A, B, C, D and G required in the numerical solution of radiation energy equation.	132

ACKNOWLEDGMENTS

I wish to thank Prof. J.C. Gunn for the provision of facilities in the department of Natural Philosophy, University of Glasgow. I would like to especially thank my supervisor, Dr. E.W. Laing for suggesting the problem, and for his great help during the course of the work. I would also like to thank Dr. R.G. Evans and Dr. D.J. Nicholas of the Rutherford Laboratory, together with Dr. J. Magill for many useful discussions. I am grateful to the departmental computer operators for their help. I also thank Mrs. Sanderson for typing this thesis.

During this period of research, I was supported by Sadr Anjuman Ahamaddyya, Rabwah, Pakistan.

PREFACE

In this thesis we present simulation studies of laser-compression of matter. We have made use of 1-D Lagrangian computer programme MEDUSA[11] and have extensively modified it to include some important geometrical and physical effects, as discussed below:

(a) MEDUSA can be used to simulate compression of a solid microsphere, but is incapable of dealing with a gas filled microballoon or a layered target. We have modified MEDUSA to allow it to handle the latter two types of targets which have more practical importance.

(b) MEDUSA does not allow ionization and recombination effects in the plasma, but assumes a fixed degree of ionization. This assumption may be valid for a D-T plasma, but when one is dealing with a medium-z target (z up to 20), the degree of ionization exhibits a large variation in space-time. To overcome this deficiency of the model, we have incorporated a steady state density and temperature dependent atomic physics package, TRIP (4) [21]. This package evaluates mean ionization and mean squared ionization as a function of local plasma density and temperature.

(c) In the standard version of MEDUSA, ions and thermal electrons are the only means of energy transport. However, it can be shown that the thermal transport due to radiation absorption and suprathermal electrons is much faster than that due to the thermal electrons. One would therefore expect the compression to be very sensitive to the latter two transport processes. We have modified MEDUSA to include the transport of continuum radiation under a diffusion approximation.

Using this modified version of MEDUSA, we have carried out extensive simulation studies to investigate the effect of the atomic physics and radiative transport processes in the laser-compression of solid micro-spheres, gas filled micro-balloons and layered targets.

CHAPTER ONE

CHAPTER 1

A Review of laser-fusion

(1.1) Introduction:

Energy is the most important need of the modern world. At the present rate of consumption, the estimated reserves of natural fuel, particularly coal and oil will be exhausted in a few decades. It is therefore essential to discover some other means of energy generation. One possibility could be to develop the use of thermonuclear fuels which are naturally abundant. The two sources of nuclear power are:

(i) Nuclear fission, in which energy is released by the splitting up of a heavy element into lighter ones, and

(ii) Nuclear fusion, in which nuclei of lighter elements are fused together to form heavier elements.

The possibility of exploiting the latter process for generation of controlled energy is more attractive for various reasons. For example, the necessary fuel is more abundant and the waste products can be more easily disposed of. The nuclear reactions which one can make use of are:[1]

$$
\begin{aligned}
D + T &\longrightarrow He^4 + n + 17.6\,(\text{Mev}) \\
D + D &\longrightarrow He^3 + n + 3.27\,(\text{"}) \\
D + D &\longrightarrow T + H + 4.03\,(\text{"})
\end{aligned}
\qquad (1.1)
$$

The cross section for a D-T reaction has a peak of 5 Barns at 100 Kev (1.16×10^9 K) whereas the two D-D reactions have a lower cross section even at a higher temperature. A D-T reaction is therefore much easier to bring about and it releases a larger amount of energy. Unlike deuterium, tritium does not exist in nature and hence must be produced, using the neutrons generated in the above D-D reactions, as follows:

$$Li^6 + n \longrightarrow He^4 + T + 5\,(\text{Mev}) \qquad (1.2)$$

The problem of controlled thermonuclear fusion has been pursued actively during the last twenty years, but until a few years ago almost all the effort was devoted to the magnetic confinement approach. The idea behind this approach is to confine a low density ($n \sim 10^{20}$ m^{-3}, where n is the electron number density), high temperature ($T \sim 10^{8}$ K) D-T plasma for a time, τ, which is long enough so that Lawson's criterion [2] - the breakeven condition - is satisfied.

$$\text{ie} \quad n\tau > 10^{20} \ m^{-3} s \tag{1.3}$$

However in 1972, Nuckolls et al [3] proposed laser-fusion as an alternative approach to this problem. In this process an intense laser beam is used to compress a small D-T pellet to 10^{4} - times solid density ($n \sim 5 \times 10^{33}$ m^{-3}). The confinement time of the plasma in this case is determined by the inertia of the matter and is $\tau \sim \frac{R}{v_{th}}$, where R is the radius of the pellet and v_{th} is the average thermal speed of the particles. For a 75-μg D-T microsphere at 8 kev ion temperature, τ has a value 10^{-10} Sec. [4] The product $n\tau$ is then 5×10^{23} m^{-3} S and the Lawson's criterion is easily satisfied. One may therefore expect an overall energy gain. The remainder of this chapter will be devoted to a review of laser-fusion.

(1.2) Principles of laser-fusion:

In its simplest conceptual form, laser-fusion can be described as follows:

A cryogenic pellet of solid or liquid D-T is uniformly irradiated by a high intensity laser pulse which heats the surface of the pellet. The heated surface then expands and within a few pico-seconds, a uniform spherical shell of plasma, a few microns thick, known as the corona region is formed around the pellet. The incoming laser energy penetrates up to the critical density surface* and heats the electrons

* The density at which the plasma frequency becomes equal to the laser frequency.

by inverse Bremsstrahlung and numerous anomalous processes. This heat is then transformed inwards by various transport mechanisms, thereby driving a thermal wave into the overdense region. The increase in pressure at the thermal front and the reactive force due to ablating material generate a series of spherically converging shocks, which move into the material, compressing and heating the central part of the pellet. In fact by proper pulse shaping one can simulate the ultra-high densities and the temperatures of thermonuclear burn [3,4].

In general one can divide the physics of laser-fusion into three main areas:

Laser-plasma interaction in the corona region.

Energy transport from the critical density surface to the ablation front.

The physics of compression.

Each of these processes will now be discussed.

(1.2a) Laser-plasma interaction:

We noted above that an outward expanding plasma is generated around a solid microsphere when it is irradiated by an intense laser pulse. The laser light penetrates the plasma up to the critical density surface and is absorbed by classical inverse Bremsstrahlung. However, the electron-ion collision frequency is $\propto \frac{1}{T_e^{3/2}}$ where T_e is the electron temperature, and therefore at high temperature ($\sim$ 1 kev) the above mechanism of energy absorption becomes ineffective. It is believed that the absorption then takes place as a result of collective processes discussed elsewhere [5, 6], including the oscillating two stream instability and the ion-acoustic decay instability which are excited near the critical density. Another parametric decay instability which is excited at $\omega = 2\omega_p$, where ω is the laser frequency and ω_p is the plasma frequency, is the two plasmon decay instability. There are also two reflective instabilities, namely,

stimulated Brillouin and Raman scattering. These instabilities are expected to occur when the laser beam is normally incident on the plasma. On the other hand if the laser is obliquely incedent at a small but a finite angle, then the energy can be absorbed by resonance absorption mechanism [7].

Excitation of these instabilities would give rise to strong heating of the plasma, generating highly energetic non-Maxwellian electrons[8]. These electrons have very large mean free path and therefore can easily penetrate deep into the target causing pre-heat of the uncompressed dense core. This problem will be discussed in the next sub-section.

(1.2b) Energy transport:

The success of laser-fusion is critically dependent on the efficiency of the energy transfer from critical density surface, the region where most of the laser energy is deposited, to the ablation surface. Electron thermal conduction, suprathermal electron transport and radiative transport are considered to be important in this respect. In the following we discuss these processes and compare their relative importance.

(i) Electron thermal conduction:

Electron thermal conduction is believed to play an important role in transferring energy in the laser-produced plasmas. The electron thermal flux is given by:

$$F_e = -\kappa_e \nabla T_e \qquad (1.4)$$

where

$$\kappa_e \propto (T_e^{5/2} \bar{Z}) / \bar{Z}^2 \qquad (1.5)$$

is the classical electron thermal conductivity[9]. It is seen from relation(1.5) that the thermal conductivity is a very rapidly increasing function of the electron temperature ($\propto T_e^{5/2}$) and is therefore expected

to produce nearly isothermal conditions in the high temperature corona region. This would help in smoothing out the effects of non-uniform deposition of the laser energy.

In order that equation (1.4) remains valid, the temperature should not change appreciably over the distance of the order of one electron mean free path. However, the electron mean free path is given by the relationship [9]

$$\bar{l}_e \propto T_e^2/(n_i \bar{Z}^2) \tag{1.6}$$

so that in the high temperature and the low density corona region, the mean free path can easily exceed the temperature scale length, causing equation (1.4) to over-estimate the thermal flux. In such a case, however, the electron flux is restricted by an upper limit, namely, the free-streaming limit, which is some fraction of the product of thermal velocity and energy density, and is given by

$$F_f = \alpha \left(\tfrac{3}{2} n_e K T_e\right)\left(\frac{3KT_e}{m_e}\right)^{1/2} \tag{1.7}$$

where $0 < \alpha \leq 1$

The value $\alpha = 1$ corresponds to the case when all the electrons are streaming in the same direction. The flux is limited according to

$$\frac{1}{F_e'} = \frac{1}{F_e} + \frac{1}{F_f} \tag{1.8}$$

and the modified thermal conductivity becomes

$$\kappa_e' = \kappa_e\left(1 + \kappa_e \left|F_f^{-1}\right| \frac{dT_e}{dx}\right)^{-1} \tag{1.9}$$

which limits the electron flux as $\frac{dT_e}{dx} \longrightarrow \infty$.

Using a simple analytic model, Ashby and Christiansen [10] have shown that the flux limiting becomes important when the ratio of the critical radius to the ablation radius

$$r_c/r_a \gtrsim \frac{\alpha}{16}\left(\frac{8AM_H}{\pi m_e Z}\right)^{1/2} \tag{1.10}$$

and the laser power at which this occurs is

$$P_{fl} = \left(\frac{a}{16}\right)^3 \left(\frac{8AM_H}{\pi m_e Z}\right) \cdot 16\pi \lambda_a^2 C_T^3 \rho_c \qquad (1.11)$$

where in their notation $\alpha = 0.14a$

and $$C_T = \left(\frac{ZKT_e}{AM_H}\right)^{1/2} \qquad (1.12)$$

is the isothermal sound speed in the corona region. In the above equations A denotes the atomic weight of the element, z the atomic number, m_H is the proton mass, m_e is the electron mass and ρ_c is the critical mass density. Using 1-D Lagrangian laser-fusion code MEDUSA [11], the above authors have found that the fusion yield is reduced for values of a of the order of 0.6. However, Malone et al[12] on the basis of detailed experimental-calculational comparison have suggested that the value $a \sim 0.6$ is highly optimistic and good agreement can be obtained between experimental results and computer simulations only if much smaller values of a, such as, $a \sim 0.075$ is used. (Note that the parameter f used in reference [12] is related to α by the relationship $f \simeq 0.4a$). Bickerton [13] has suggested that this severe flux limitation can be the result of ion-acoustic turbulence in the plasma. He has shown that this phenomenon can limit the thermal flux to $\frac{3}{8}\left(\frac{m_e}{Am_H}\right)^{\frac{1}{2}} n_e v_e k T_e$ which corresponds to $a \sim 0.02$ for an equi-molar D-T plasma.

(ii) Suprathermal electron transport:

At high laser powers the laser light is believed to be absorbed by various anomalous processes and as a result strong electron heating is expected, generating highly energetic electrons. These fast electrons can cause degradation of compression as a result of preheat of the target core and can also cause the plasma energy to be lost through a low-density high-velocity expansion of the plasma surface, at a rate much faster than that predicted by a single temperature fluid expansion.

Morse and Nielson [8] have proposed a simple model which can estimate the magnitude of the electron heating and can calculate the blow-off velocity of the material, as described below.

Preheat effects:

This model assumes that the laser flux Φ_L which is deposited at the critical density surface as a result of anomalous processes is removed by an inward flux Φ_h of hot electrons. In order to maintain quasi-neutrality, a flux Φ_c of cold electrons counter streams outwards. Assuming the one-dimensional electron distribution as in figure (1-1)

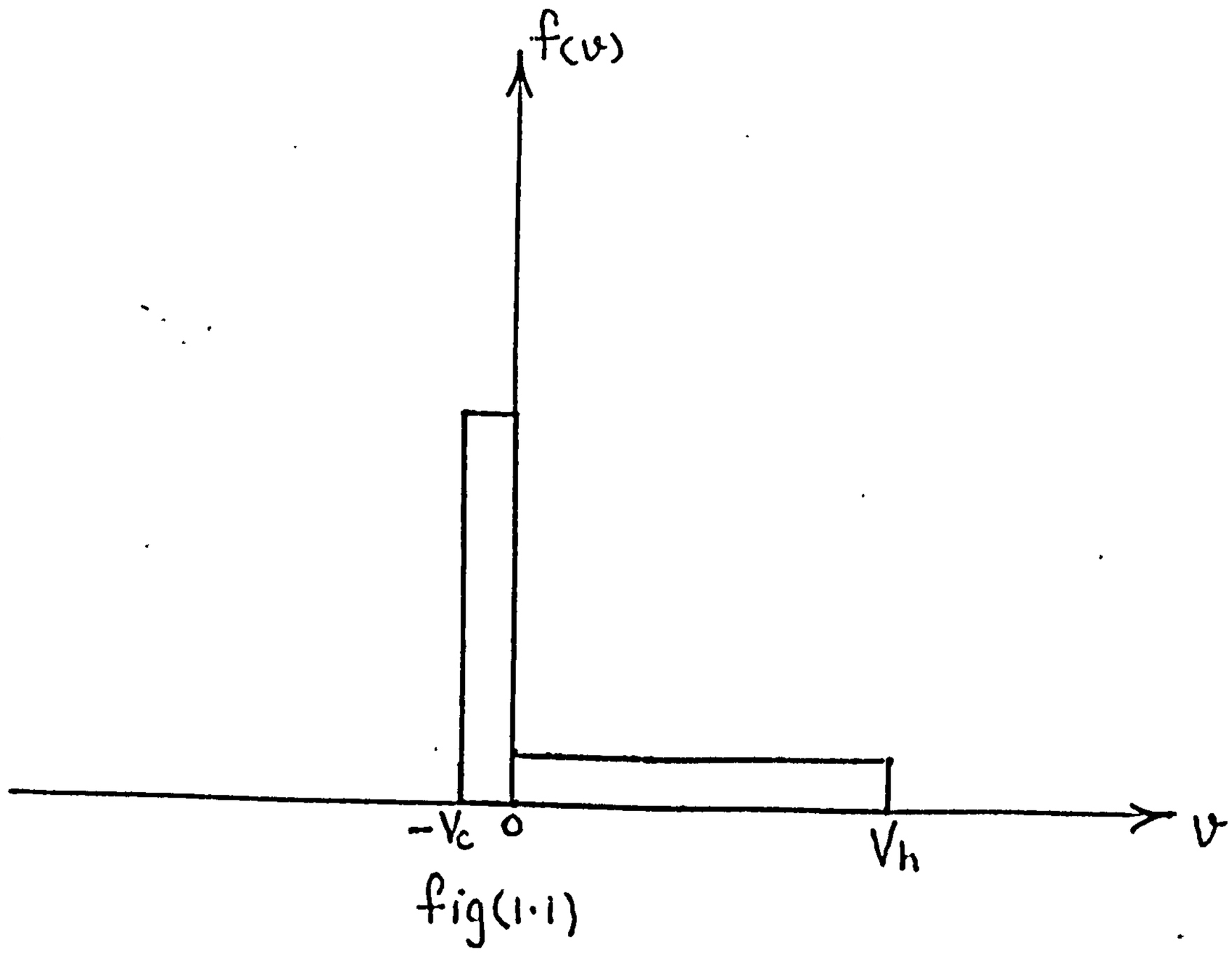

fig(1·1)

$$f(v) = n_H/V_h \qquad 0 < v \leq V_h$$

$$= n_c/V_c \qquad -V_c \leq v < 0$$

The energy flux is defined as

$$\phi = \frac{1}{2} m_e \int_{-\infty}^{\infty} dv . v^3 f(v) \qquad (1.13)$$

which gives

$$\Phi_h = \frac{1}{8} m_e n_h V_h^3 \tag{1.14}$$

and

$$\Phi_c = \frac{1}{8} m_e n_c V_c^3 \tag{1.15}$$

For a current-free situation one has

$$J = \int_{-\infty}^{\infty} dv \cdot v \cdot f(v) = \frac{1}{2}(n_h V_h - n_c V_c)$$

or

$$n_h V_h = n_c V_c \tag{1.16}$$

Also we have $n_{crit} = n_h + n_c$ (1.17)

In the above equations n_h is the number density of hot electrons, n_c is the number density of cold electrons and n_{crit} is the critical electron density. Using equations (13) - (17) one gets

$$\Phi_L = \frac{1}{2}(n_{crit} m_e V_h^3)\left[\frac{n_h}{4n_{crit}}\left\{1 - \left(\frac{n_h}{n_{crit} - n_h}\right)^2\right\}\right] \tag{1.18}$$

A plot of $\Phi_L/(n_{crit} \cdot m_e V_{h/2}^3)$ against $n_{h/n_{crit}}$ shows that for a given value of Φ_L there is a minimum value of V_h ($V_{h\ min}$) given by:

$$\Phi_L/(\tfrac{1}{2} n_{crit} m_e V_{hmin}^3) = \frac{1}{16} \tag{1.19}$$

which is achieved when $n_{h/n_{crit}} = 1/3$. The physical significance of this result is that the fluxes adjust themselves to minimize the fast-electron flux. It is clear from equation(1.19)that the effect of hot electrons is more important for longer wavelengths. For example, if $\Phi_L \sim 10^{17}$ W/cm^2 is to be transported through a density 3×10^{22} cm^{-3}, then equation(1.19)would give $V_{min} \sim 0.95\times10^{10}$ cms/sec which correspond to electron energy $\sim$ 25-Kev. However, if this energy were to be absorbed $n=10^{21}$ cm^{-3} which is the critical density for Nd-glass laser ($\lambda \sim 1.06$ micron), the maximum electron energy will be $\sim$340-kev. The critical

density for a CO2 laser is even smaller, $\sim 10^{19}$ cm^{-3} and will produce 340-kev electrons even at $\Phi_L \sim 10^{15}$ W/cm^2. If the dimensions of the target are of the order of the mean free path of the fast-electrons, then these fast electrons will deposit their energy deep into the target, thus pre-heating the uncompressed core. However, the mean free path is shorter in a high z material, and thus one can avoid pre-heat by using a structured pellet [14] with a thin high z shell outside the D-T pellet.

High velocity surface expansion:

In the above we considered only the inward motion of the fast electrons, whereas now we discuss the effect of escape of these electrons from the plasma. In the former case charge neutrality is maintained by a counter streaming cold electron flux while in the latter case an abrupt potential step $\Phi_1 < o$ will be created at the plasma-vacuum boundary as soon as a small fraction of fast electrons escapes from the plasma. This potential will accelerate ions to energies higher than the mean energy of the fast electrons. It is shown [8] that the fast ion energy is

$$E_i \doteq 0.153\, C_h T_h \frac{3}{2}(n_{ho} K T_h) \tag{1.20}$$

where $c_h = \left(\frac{zkT_h}{m_i}\right)^{\frac{1}{2}}$ is the ion-acoustic velocity. T_h denotes the temperature of the hot electrons and n_{ho} is the hot electron number density at t=o. It is seen from (1.20) that the rate of energy lost by fast ions will be reduced if ratio $m_{i/z}$ is made larger, which can be achieved by using a weakly ionized high-z material.

(iii) Radiative transport:

The high temperature laser-produced plasmas are very rich in radiation over a wide range of the spectrum. The mean free path of the photons created near the critical density surface is large enough to cross the ablation surface and deposit their energy into the

target, pre-heating the uncompressed core. Computer simulations of Fraley and Mason [15] predict a decrease by a factor of 2 in compression as a result of pre-heat by medium energy Bremsstrahlung radiation. Inclusion of recombination and line radiation will have even more severe effect on the compression. The effect of radiative pre-heat in laser-compression simulations will be discussed in chapter 6.

(1.2c) Compression:

The key idea involved in laser-fusion is to compress the D-T fuel to ultra-high densities (10^4 solid density), hence greatly increasing the reaction rate. In practice one can achieve such high density if the pellet is subject to a series of shocks of increasing strength which are adjusted in time so that the successive shocks do not overtake each other before arriving at the centre of convergence. This behaviour may be achieved by properly programming the laser pulse. We now calculate the pulse shape required to compress the fuel adiabatically [3,4].

For a pulse driving the surface of the pellet towards the centre at perfect gas sound speed, we have

$$-\frac{dR}{dt} = v(t) = \left(\frac{\gamma P}{\rho}\right)^{1/2} \qquad (1.21)$$

and also

$$v(t) = v_0 \left(T/T_0\right)^{1/2}. \qquad (1.22)$$

where $$v_o = \frac{dR_o}{dt} \tag{1.23}$$

In the above equations, γ is the specific heat ratio of the gas, P is the pressure, ρ is the density, T is the temperature and R is the radius at time t, R_o and T_o denote initial pellet radius and initial temperature respectively.

For an adiabatic compression of a perfect gas

$$P R^{3\gamma} = P_o R_o^{3\gamma} \tag{1.24}$$

and $$\frac{P}{P_o}\left(\frac{R}{R_o}\right)^3 = \frac{T}{T_o} \tag{1.25}$$

(1.21) - (1.23) give $$\frac{dR}{dt} = \dot{R}_o \left(\frac{T}{T_o}\right)^{1/2} \tag{1.26}$$

and from (1.24) and (1.25)

$$\frac{T_o}{T} = R_o^{3(1-\gamma)} \cdot R^{3(\gamma-1)} \tag{1.27}$$

Hence $$R(t) = R_o\left(1 - \frac{t}{\tau}\right)^{\frac{2}{3\gamma-1}} \tag{1.28}$$

where $$\tau = \frac{2}{3\gamma-1} \cdot \frac{R_o}{\dot{R}_o} \tag{1.29}$$

and $$P(t) = P_o\left(1 - \frac{t}{\tau}\right)^{-\frac{6\gamma}{3\gamma-1}} \tag{1.30}$$

Assuming that all the laser energy is used in the compression process, we can equate the instantaneous laser power E(t) to the rate at which work is done.

$$\dot{E}_o = -4\pi R^2 \dot{R} P \tag{1.31}$$

giving $$\dot{E}(t) = \dot{E}_o\left(1 - \frac{t}{\tau}\right)^{-p} \tag{1.32}$$

where $$p = \frac{9\gamma - 7}{3\gamma - 1} \tag{1.33}$$

and $E_o = 4\pi R_o^2 \dot{R}_o P_o$ is the initial power level.

For a perfect gas, $\gamma = 5/3$, $p = 2$ and

$$\dot{E} = \dot{E}_o \left(1 - \frac{t}{\tau}\right)^{-2} \tag{1.34}$$

This model is over-simplified, neglecting such important physical effects as ionization, recombination and the degeneracy of the electrons. Nuckolls et al [3] have shown that $p = 15/18$ for the compression of a fully degenerate electron gas.

We now discuss the case when ionization and recombination are included. We consider the simplest atomic physics model, namely, the Steady State Corona model [16], in which the degree of ionization is a function only of electron temperature. The equation of state for a partially ionized gas in coronal equilibrium may be written

$$PV = R_{(T)} T \tag{1.35}$$

where $$R_{(T)} = R_o (1 + \langle z \rangle) \tag{1.36}$$

R_o is the ordinary gas constant of a perfect gas and $\langle z \rangle$ is the mean ionization as a function of electron temperature. The specific heat ratio for such a gas (as shown in appendix 1)

(1.37)

$$\gamma = 1 + \frac{\left[1 + \frac{T}{(1+\langle z \rangle)} \cdot \frac{d\langle z \rangle}{dT}\right]^2}{\frac{3}{2}\left[1 + \frac{T}{(1+\langle z \rangle)} \cdot \frac{d\langle z \rangle}{dT}\right] + \frac{1}{K(1+\langle z \rangle)} \frac{d\langle E_z \rangle}{dT}}$$

In the limiting case when $\frac{d\langle z\rangle}{dT} \longrightarrow o$ and $\frac{d\langle E_z\rangle}{dT} \longrightarrow o$, $\gamma \longrightarrow 5/3$.

$\langle E_z \rangle$ is the ionizational energy per atom averaged over population fractions.

The adiabatic law in differential form is:

$$\frac{dP}{dV} \cdot \frac{V}{P} + \gamma(T) = 0 \qquad (1.38)$$

In general it is not possible to integrate this equation and so one cannot obtain a condition of the type (1.30) for adiabatic compression of a partially ionized gas in Steady State coronal equilibrium. More sophisticated models will make the problem more difficult. However, it has been found that a plasma which is represented by a more realistic equation of state, gives reasonably good results when compressed by the pulse shape given by equation (1.32). Using this pulse shape, Clark et al [4] have derived energy-mass scaling laws for maximum neutron yield Y from a mass m, compressed by an amount of energy E. Their results can be summarized as follows:

(1) $E/_m$ should be of the order of 700 $J/\mu g$

(2) Y is found to be very sensitive to $\dot{E}_o$, especially for small masses and $\dot{E}_o$ should be $\propto m^n$ where n = 1.5 for micro-spheres and 1.38 for shells.

(3) Y is not sensitive to the pulse shaping parameter p in the range $1.5 \leq p \leq 2.5$ and for pulse length τ in the range $0.5t_1 \leq \tau \leq 3t_1$, where t_1 is the time for the first shock to reach the centre and is $\sim \frac{R_o}{C_s}$, C_s is the sound speed.

(4) Y is of the order of $(E)^{0.9}$ for E>8KJ and is of the order of $(E)^{0.45}$ for E<8KJ.

These results have been cross checked by the author using 1-d Lagrangian computer program MEDUSA [11].

The work presented in this thesis is mainly connected with the study of the effect of various processes, including atomic physics and radiative pre-heat on compression, using the above mentioned computer program MEDUSA. In chapters 3 and 4 we describe the incorporation of atomic physics and transport of continuum radiation into MEDUSA presenting results in chapters 5 and 6 respectively.

CHAPTER 2

MEDUSA: A 1-D Lagrangian Laser-fusion computer Program:

In this chapter we describe the computer program MEDUSA [11] which simulates a simple laser-fusion model including the following processes.

(a) Absorption of laser energy by electrons.

(b) Energy exchange between electrons and ions

(c) Energy transport by electron and ion thermal conduction.

(d) Hydrodynamic plasma motion, treating shocks by artificial viscosity.

(e) Thermonuclear burning and energy deposition.

Details of the physical model of this program are given in section (2.1). The system of equations of the code is described in (2.2). The geometry of the target, the initial and boundary conditions are discussed in (2.3). A description of the mesh and integration scheme is presented in (2.4). The method of solution of energy equation and equation of motion is treated in (2.5) and the limitations of this code are discussed in section (2.6).

(2.1) Physical Model:

The standard version of MEDUSA is a two-temperature Lagrangian computer program which can simulate the one-dimensional hydrodynamic and thermodynamic behaviour of a plasma irradiated by an intense laser beam. The plasma is treated as a quasi-neutral mixture of electrons and ions of one or more species with a fixed degree of ionization. The electron temperature T_e, the ion temperature T_i, the plasma mass density ρ and hydrodynamic plasma velocity u are the four dependent variables which determine the state of the system in space-time. The eight species considered in the published code are H (hydrogen), D (deuterium), T (tritium), He^3 ($helium^3$), He^4 ($helium^4$), N (an arbitrary neutral atom with mass number M_x), X (an arbitrary ion with mass number M_x and charge Z_x) and N (neutrons).

The charged particles produced in the thermonuclear reactions dump their energy locally while the neutrons escape freely.

(2.2) System of Equations:

Instantaneous local chemical composition of the plasma is described by

$$n_k = n_i f_k \tag{2.1}$$

where f_k is the fraction of ions of species k and n_i is the total ion number density; $\sum_k f_k = 1$

The average ion mass number: $$M = \sum_k f_k M_k \tag{2.2}$$

and the average ion charge number: $$Z = \sum_k f_k Z_k \tag{2.3}$$

where M_k and Z_k are the mass and charge number of the ions of species k respectively.

The physical plasma mass density: $$\rho = m_H M n_i = \frac{1}{V} \tag{2.4}$$

where m_H is the proton mass and V is specific volume.

In general, the internal energy U and pressure P will be functions of density and temperature,

$$U = U(\rho, T) \quad \text{and} \quad P = P(\rho, T) \tag{2.5}$$

We drop the subscripts i and e for simplicity. The energy equation of the system may be written as

$$C_v \frac{dT}{dt} + B_T \frac{d\rho}{dt} + P \frac{dV}{dt} = S \tag{2.6}$$

(See appendix 2)

where $$C_v = \left(\frac{\partial U}{\partial T}\right)_\rho \quad \text{and} \quad B_T = \left(\frac{\partial U}{\partial \rho}\right)_T \tag{2.7}$$

Equation (2.6) holds for ions and electrons separately. For ions

$$S_i = H_i - K_{ie} + Y_i + Q \tag{2.8}$$

and for electrons

$$S_e = H_e + K_{ie} + Y_e + X_L + J \tag{2.9}$$

where H denotes the rate of energy flow due to thermal conduction, K_{ie} is the rate of energy exchange between ions and electrons, Y is the rate of energy release due to thermonuclear reactions, J is the rate of energy loss due to bremsstrahlung and X_L is the rate of

energy absorption from the laser. The expressions for these source terms are all well known. We shall deal with the evaluation of H in this section, K_{ie} will be treated in section (2.5) and the remainder in appendix (3) . To calculate electron and ion temperatures from equation (2.6) we need to know the coefficients C_V, B_T, P and the source terms S. These quantities are evaluated separately for electrons and ions.

Ions:

The ions are always treated as a classical ideal gas and therefore the density dependent term $B_T \equiv 0$. Thus the internal energy of the ions is given by

$$U_i = 3/2 \left(\frac{K T_i}{m_H M}\right) \tag{2.10}$$

the specific heat by

$$(C_V)_i = 3/2 \left(\frac{K}{m_H M}\right) \tag{2.11}$$

and the pressure by

$$P_i = n_i K T_i \tag{2.12}$$

where K is Boltzmann constant.

Electrons:

The electrons may be classical or degenerate depending upon their density and temperature. The degree of degeneracy is determined by a parameter $\xi = T_e / T_F$ where T_F is the Fermi temperature given by:

$$K T_F = \frac{h^2}{8 m_e} \left(\frac{3}{\pi}\right)^{2/3} \left(\frac{Z}{m_H M}\right)^{2/3} \rho^{2/3}$$

where m_e is the electron mass and h is the Planck's constant. The electrons are considered to be strongly degenerate if $\xi < \xi_{min}$ weakly degenerate if $\xi_{min} \leq \xi < \xi_{max}$ and classical if $\xi \geq \xi_{max}$, where $\xi_{max} = 100$ and $\xi_{min} = 0.10$. The expressions for P_e, $(C_V)_e$ and $(B_T)_e$ are as follows.

$$P_e = \frac{K Z}{m_H M} (\rho T_e) \begin{cases} 2/5\,\xi^{-1} + \pi^2/6\,\xi - \pi^4/40\,\xi^3 & \xi < \xi_{min} \\ 1 + (3\sqrt{2\pi})^{-1} \xi^{-3/2} & \xi_{min} \leq \xi < \xi_{max} \\ 1 & \xi \geq \xi_{max} \end{cases} \tag{2.13}$$

$$(C_V)_e = \frac{3}{2}\left(\frac{KZ}{m_H M}\right)\begin{cases} \frac{\pi^2}{3}\xi - \frac{\pi^4}{10}\xi^3 & \xi < \xi_{min} \\ 1 - (6\sqrt{2\pi})^{-1}\xi^{-3/2} & \xi_{min} \le \xi < \xi_{max} \\ 1 & \xi_{max} \le \xi \end{cases} \tag{2.14}$$

$$B_T = \frac{3}{2}\frac{P_F}{\rho^2}\begin{cases} 2/3 - \frac{5}{18}\pi^2\xi^2 + \frac{\pi^4}{8}\xi^4 & \xi < \xi_{min} \\ 5(6\sqrt{2\pi})^{-1}\xi^{-1/2} & \xi_{min} \le \xi < \xi_{max} \\ 0 & \xi_{max} \le \xi \end{cases} \tag{2.15}$$

where $P_F = \frac{h^2}{20\, m_e}\left(\frac{3}{\pi}\right)^{2/3}\left(\frac{Z}{m_H M}\right)^{5/3}\rho^{5/3}$ (2.16)

is the Fermi pressure of a fully degenerate gas. However one can simulate degeneracy effects by choosing an initial temperature which yields the same pressure as that of a fully degenerate gas at zero temperature.

Heat Conduction Term:

Although the heat conduction is assumed to satisfy Fourier's equation

$$H = \tfrac{1}{\rho}\nabla\cdot(\kappa\nabla T) \tag{2.17}$$

where κ is the thermal conductivity of the fluid, in the case of electrons, for large temperature gradients, the thermal flux ($\kappa_e \nabla T$) becomes unphysically large. As discussed in chapter 1, an upper limit, namely, the free streaming limit

$$F_{max} = \frac{1}{a_1}\left(\frac{1}{4} n_e v_e K T_e\right) \tag{2.18}$$

is then imposed on the electron flux and the modified electron flux is given by

$$F_e' = \frac{F_e F_{max}}{F_e + F_{max}} \tag{2.19}$$

where $F_e = \kappa|\nabla T_e|$

Equation (2.19) can be simplified to

$$F_e = \left[\kappa_e\left(1 + \frac{a_1 \bar{l}_e}{T_e}\left|\frac{dT_e}{dx}\right|\right)^{-1}\right]\left|\nabla T_e\right| \tag{2.20}$$

where a_1 is a +ve number ≥ 1, $v_e = (8KT_e/m_e\pi)^{1/2}$ and

$$\bar{l}_e = 5.9\times 10^9\, T_e^2/(n_i \log\Lambda) \tag{2.21}$$

is the electron mean free path.

From (2.20), the modified electron thermal conductivity is

$$\kappa_e' = \kappa_e \left(1 + \frac{a_1 \bar{l}_e}{T_e} \left|\frac{dT_e}{dx}\right|\right)^{-1} \qquad (2.22)$$

It is obvious that as $\left|\frac{d\,T_e}{dx}\right|$ increases, K_e decreases and remains within required physical limits.

(2.3):

(a) Geometry of the target:

With an appropriate choice of parameter g we can assign one of the following geometries to the target.

g = 1 corresponds to a slab of unit cross-section.

g = 2 corresponds to a section of a cylinder of unit length and one radian in angle.

g = 3 corresponds to a section of a sphere of one steradian in solid angle.

For laser compression studies, spherical geometry is preferred over the other two and therefore in our calculations we shall always consider a spherical target.

(b) Initial and boundary conditions:

The standard version of MEDUSA does not allow for hollow shells and layered targets but can only deal with spheres. The initial density and temperature profiles and hence the pressure profile is uniform throughout the radius of the target. 3)

At the outer boundary $r = R_o$ we apply

1) zero thermal flux, 4)

2) $u(R_o) = u(t)$,

3) $P(R_o) = P(t)$

So that the outer boundary can move freely.

MISSING

PRINT

Because of the complexity of the problem, the above system of equations cannot be solved analytically and therefore numerical techniques are required. The two standard techniques employed in numerical methods are explicit and implicit schemes. Using an explicit scheme the time step must be restricted by C-F-L condition to avoid numerical instability. An implicit scheme on the other hand guarantees a numerically stable solution. For reasons of accuracy however, the time step is monitored by the time rate of change of the fundamental variables of the problem such as temperature, density etc. MEDUSA solves the equation of motion explicitly while the energy equation is treated implicitly. In the following we discuss the details of these schemes.

(2.4) Mesh and numerical scheme:

The target radius r = o to r = R is replaced by a Lagrangian mesh containing N cells. The cell boundary is labelled by j and the cell centre by ℓ, as shown below.

The cell boundaries move, thereby changing the volume of the cell.

Each cell carries a mass dM_ℓ so that its specific volume

$$V_\ell = \frac{1}{g}\left(R^g_{j+1} - R^g_j \right) \tag{2.23}$$

The mass dM_ℓ will only change if the cell undergoes thermonuclear burning. Any quantity known at the cell boundaries can be evaluated at the cell centre by simple average:

$$R_\ell = \frac{1}{2}\left(R_{j+1} + R_j\right) \tag{2.24}$$

The quantities are advanced in time by using a five time level scheme as shown below:

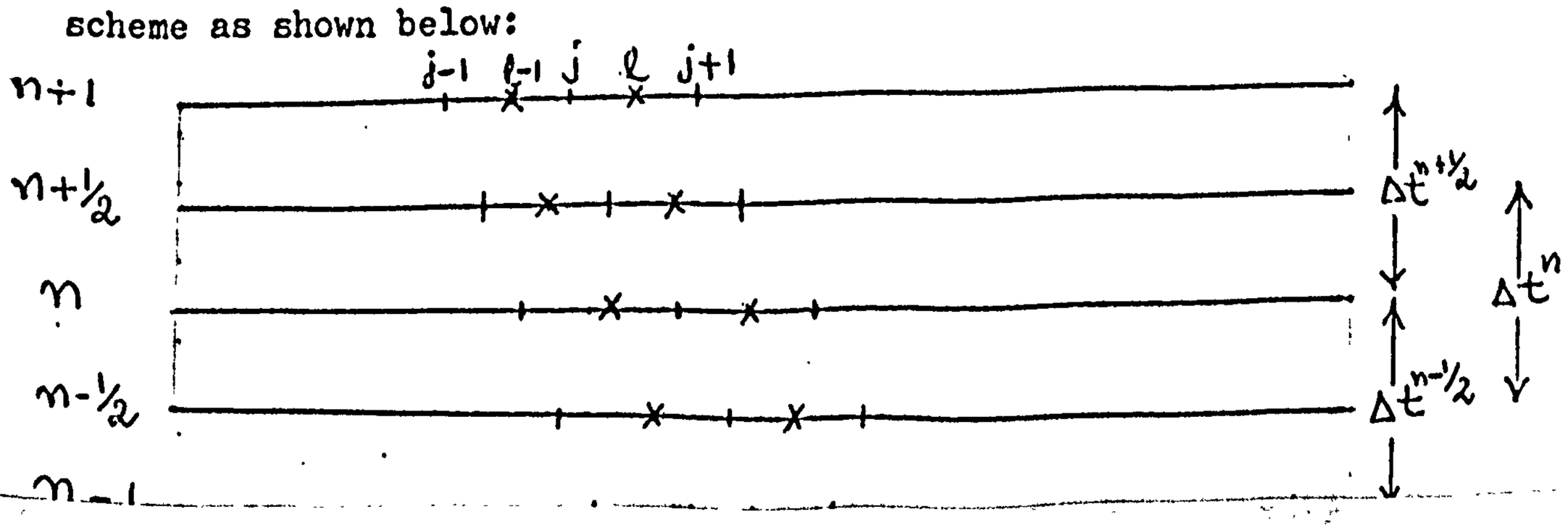

Knowing T_ℓ, ρ_ℓ, R_j and f_ℓ at time level n-1 also knowing Uj at time level $n-\frac{1}{2}$ and knowing R_j and ρ_ℓ at time level n, these quantities are evaluated at advanced time levels as:

T_ℓ, f_ℓ at time level n

U_j at time level $n+\frac{1}{2}$

and R_j, ρ_ℓ at time level n+1.

The quantities with subscript ℓ are evaluated at the cell centre whereas those with subscript j are evaluated at cell boundary.

For further details of the numerical scheme see reference (11).

(2.5) Solution of the system of Equations:

(a) Energy Equation

Using Crank-Nicolson implicit scheme the energy equation can be written as follows.

$$(C_v)_\ell^{n-1/2}\left(\frac{T_\ell^{n}-T_\ell^{n-1}}{\Delta t^{n-1/2}}\right)+(B_T)_\ell^{n-1/2}\left(\frac{\rho_\ell^{n}-\rho_\ell^{n-1}}{\Delta t^{n-1/2}}\right)+P_\ell^{n-1/2}\left(\frac{V_\ell^{n}-V_\ell^{n-1}}{\Delta t^{n-1/2}}\right)=S_\ell^{n-1/2} \qquad (2.25)$$

The subscripts i and e are dropped for simplicity. The coefficients $(Cv)_\ell^{n-\frac{1}{2}}$, $(B_T)_\ell^{n-\frac{1}{2}}$ and $P_\ell^{n-\frac{1}{2}}$ are evaluated by taking an average of the corresponding quantities at levels n and n-1. The source terms $S_e^{n-\frac{1}{2}}$ for the electrons and ions are evaluated as below:

$$S_e^{n-1/2} = H_\ell^{n-1/2} + K_{ie}^{n-1/2} + Y_e^{n-1/2} + J^{n-1/2} + X^{n-1/2} \qquad (2.26)$$

and

$$S_i^{n-1/2} = H_i^{n-1/2} - K_{ie}^{n-1/2} + Y_i^{n-1/2} + Q^{n-1/2} \qquad (2.27)$$

In this section we will deal with the heat conduction term and the energy exchange term which require special techniques for computation while the remaining quantities in equations (2.26) and (2.27) are evaluated by taking an average of the corresponding quantities at levels n and n-1 respectively.

Heat Conduction term:

The rate of energy absorbed in a cell due to heat conduction is the difference of the rate at which the energy flows into that cell through wall j+1 and the rate at which energy flows out of that cell

through wall j as shown below:

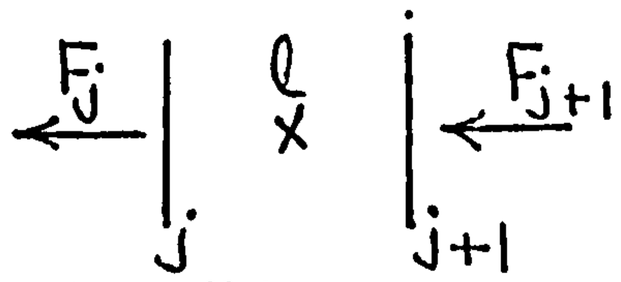

The heat conduction term H becomes

$$H_\ell^n = \frac{1}{dM_\ell}\left(F_{j+1}^n - F_j^n \right) \tag{2.28}$$

where $$F_j^n = (R_j^n)^2 q K_j^n \frac{T_\ell^n - T_{\ell-1}^n}{R_\ell^n - R_{\ell-1}^n} \tag{2.29}$$

An average is then taken to evaluate $H_e^{n+\frac{1}{2}}$ as:

$$H_\ell^{n+1/2} = \frac{1}{2}\left(H_\ell^n + H_\ell^{n-1} \right) \tag{2.30}$$

Energy exchange term

Special care must be taken in choice of time step when studying a system involving processes with widely disparate time scales. It was mentioned in (2.3) that an implicit scheme does not impose any restrictions on the time step other than those determined by the accuracy of the solution. This scheme, however, does have some drawbacks which we discuss in this section. Consider the following simple differential equation

$$\frac{\partial f}{\partial t} = -\omega f \tag{2.31}$$

where f may be fraction of some radio-active element which decays on a time scale. $\tau \sim \frac{1}{\omega}$

Analytic solution to equation (2.31) is

$$f = f_o\, e^{-\omega t} \tag{2.32}$$

where f_0 is the fraction of the element present at time t = o. Equation (2.31) can be written in implicit finite difference form as

$$\frac{f^{n+1} - f^n}{\Delta t} = -\omega\left(\theta f^{n+1} + (1-\theta) f^n \right) \tag{2.33}$$

where θ determines the degree of implicitness.

Equation (2.33) can be written as

$$f^{n+1} = f^n \frac{1 - \Delta t\, \omega(1-\theta)}{1 + \Delta t\, \omega \theta} \tag{2.34}$$

From equation (2.34) it can be seen that f^{n+1} can become zero or even

-ve, if Δt is chosen bigger than the time scale of the process.

In case when $f_o < 0$, one can replace its value by zero. If we now like to evaluate $f^{n+\frac{1}{2}}$ by taking an average of f^{n+1} and f^n, it will be a very bad approximation as shown below.

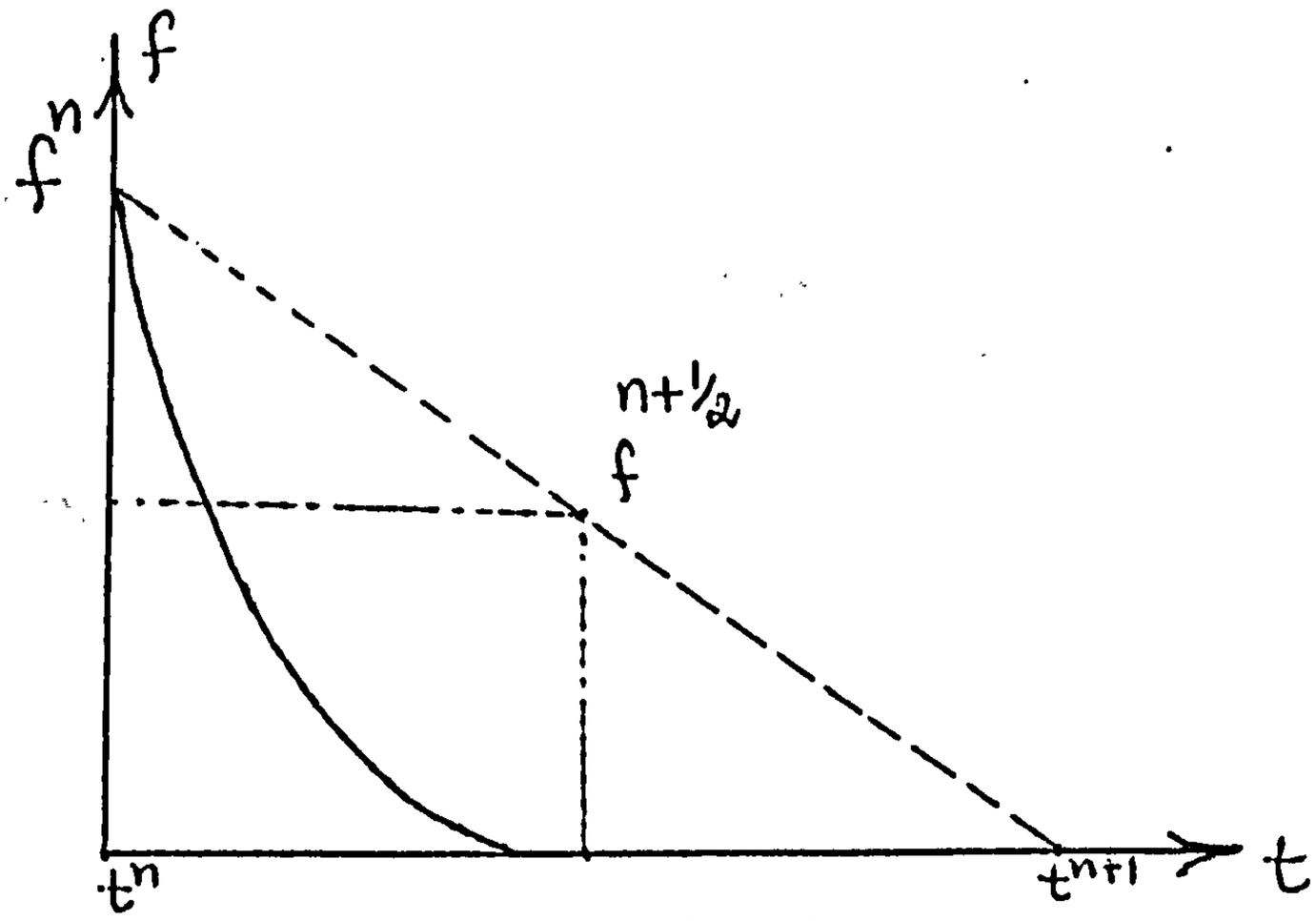

If we take the analytic solution (2.32) and compute an average of f^{n+1} over time step Δt we get

$$\langle f^{n+1} \rangle = f^n \langle \bar{e}^{\omega t} \rangle$$

where

$$\langle \bar{e}^{\omega t} \rangle = \frac{1}{\Delta t} \int_0^{\Delta t} e^{-\omega t} dt = \frac{1}{\omega \cdot \Delta t} \left(1 - \bar{e}^{\omega \cdot \Delta t}\right) \qquad (2.35)$$

In laser plasma calculations simulated by MEDUSA the electron-ion energy exchange time scale τ_{ie} in some circumstances, may become many orders of magnitude smaller than the hydrodynamic time scale τ_{hd} where as the time scale of our interest is τ_{hd}. To overcome this problem of time scales, MEDUSA employs the above technique to evaluate the energy exchange term $K_{ie}^{n-\frac{1}{2}}$ as explained below [17].

The ion and electron energy equations can be written as:

$$\frac{dT_i}{dt} = \frac{W_i}{(Cv)_i} - \frac{K_{ie}}{(Cv)_i} \qquad (2.36)$$

$$\frac{dT_e}{dt} = \frac{W_e}{(Cv)_e} + \frac{K_{ie}}{(Cv)_e} \qquad (2.37)$$

where W contains the rest of source terms and also the $p \cdot \frac{dv}{dt}$ term.

Hence

$$\frac{d}{dt}(T_i - T_e) = \left(\frac{W_i}{(Cv)_i} - \frac{W_e}{(Cv)_e}\right) - \left(\frac{1}{(Cv)_i} + \frac{1}{(Cv)_e}\right) K_{ie} \qquad (2.38)$$

We suppose that $$K_{ie} = (C_v)_i (T_i - T_e)\omega_{ie} \quad (2.39)$$

where $$\omega_{ie} = \frac{Z^2 e^4 \log\Lambda \, m_e^{1/2}}{32\sqrt{2\pi}\,\varepsilon_0^2 m_H M}(KT_e)^{-3/2} \quad (2.40)$$

is the electron-ion collision frequency, e is the electron charge and m_e is the electron mass.

Let $\xi = T_i - T_e$, $\beta = 1 + (C_v)_i/(C_v)_e$

and $$\Phi = \frac{W_i}{(C_v)_i} - \frac{W_e}{(C_v)_e} \quad (2.40A)$$

also substituting K_{ie} from (2.39) into (2.38) we get

$$\frac{d\xi}{dt} = \Phi - \beta\omega_{ie}\xi \quad (2.41)$$

In the high density core region, the energy equipartition rate is very large and therefore any difference between the temperatures of the two fluids (electrons and ions) will smooth out rapidly. In such a case we can treat Φ, β and ω_{ie} constant over the time step Δt. Under this assumption, equation (2.41) leads to a solution

$$\xi(t) = \left(\xi_0 - \frac{\Phi}{\beta\omega_{ie}}\right)e^{-\beta\omega_{ie}t} + \frac{\Phi}{\beta\omega_{ie}} \quad 0 < t < \Delta t \quad (2.42)$$

where $\xi_0 = \xi(t=0)$

However in the low density corona region the electron-ion collision frequency is amall and ξ is almost constant over the time step i.e.

$$\xi(t) \cong \xi_0 \quad (2.42A)$$

Case 1. Rapid Energy Exchange

Averaging equation (2.42) over time step $\Delta t^{n-1/2}$ we get

$$\xi^{n-1/2} = \left[\xi^{n-1} - \left(\frac{\Phi}{\beta\omega_{ie}}\right)^{n-1/2}\right]\left[\frac{1-e^{-\beta\omega_{ie}^{n-1/2}\Delta t^{n-1/2}}}{\beta\omega_{ie}^{n-1/2}\Delta t^{n-1/2}}\right] + \left(\frac{\Phi}{\beta\omega_{ie}}\right)^{n-1/2} \quad (2.43)$$

Thus to update ξ we require $\Phi^{n-1/2}$, which should be evaluated from equation (2.40A). This would be a cumbersome process and since in the core region the temperature difference ξ is always small then Φ is always small. Hence we can approximate the updating of Φ by

$$\Phi^{n-1/2} = \frac{\xi^{n} - \xi^{n-1}}{\Delta t^{n-1/2}} + \frac{K_{ie}^{n-1/2}}{(C_v)_i} \cdot \beta \quad (2.43A)$$

This treatment of fitting exponentials to the numerical solution is adopted to avoid a numerical instability in the core region wherever the two temperatures should deviate from each other. e.g. the ion temperature may rise as a result of shock heating.

Case 2. Slow Energy Exchange

In this case we have from (2.42A)

$$\xi^{n-1/2} = \xi^{n-1}$$

Method of Solution:

Substituting the expressions for $H_e^{n-1/2}$ and $K_{ie}^{n-1/2}$ in equation (2.25)

for electrons we get

$$A_\ell^n T_{\ell-1}^n + B_\ell^n T_\ell^n + C_\ell^n T_{\ell+1} = D_\ell^n + G_\ell^{n-1} \tag{2.47}$$

where $$A_\ell^n = -\frac{1}{dM_\ell}\cdot\frac{(R_i^n)^2 K_i^n}{(R_{j+1}^n - R_{j-1}^n)}\Delta t^{n-1/2} \tag{2.48}$$

$$C_\ell^n = -\frac{1}{dM_\ell}\cdot\frac{(R_{j+1})^2 K_{j+1}^n}{(R_{j+2}^n - R_j^n)}\Delta t^{n-1/2} \tag{2.49}$$

$$B_\ell^n = 0.5\left((Cv)_\ell^{n-1} + (Cv)_\ell^n\right) - A_\ell^n - C_\ell^n \tag{2.50}$$

$$D_\ell^n = 0.5\left[\left(X_\ell^n + J_\ell^n + Y_\ell^n + 2K_{ie}^n\right)\Delta t^{n-1/2} - (\rho_\ell^n - \rho_\ell^{n-1})\cdot\right.$$
$$\left.\cdot\left((B_T)_\ell^{n-1} + (B_T)_\ell^n\right) - (V_\ell^n - V_\ell^{n-1})(P_\ell^{n-1} - P_\ell^n) + T_\ell^{n-1}\left((Cv)_\ell^{n-1} + (Cv)_\ell^n\right)\right] \tag{2.51}$$

$$G_\ell^{n-1} = 0.5\,\Delta t^{n-1/2}\left(X_\ell^{n-1} + J_\ell^{n-1} + Y_\ell^{n-1}\right) - C_\ell^{n-1}\left(T_{\ell+1}^{n-1} - T_\ell^{n-1}\right)$$
$$+ A_\ell^{n-1}\left(T_\ell^{n-1} - T_{\ell-1}^{n-1}\right) \tag{2.52}$$

Similarly these expressions can be evaluated for ions provided J_ℓ^n and X_ℓ^n are replaced by Q_ℓ^n in equations (2.51) and (2.52) and +2Kie is replaced by -2Kie in equation (2.51).

It is obvious that the coefficients A_ℓ^n etc. are functions of T_ℓ^n and therefore equation (2.47) must be solved iteratively. For first iteration we take $T_\ell^n = T_\ell^{n-1}$ and evaluate the coefficients. Substituting these values of coefficients in equation (2.47) we compute the temperature using Gauss's elimination scheme . This new value of temperature is accepted after checking the convergence of iterations.

(b) Equation of motion:

Using explicit difference scheme the equation of motion can be written as

$$U_j^{n+\frac{1}{2}} - U_j^{n-\frac{1}{2}} = -(R_j^n)^2\frac{P_\ell^n - P_{\ell-1}^n + q_\ell^n - q_{\ell-1}^n}{dM_j}\Delta t^n \tag{2.53}$$

where $dM_j = \frac{1}{2}(dM_\ell + dM_{\ell-1})$.

After evaluating $U_j^{n+\frac{1}{2}}$, the cell boundary can be moved to the new

position

$$R_j^{n+1} = R_j^n + U_j^{n+1/2} \cdot \Delta t^{n+1/2} \tag{2.54}$$

Time step control:

Since the equation of motion is solved explicitly, the solution obtained will be stable only if the time step is restricted by the C-F-L condition

i.e.

$$\Delta t^{n+1/2} \leq a_1 \, \mathrm{Min}\left(\frac{R_{i+1}^n - R_i^n}{C_\ell^n}\right) \tag{2.55}$$

where C_ℓ^n is the speed of sound in cell ℓ and a_1 is an adjustable parameter < 1. The energy equation on the other hand is solved implicitly and thus provides numerically stable solution, but for reasons of accuracy $\Delta t^{n+1/2}$ is monitored by time rate of change of T_i and T_e. We also restrict $\Delta t^{n+1/2}$ by time rate of change of V. The expressions used for this purpose are

$$\Delta t^{n+1/2} \leq a_2 \, \mathrm{Min}\left|\frac{T_\ell^{n+1} - T_\ell^n}{T_\ell^{n+1} + T_\ell^n}\right|_i \tag{2.56}$$

with two similar expressions for T_e and V.

Having chosen the smallest time step out of these four conditions we check the convergence of iterations on the values of temperature obtained from equation (2.47) by examining

$$\left|\frac{T_i^m - T_i^{m-1}}{T_i^m + T_i^{m-1}}\right| = \delta T_i \tag{2.57}$$

where T_i^m denotes the value of the ion temperature after mth iteration. Similarly iterations on T_e and V are checked by evaluating two expressions similar to (2.57). If δT_i is below a specified value then convergence has been achieved and we prepare for the next time step.

(2.6) Limitations of MEDUSA:

In order to predict sensible results a computer code must have all the physics relevant to the experiment which it simulates. As mentioned at the beginning of this chapter, MEDUSA simulates a very

simple laser-compression model which neglects many important physical processes taking place in the laser plasma. As a consequence, in many cases the compression results predicted by MEDUSA differ from the experimental results by many orders of magnitude. In the following we present a few physical phenomena which are outside the scope of MEDUSA.

(a) Atomic Physics:

MEDUSA treats the plasma as a charge neutral mixture of ions and electrons with a fixed degree of ionization. This assumption may be correct for a D-T plasma but in the case of medium z targets ($z \sim 20$) important physical effects are neglected. For example, the degree of ionization may change significantly during the compression and expansion, due to microscopic processes taking place in the plasma. A variation in $\langle z \rangle$ would change all z-dependent quantities of the plasma such as thermal conductivity, laser light absorption, plasma pressure, radiation loss etc., which in turn affect qualitatively the implosion. In practice, one deals with a medium z (glass) micro-shell filled with solid or gaseous D-T. It is therefore important to include atomic physics effects into the code for realistic compression studies. In Chapter 3 we present the incorporation of a steady state density and temperature dependent atomic physics package into MEDUSA. The results obtained by using this modified version of the code will be discussed in Chapter 5.

(b) Energy transfer:

In the standard version of MEDUSA, ions and thermal electrons are the only means of energy transfer. In fact it can be shown that the mean free path of suprathermal electrons, and under certain conditions the mean free path of photons, becomes very large as compared to the thermal electrons. The suprathermal electrons and the photons can therefore penetrate the target at a much faster rate, preheating the core. As a result, the shock front would be weakened and the quality

of implosion will be degraded. It is therefore very important to include energy transfer by fast electrons and radiation into MEDUSA.

In Chapter 4 we describe the incorporation of the transport of continuum radiation, namely, free-free and free-bound radiation into MEDUSA, using a diffusion approximation. The radiation field is represented by a radiation temperature T_r and it interacts with the electrons as a function of local temperature difference between the fluids i.e. $(T_e - T_r)$.

The diffusion approximation is correct only for an optically thick medium and is therefore not satisfactory in the corona region. But since in 1-D simulations we are mainly interested in the physics of the core, this discrepancy of the model will be overlooked for the present case. The line radiation is absorbed locally in the compressed core while it escapes freely from the underdense corona region.

(c) Target design:

The standard version of MEDUSA can only deal with solid microspheres and is incapable of dealing with micro-shells and layered targets. We have modified MEDUSA to be able to handle the latter two types of targets which have more practical importance. The modifications made in the code in this context are described in appendix 4.

CHAPTER 3

ATOMIC PHYSICS

Numerous atomic processes take place in a high density and high temperature laser produced plasma, including collisional ionization, collisional excitation and de-excitation, radiative recombination, dielectronic recombination, spontaneous radiative decay, photo-ionization and photoexcitation. For one and two electron systems the cross-sections for these processes are known with reasonable accuracy. But the problem becomes extremely complicated when one is dealing with a many-electron system and thus many approximations need to be made. The accuracy of the rate coefficients for the above processes in the case of many-electron atoms is therefore limited, typically to within a factor of 2 [18]. If the plasma is assumed optically thin, the processes of photo-ionization and photo-excitation become unimportant. In the present work only those processes will be considered which have relatively larger cross-section, namely, collisional ionization, collisional excitation and de-excitation, radiative recombination and three-body recombination.

The rate equations governing the time evolution of population densities of ions with different ionization levels is given in section (3.1). The rate coefficients for the various atomic processes are presented in section (3.2). Some well known atomic physics models are described in section (3.3) and the limitations of these models are also discussed. In section (3.4), incorporation of a steady state density and temperature dependent atomic physics package, namely, TRIP (4), into MEDUSA is described. The limitations of this new version of the code are also stated.

(3.1) Rate Equations:

The various atomic processes mentioned in the introduction to this chapter give rise to changes in the ionization and excitation states of

the ions in the plasma. The rate of evolution of the population densities of the ions in different ionization and excitation states is described by a set of differential equations, known as plasma rate equations. These rate equations reduce to a simple but nevertheless useful form if the following assumptions are considered [19].

(i) The collisional ionization rate from any bound level is partially balanced by the three-body recombination rate into any level:

i.e. $$I_{(z,p)} + e \rightleftharpoons I_{(z+1,p)} + e + e \quad (3.1)$$

where I (z,p) denotes a z-times ionized atom whose external electron is in quantum state p and e represents an electron.

(ii) Transitions between bound levels are caused by electron collisions only:

i.e. $$I_{(z,p)} + e \rightleftharpoons I_{(z,q)} + e \quad (3.2)$$

where $p > q$.

(iii) The radiative processes taking place in the plasma are radiative recombination and spontaneous radiative decay:

i.e. $$I_{(z+1,p)} + e \longrightarrow I_{(z,q)} + h\nu \quad (3.3)$$

and $$I_{(z,p)} + e \longrightarrow I_{(z,q)} + h\nu \quad (3.4)$$

(iv) The plasma is assumed to be optically thin.

When studying the changes in the degree of ionization of the plasma, the processes of spontaneous radiative decay, collisional excitation and collisional de-excitation can be neglected, since these processes do not change the population density of a given ionization stage but only affect the internal structure of the ions within that ion stage.

With the above assumptions, the population density of, say, z-times ionized atoms in a quantum state p, is governed by the following differential equation:

$$\begin{aligned}\frac{dn_{(z,p)}}{dt} = &- n_e n_{(z,p)} S_{(T_e,z,p)} + n_e n_{(z-1,p)} S_{(T_e,z-1,p)} \\ &- n_e^2 n_{(z,p)} \beta_{(T_e,z,p)} + n_e^2 n_{(z+1,p)} \beta_{(T_e,z+1,p)} \\ &- n_e n_{(z,p)} \alpha_{(T_e,z,p)} + n_e n_{(z+1,p)} \alpha_{(T_e,z+1,p)}\end{aligned} \quad (3.5)$$

where S, β and α represent rate coefficients for collisional ionization, three-body recombination and radiative recombination for the corresponding ion stage respectively. Summing over all possible excitation levels, (3.5) can be written as:

$$\frac{dn(z)}{dt} = -\sum_p n_e n(z,p) S(T_e,z,p) + \sum_p n_e n(z-1,p) S(T_e,z-1,p) - \sum_p n_e^2 n(z,p) \beta(T_e,z,p) + \sum_p n_e^2 n(z+1,p) \beta(T_e,z+1,p) - \sum_p n_e n(z,p) \alpha(T_e,z,p) + \sum_p n_e n(z+1,p) \alpha(T_e,z+1,p) \quad (3.6)$$

where $n(z) = \sum_p n(z,p)$

For any given rate coefficient, say, $A(T_e,z,p)$ one can write

$$\sum_p n(z,p) A(T_e,z,p) = n(z) \langle A(T_e,z,p) \rangle \quad (3.7)$$

For simplicity let $\langle A(T_e,z,p) \rangle = A(z)$

then $\sum_p n_e n(z,p) A(T_e,z,p) = n_e n(z) A(z)$

Equation (3.6) can then be written as

$$\frac{dn(z)}{dt} = -n_e n(z) S(z) + n_e n(z-1) S(z-1) - n_e^2 n(z) \beta(z) + n_e^2 n(z+1) \beta(z+1) - n_e n(z) \alpha(z) + n_e n(z+1) \alpha(z+1) \quad (3.8)$$

where $z=0,1,2\ldots Z_M$ and Z_M is the atomic number of the element.

(3.2) Rate Coefficients:

The rate coefficients used in equation (3.8) are discussed in [20] The analytic expressions for these rate coefficients are as follows.

(i) Collisional Ionization:

The ionization of an atom due to electron impact can either proceed directly from the ground state or from an excited state. The rate coefficient for ionization from the ground state of a μ-times ionized atom is

$$S_\mu = 1.55 \times 10^{-40} \xi_\mu \left(\frac{KT_e}{\chi_\mu}\right)^{1/4} \exp\left(-\frac{\chi_\mu}{KT_e}\right) \chi_\mu^{-3/2} \quad m^3 s^{-1} \quad (3.9)$$

where χ_μ is the ionization potential for ions in state μ, ξ_μ is the number of electrons in the outermost shell, K is the Boltzmann constant and T_e is the electron temperature.

(ii) Radiative Recombination:

The rate coefficient for the capture of a free electron in

the ground state of a $(\mu-1)$-times ionized atom is:

$$\alpha_\mu = 47.5 \times 10^{-12} \chi_{\mu-1} / (K T_e)^{1/2} \quad m^3 s^{-1} \qquad (3.10)$$

(iii) Three-body Recombination:

$$\beta_\mu = 1.6 \times 10^{-96} / (K T_e)^{5/4} (\chi_\mu)^{7/4} \quad m^6 s^{-1} \qquad (3.11)$$

(3.3) Atomic Physics Models:

The ionization state of a plasma can be fully determined by population fractions f_z(z=o,1,2...) of ions with different degrees of ionization. Complete information about the densities of these population fractions, which in general are function of electron number density, electron temperature and time, can be obtained from the set of differential equations (3.8). However in some circumstances the relaxation times for atomic processes are very small as compared with the time over which macroscopic plasma parameters vary. In such cases one can neglect the time evolution of f_z and the plasma can be regarded as in a state of equilibrium. A steady state model is then sufficient to determine the degree of ionization of such a system. The atomic physics models used to represent the state of a plasma can therefore, in general, be divided into two groups, namely, steady state models and time dependent models. In the following we present some well known atomic physics models and discuss their advantages and limitations.

(3.3a) Steady State Models:

(a-i) Local Thermodynamic Equilibrium Model (LTE):[19]

This model assumes that the population density of electrons in the plasma is completely determined by the particle collisional processes. Also it is assumed that collisions occur at a sufficiently rapid rate that the distribution responds instantaneously to any change in the plasma conditions. When such a situation holds then each collision is accompanied by its inverse collision and, according to the principle of detailed balancing, these pairs of processes take place at equal rates. Thus the distribution of population densities of the energy levels of electrons is analogous to that of a system in complete thermodynamic

equilibrium. The population distribution of such a system is completely determined by the laws of statistical mechanics (Boltzmann, Fermi-Dirac or Bose-Einstein) and does not require the knowledge of atomic cross sections. Thus the distribution of the population densities, at a certain point in space and at any instant in time is determined by the local plasma density, temperature and chemical composition, although the density and temperature may vary in space-time.

If the free electrons are distributed among the available energy levels, according to the laws of statistical mechanics, their velocities will have a Maxwellian distribution. The number of electrons with velocities between v and v+ dv is given by

$$dn_v = n_e\, 4\pi \left(\frac{m_e}{2\pi K T_e}\right)^{3/2} \exp\left(-\frac{m_e v^2}{2KT_e}\right) v^2\, dv \qquad (3.12)$$

where n_e is the electron number density and m_e is the electron mass.

For bound electrons the distribution of population densities is given by Boltzmann and Saha equations:

$$\frac{n(p)}{n(q)} = \frac{\omega(p)}{\omega(q)} \cdot \exp\left(\frac{\chi(p,q)}{KT_e}\right) \qquad (3.13)$$

$$\frac{n_e n(z+1,g)}{n(z,g)} = \frac{\omega(z+1,g)}{\omega(z,g)} \cdot 2\left(\frac{2\pi m_e K T_e}{h}\right)^{3/2} \exp\left(\frac{\chi(z,g)}{KT_e}\right) \qquad (3.14)$$

where n(p), n(q), n(z+1,g) and n(z,g) are the population densities of the various levels designated by their quantum numbers p,q and g (ground level) and ionic charge z+1 and z. Equations (3.12) to (3.14) describe the state of electrons in an LTE model.

Limitations:

As mentioned above, in an LTE model, each process is balanced by its inverse process. Consider the processes of collisional ionization and three-body recombination:

$$e + A(z) \longrightarrow A(z+1)' + e + e \qquad (3.15)$$

i.e. an electron e collides with a z-times ionized atom, A(z), and knocks out one of its electrons, producing a (z+1)-times ionized atom.

$$A(z+1) + e + e \longrightarrow A(z) + e \qquad (3.16)$$

i.e. two electrons collide with a (z+1)-times ionized atom, one electron is captured by the atom and the other carries away the extra energy of the captured electron.

For the LTE model to hold, these two processes must occur at equal rates. From (3.15) and (3.16) one can see that the rate of collisional ionization is proportional to n_e while the rate of three-body recombination is proportional to n_e^2. The latter process would therefore decrease rapidly with n_e and at sufficiently low densities the balance between the rates of the above mentioned two processes will break up. However at such low densities radiative recombination becomes important since its rate is proportional to n_e. Therefore at sufficiently low densities the LTE model is completely invalid.

Criterion For Applicability of LTE:

In the following we derive a simple criterion which is a necessary, but not a sufficient condition for a plasma to be in LTE.

The electrons, because of their high velocities, mainly bring about collisional transitions in the plasma. To check the validity of LTE model we compare the collisional de-excitation rate with the radiative decay rate - consider atoms (or ions), in a certain level p, undergoing transitions to a lower level q due to electron impact.

The rate at which these transitions take place

$$= n_e n(p) X(T_e, p, q)$$

where $X(T_e, p, q)$ is the de-excitation coefficient.

The radiative decay rate, on the other hand

$$= n(p) A(p, q)$$

For a 10% deviation from LTE we get

$$n_e n(p) X(T_e, p, q) \geqslant 10\, n(p) A(p, q) \qquad (3.17)$$

Substituting appropriate expressions for $X(T_e, p, q)$ and $A(p, q)$ the above inequality reduces to a simpler form[19]

$$n_e \geqslant 1.6 \times 10^{12} T_e^{1/2} X(p, q) \quad /cm^3 \qquad (3.18)$$

where T_e is in K^o and X(p,q) is in electron volts.

(a-ii) Steady State Corona Model:[16]

Unlike LTE model, where each collisional process is balanced by its inverse collisional process, the steady state corona model assumes the plasma to be in ionizational equilibrium due to a balance between collisional ionization (excitation) and radiative recombination (spontaneous radiative decay). Let us assume that if there is a change in the plasma parameters, it takes place sufficiently slowly that the plasma effectively remains in a steady state. The question of intrinsic relaxation times of atomic processes will be treated later.

The equations which describe the steady state corona model are as follows:

(i) The electrons are assumed to have a Maxwellian distribution. The velocities of free electrons will therefore be distributed according to (3.12). It is not necessary to make any specific assumption about the velocity distribution of ions, except that their mean energy should be of the same order or less than that of electrons, otherwise ion-ion collisions will become important.

(ii) It is also assumed in this model that the majority of ions are in the ground state and that only a negligibly small number of ions are in excited levels. Thus the equation representing the ionization and recombination balance may be written as:

$$n_e n(z,g)\, S(T_e,z,g) = n_e n(z+1,g)\, \alpha(T_e,z+1,g) \quad (3.19)$$

i.e.

$$\frac{n(z,g)}{n(z+1,g)} = \frac{\alpha(T_e,z+1,g)}{S(T_e,z,g)} \quad (3.20)$$

where α and S denote the rate coefficients for radiative recombination and collisional ionization for the corresponding ions respectively.

Since these two processes are both two-body processes, the distribution of ions in a corona model is therefore

independent of density.

(iii) The population density of the excited levels is determined by equating the rate of collisional excitation from ground level and the rate of spontaneous decay:

So that

$$n_e n(z,g) X(T_e,g,p) = n(z,p) \sum_{q<p} A(p,q) \quad (3.21)$$

Limitations:

The steady state corona model was developed for plasmas with a density low enough to ensure that ion-ion collisions are unimportant. It may be shown [16] that in order to meet this requirement the electron temperature should be greater than $10^4 K^o$. The maximum density at which the corona model breaks down is reached at a point where collisional de-excitation becomes comparable with radiative decay process. At this limiting value of n_e there are as many collisional transitions out of a level p as radiative decays of level p. Thus the line intensity deviates by 50% from the value predicted by the corona model at that density.

Hence for a 50% deviation, it is sufficient to take the following as the criterion of applicability of the corona model:

$$\sum_{s<p}^{g} A(p,s) \geq n_e X(T_e,p,q) \quad (3.22)$$

where A(p,q) is the spontaneous radiative decay coefficient between levels p and q ($q<p$) and $X(T_e,p,q)$ is the collisional de-excitation coefficient. Ideally equation (3.22) should hold for all values of p. But this is not true because, as the quantum number increases, the probability of spontaneous radiative decay decreases while that of collisional de-excitation increases. Therefore there always exists some value of p for which the relation (3.22) is not satisfied no matter how low the density may be. The problem now is to select a value of p such that a density limit may be set for practical interest. It has been shown [19] that p=6 is a reasonable value. Substituting the analytic expressions for X and A [19], the relation (3.22)

reduces to

$$n_e < 5.6 \times 10^8 (z+1)^6 T_e^{1/2} \exp\left(\frac{1.162 \times 10^3 (z+1)^2}{T_e}\right) \qquad (3.23)$$

Thus we have seen that the steady state corona model is a high temperature and low density model and therefore has a limited use in the case of laser plasmas.

(a-iii) TRIP (4) - A steady state density and temperature dependent model: (21)

As has been discussed above, the LTE model and steady state corona model have limited application. The former model can be applied to a high density plasma while the latter is valid for a low density, high temperature regime only.

The electron density in laser produced plasmas exhibits considerable spatial variation. Therefore neither of the above two models can be applied to such a system. A very simple solution to this problem is to use a standard corona-like relation

$$\frac{n_{z+1}}{n_z} = \frac{S(T_e, Z)}{R_v(T_e, z+1)} \qquad (3.24)$$

where $$R(T_e, z+1) = \alpha(T_e, z+1) + n_e \beta(T_e, z+1) \qquad (3.25)$$

i.e. the sum of radiative and three-body recombination rate coefficients. n_z denotes the number density of z-times ionized ions. Since the recombination rate in this model is the sum of the radiative and the three-body recombination rates, either of which may dominate depending upon the density and temperature regime. Therefore this model can quite successfully be applied to a laser produced plasma.

Comparison between 3-body recombination and radiative recombination rates in a laser plasma:

It is of interest to compute the radiative recombination rate and the three body recombination rate using the criterion (3.18). Strictly speaking it is not possible to draw a sharp boundary between these two processes; nevertheless, one can picture the relative importance of the two by plotting their rates in a density, temperature

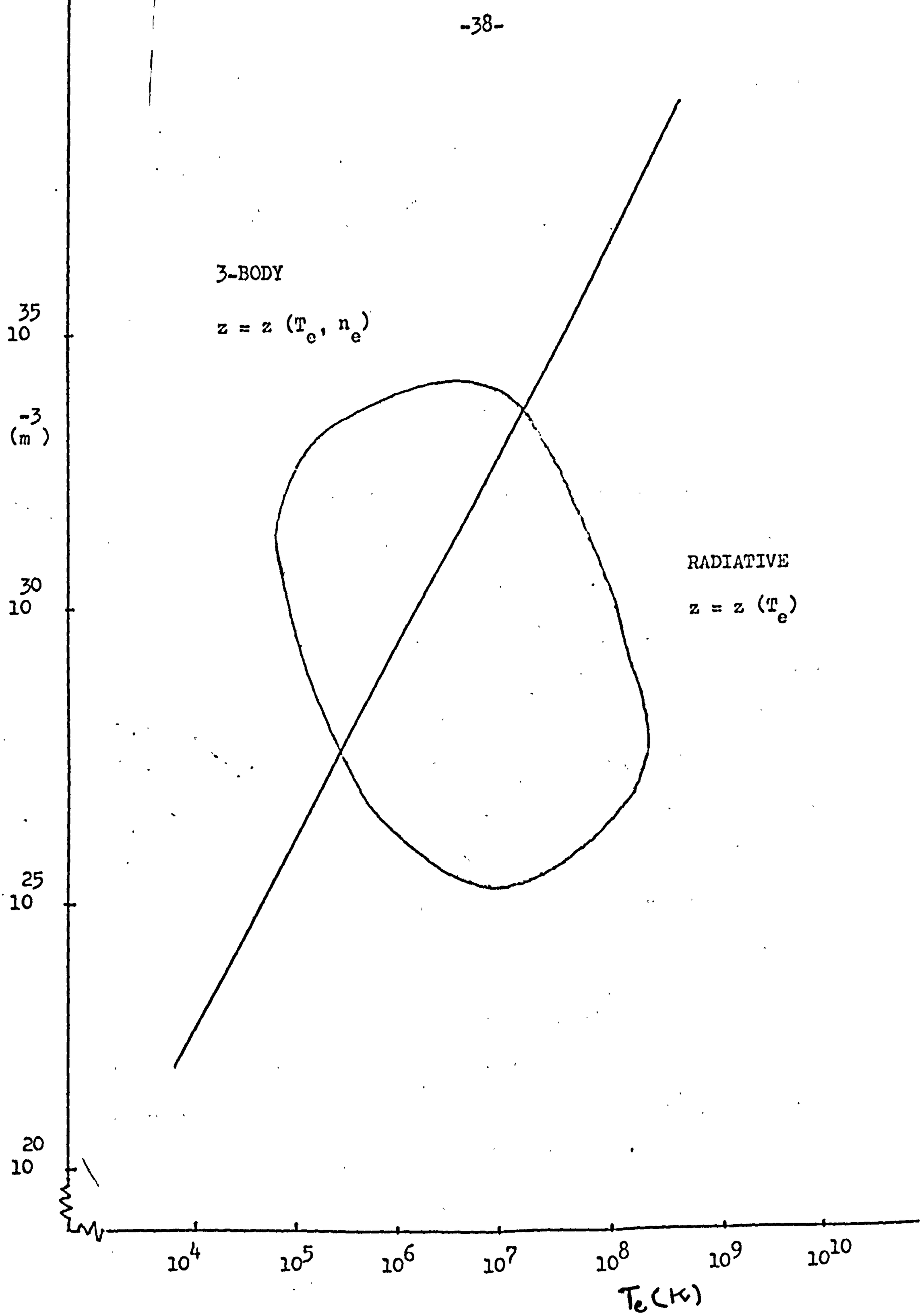

RECOMBINATION REGIMES

Fig. (3.1)

diagram. Figure (3.1) shows the recombination state of a carbon plasma produced by adiabatic compression of a 1 μ-g carbon microsphere. The three-body recombination rate dominates in the high density, compressed core region while the radiative recombination rate is important in the low density, high temperature corona region.

(3.3b): Time dependent atomic physics models:

(b-1) Time dependent corona model:- [19]

In the steady state corona model it has been assumed that the relaxation times for various important atomic physics processes are very short as compared to the time over which microscopic plasma variables such as density, temperature etc. change significantly. In this section we give consideration to the rates of these processes.

Suppose the conditions in the corona model plasma are changed suddenly. For example, there may be an abrupt change in the electron temperature. The bound electrons will take a finite time to arrange themselves into the new population distribution. This relaxation time will be controlled by the slowest atomic process. Imagine a plasma close to equilibrium. The population of z-times ionized atoms in their ground state will have a time dependence according to:

$$\frac{dn(z,g)}{dt} = n_e n(z-1,g) S(z-1) - n_e n(z,g) \alpha(z,g) \qquad (3.26)$$

First term on the R.H.S. is the rate at which (z-1)-times ionized atoms are ionized to state z while the second term represents the rate of recombination of z-times ionized atoms back to state z-1.

Also $$n(z-1,g) + n(z,g) = \text{Constant} \qquad (3.27)$$

Solution of equation (3.26) leads to

$$n(z,g) = \frac{(n(z-1,g) + n(z,g)) S(z-1,g) \left[1 - \exp\{-n_e(S(z-1,g)+\alpha(z,g))t\}\right]}{S(z-1,g) + \alpha(z,g)} \qquad (3.28)$$

Therefore the characteristic time for the plasma to approach towards final equilibrium is:

$$\tau \geq \frac{1}{n_e (S(z-1,g) + \alpha(z,g))} \qquad (3.29)$$

It is shown [19] that the above equation leads to the simple expression

$$\tau \geq \frac{10^{18}}{n_e} \quad Sec \tag{3.30}$$

or $$n_e \geq 10^{18}\,\tau^{-1}\ m^{-3}, \tag{3.31}$$

which is a lower limit on the electron density for the corona model to be valid. To check the validity of the steady state approximation in case of the laser plasmas, we apply relation (3.31) to a carbon plasma obtained by the compression of a 1-μg solid carbon microsphere. τ in this case, is considered as the time over which the electron temperature changes by a factor of e or it is the e-folding time for the electron temperature. Figure (3.2) represents a graph of τ against n_e which shows that the steady state assumption is valid in the greater part of the plasma region, except in the very tenuous outermost part of the corona.

The equations which describe the time dependent corona model can be written as follows:

(1) The free electrons are assumed to interchange energy at a sufficiently rapid rate by elastic collisions that, despite the changing conditions of the plasma, the velocity distribution is always Maxwellian and is represented by equation (3.12).

(2) The rate of change of population density of the ground level of z-times ionized atoms is written as

$$\frac{dn(z,g)}{dt} = n(z-1,g)\,n_e S(T_e,z-1,g) - n(z,g)\,n_e S(T_e,z,g) - n(z,g)\,n_e \alpha(T_e,z,g) + n(z+1,g)\,n_e \alpha(T_e,z+1,g) \tag{3.32}$$

The first two terms on the R.H.S. of the above equation represent the rates of collisional ionization from the ground state of (z-1) and z-times ionized atoms respectively. The latter two terms give the rates at which free electrons are captured into the ground state of z and (z+1)-times ionized atoms respectively.

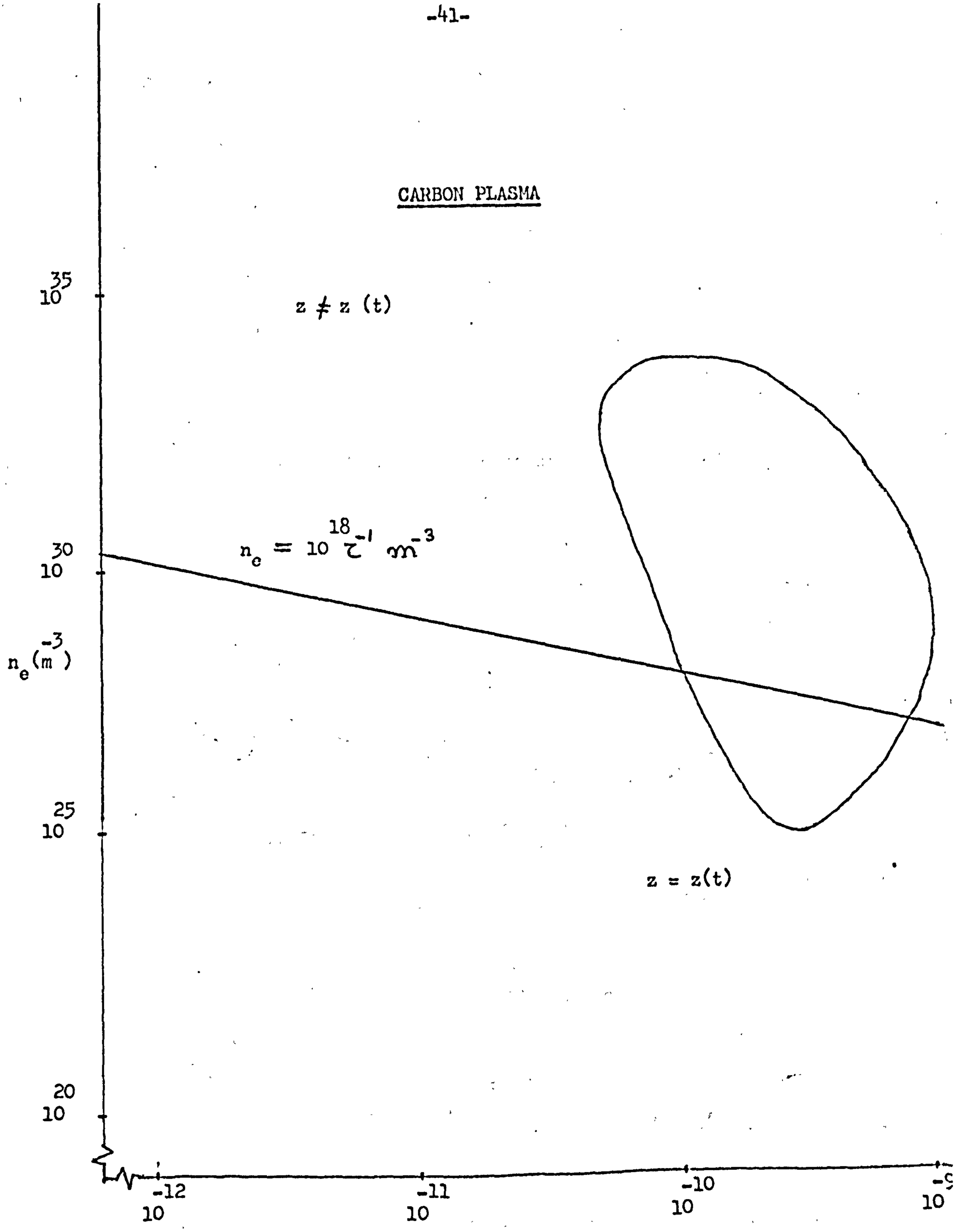

Ionization equilibrium regimes

Fig. (3.2)

(b-ii) TRIP (2) - A Time-Dependent Recombination And Ionization Package:- (21)

This time dependent ionization and recombination model is more general than the time dependent corona model. The atomic processes considered in this model are collisional ionization, radiative recombination and the three-body recombination. The approximation made is that at any point in space-time only three fractions are effectively present. The effect of excited levels is neglected and only ground state population densities are considered. The problem of radiative transfer is avoided by assuming the plasma to be optically thin.

Mathematical Model And Numerical Details:

Under the assumption of three fractions only being present at any point in space time, the rate equations (3.8) reduce to the following set of equations

$$\left.\begin{aligned}
\frac{df_{\mu-1}}{dt} &= -n_e S_{\mu-1} f_{\mu-1} + n_e R_\mu f_\mu \\
\frac{df_\mu}{dt} &= n_e S_{\mu-1} f_{\mu-1} - n_e (S_\mu + R_\mu) f_\mu + n_e R_{\mu+1} f_{\mu+1} \\
\frac{df_{\mu+1}}{dt} &= n_e S_\mu f_\mu - n_e R_{\mu+1} f_{\mu+1}
\end{aligned}\right\} \quad (3.32)$$

The moments of the distribution function are defined as $\langle z^n \rangle = \sum_\mu^n \mu^+ f_\mu$ (3.33A

The set of equations (3.32) can be written as

$$\frac{df_\mu}{dt} = n_e A_{\mu\nu} f_\nu \quad (3.33)$$

where $A_{\mu\nu}$ is the matrix of the rate coefficients.

It has been shown (22) that (3.33) can be written as

$$\frac{d\langle z^q \rangle}{dt} = n_e B_{q\nu} f_\nu \quad (3.34)$$

$$\nu = 1, 2 \text{-----} z_M$$

$$\text{where } B_{q\nu} = \left[(\nu+1)^q - \nu^q\right] S_\nu - \left[\nu^q - (\nu+1)^q\right] R_\nu \quad (3.35)$$

The distribution function f_μ can be expressed in terms of $\langle z^n \rangle$ with the help of eq.(3.33A) Substituting f_μ as a function of $\langle z^n \rangle$ and using three fraction model, eq.(3.34) can be written as

$$\frac{d\langle z^q \rangle}{dt} = n_e \sum_{q=0}^{2} a_{pq} \langle z^q \rangle \quad , p = 1, 2 \quad (3.36)$$

where vector (3.37)

$$\underline{a}_p = \underline{\underline{b}} \cdot \underline{B}_p$$

with

$$\underline{\underline{b}} = \begin{bmatrix} \frac{1}{2}i(i+1) & -(i+1)(i-1) & \frac{1}{2}i(i-1) \\ -\frac{1}{2}(1+2i) & 2i & \frac{1}{2}(1-2i) \\ 1/2 & -1 & 1/2 \end{bmatrix} \qquad (3.38)$$

and with B_p has elements $B_{pr} = \left[(r+1)^P - r^P\right] S_r - \left[r^P - (r-1)^P\right] R_r$

$\therefore$ $r = i-1, i, i+1$ $\quad$ R_{i-1} and $S_{i+1} = 0$

Equation (3.36) is then solved implicitly to determine $\langle z \rangle$ and $\langle z^2 \rangle$.

One can then construct three fractions at any time

i.e.

$$\begin{aligned} f_{i-1} &= 0.5\left[-\langle z\rangle(1+2i) + \langle z^2\rangle + i(i+1)\right] \\ f_i &= 2i\langle z\rangle - \langle z^2\rangle - (i-1)(i+1) \\ f_{i+1} &= 0.5\left[(1-2i)\langle z\rangle + \langle z^2\rangle + i(i-1)\right] \end{aligned} \qquad (3.39)$$

Knowing these three fractions, the microscopic plasma variables can be constructed.

(3.4) Incorporation of Atomic Physics into MEDUSA:-

It has been shown in section 3.3 (b-i) that a steady state assumption can be applied to a plasma with life time $\sim$ 100 p sec. The laser-produced plasmas generally evolve on a nano-second time scale. To a good approximation, one can therefore apply a steady state model to evaluate the degree of ionization in the matter while doing compression studies simulated by MEDUSA. The presence of large density and temperature variations in the laser produced plasmas requires that the degree of ionization be a function of density and temperature. In the following we describe the incorporation of such a model, namely, TRIP (4) into MEDUSA.

Mathematical Model:

This model assumes the plasma to be in equilibrium as a result of a balance between collisional ionization and radiative as well as three body recombination. Mathematically one can write

$$S_{z-1} f_{z-1} = R_z f_z \qquad (3.40)$$

and

$$R_z = \alpha_z + n_e \beta_z \qquad (3.41)$$

where S_{z-1}, α_z and β_z are the rate coefficients for collisional ionization of (z-1)-times ionized atoms, radiative recombination of

z-times ionized atoms and three body recombination of z-times ionized atoms respectively given in section (3.2). f_z is the fraction of z-times ionized atom ground state.

Solving the set of equations (3.40) we get

$$f_z = f_o \prod_{i=1}^{z} \left(\frac{S_{i-1}}{R_i}\right) \tag{3.42}$$

Applying the constraint

$$\sum_z f_z = 1 \tag{3.43}$$

$$f_o = \left[1 + \sum_{i=1}^{z} \prod_{j=1}^{i} \left(\frac{S_{j-1}}{R_j}\right)\right]^{-1} \tag{3.44}$$

Knowing the values of S and R at a given density and temperature one can evaluate f_o from (3.44) where f_o is the fraction of neutral atoms. The term $\eta_e \beta_z$ makes Rz density dependent. We must therefore iterate on equation (3.44). In general less than 5 iterations will be required. Once f_o is evaluated the rest of the fractions fz can be computed with the help of equation (3.42). The mean ionization and mean-squared ionization can then be evaluated from the following expressions

$$\langle z \rangle = \sum_i i f_i \tag{3.45}$$

$$\langle z^2 \rangle = \sum_i i^2 f_i \tag{3.46}$$

By calling Subroutine TRIP (4) at appropriate points in MEDUSA, the degree of ionization in the plasma is determined as a function of local electron temperature and density. The quantities $\langle z \rangle$ and $\langle z^2 \rangle$, provided by TRIP (4), can be used in the evaluation of various plasma parameters. In the following we present modifications in the equations of MEDUSA in order to allow variation in z.

Modifications in MEDUSA

The incorporation of atomic physics only affects the microscopic variables of the electron gas which those for ions remain unaltered. The electrons are treated as a classical gas. Degeneracy effects are simulated by starting with a high initial electron temperature.

Internal Energy

$$U_e = \frac{3}{2} \frac{K \langle z \rangle T_e}{m_H M} + \frac{\langle E_z \rangle}{m_H M} \tag{3.47}$$

where $$\langle E_z \rangle = \sum_z f_z E_z \tag{3.48}$$

and $$E_z = \sum_j^z \chi_j \tag{3.49}$$

χ_j is the ionization potential for the atom in state j.

Specific Heat

$$(C_v)_e = \left(\frac{\partial U_e}{\partial T_e}\right)_\rho = \frac{1}{m_H M}\left[\frac{3}{2} K\left(\langle z\rangle + T_e \frac{\partial \langle z\rangle}{\partial T_e}\right) + \frac{\partial \langle E_z\rangle}{\partial T_e}\right] \tag{3.50}$$

Pressure

$$P_e = \langle z\rangle n_i K T_e \tag{3.51}$$

Total Energy

$$E_{TOTAL} = E_K + E_{TH} + E_I \tag{3.52}$$

Where E_k denotes the Kinetic energy of the plasma, E_{TH} is the thermal energy and E_I is the ionizational energy stored in the plasma.

Radiation Loss

In MEDUSA Bremsstrahlung is the only radiation loss mechanism. In the present model, however, recombination and line radiation losses are also included. The expressions for these radiation losses are

$$P_{ff} = 1.57\times10^{-40} T_e^{1/2} n_i^2 \langle z\rangle\langle z^2\rangle \quad W/m^3 \tag{3.53}$$

$$P_{fb} = 1.57\times10^{-40} T_e^{1/2} n_i^2 \langle z\rangle\langle z^2 \mu_z\rangle \quad W/m^3 \tag{3.54}$$

$$P_{bb} = 3.7\times10^{-29} T_e^{-1/2} n_i^2 \langle z\rangle\langle \bar{e}^{\mu_z}\rangle \quad W/m^3 \tag{3.55}$$

where $$\mu_z = \chi_z / KT_e . \tag{3.56}$$

The total radiation loss from the plasma will therefore be

$$P_R = P_{ff} + P_{fb} + P_{bb} \tag{3.57}$$

which must not exceed the black body limit, namely,

$$P_B = \frac{1}{\lambda_B}\sigma T_e^4 \tag{3.58}$$

where λ_B is an appropriate opacity.

Electron critical density:

The critical electron density for a radiation of frequency ω_L is

$$n_e^c = \frac{\varepsilon_0 m_e}{e^2}\omega_L^2 \tag{3.59}$$

Critical mass density can be written as

$$\rho_c = \frac{\varepsilon_0 m_H m_e M}{\langle z\rangle_c e^2}\omega_L^2$$

(3.60)

In this model $\langle z \rangle$ is a variable and hence ρ_c is also a variable. $\langle z \rangle_c$ therefore must be evaluated at every time step from the relation

$$\langle z \rangle_c = n_e^c / n_i^c$$

where n_i^c is the ion number density in the critical density cell.

Limitations:

(1) The accuracy of the rate coefficients used in the plasma rate equations is limited. This will affect the accuracy with which the degree of ionization is calculated and therefore affect the accuracy of all z-dependent plasma quantities.

(2) This model ignores the calculation of excited states, and thus a detailed study of the line spectra emitted from plasma is not possible by this model.

(3) The radiation loss rates used in this model are correct for an optically thin plasma only, and therefore not always valid for laser plasmas. In an optically thick medium radiation re-absorption must be considered.

CHAPTER 4

RADIATIVE TRANSPORT

The theory of radiative transfer was developed by astrophysicists to understand radiative energy transfer in stars, and to a great extent this theory may be applied to the study of radiative energy transfer in other high temperature systems, such as laser produced plasmas. To study the effect of radiation on laser-compression, simulated by the computer program MEDUSA, requires that an appropriate radiative transfer model be included in the program. In section (4.1), we present a brief review of the theory of radiative transport and in (4.2) we describe the numerical details of the incorporation of a diffusion treatment for continuum radiation into MEDUSA. The limitations of this model are also discussed and the results obtained by the use of this model will be presented in chapter 6.

(4.1): A Review of Radiative Transport

(1.a) Basic definitions:[23]

Spectral intensity:-

The spectral intensity $I_\nu(\underline{r}, \underline{s}, t)$ at a position $\underline{r}$, travelling in a direction specified by a unit vector $\underline{s}$, at time t is the amount of radiant energy of frequency ν passing through a unit area oriented normal to the beam, per unit solid angle, per unit frequency interval, per unit time. Treating radiation as a collection of particles (photons), the radiation field may be described by a photon distribution function $f(\nu, \underline{r}, \underline{s}, t)$ related to the spectral intensity by the relationship

$$I_\nu(\underline{r}, \underline{s}, t)\, d\nu\, d\omega = h\nu c f(\nu, \underline{r}, \underline{s}, t) \tag{4.1}$$

where c is the velocity of the radiation and $h\nu$ is the energy corresponding to the radiation of frequency ν.

Spectral energy density:-

The spectral energy density $u_\nu(r,t)$ is defined as the amount of

energy included in a unit volume located at a position r in a unit spectral interval at a time t, given by

$$U_\nu(r,t) = h\nu \int_{4\pi} f \, d\omega = \frac{1}{c} \int_{4\pi} I_\nu \, d\omega \qquad (4.2)$$

For an isotropic radiation field, I_ν is independent of direction $\underline{s}$ and then one can write the above equation as

$$U_\nu = 4\pi h\nu f = \frac{4\pi}{c} I_\nu \qquad (4.3)$$

Emission Coefficient J_ν :-

J_ν is defined as the amount of energy of frequency ν emitted spontaneously by a unit volume of matter per unit time per unit frequency interval. Because of the random orientation and chaotic motion of gas molecules the emitted radiation can be treated as isotropic. Then the amount of radiation emitted into the solid angle $d\omega$ is written as

$$j_\nu \, d\omega = J_\nu \frac{d\omega}{4\pi} \qquad (4.4)$$

where j_ν is defined as emission coefficient per unit solid angle.

Absorption coefficient μ_ν :-

When a beam of radiation of frequency ν and initial intensity $I_{\nu 0}$ passes through a thickness x of matter, the intensity of the beam is reduced according to

$$I_\nu = I_{\nu 0} \exp\left(-\int_0^\infty \mu_\nu \, dx\right) \qquad (4.5)$$

where μ_ν is known as attenuation coefficient. Radiation, while passing through matter, is attenuated as a result of absorption and scattering by the atoms of the medium. So the attenuation coefficient μ_ν can be expressed as a sum of an absorption coefficient $k_{\nu a}$ and a scattering coefficient $k_{\nu s}$.

i.e.
$$\mu_\nu = K_{\nu a} + K_{\nu s} \qquad (4.6)$$

The reciprocals of these coefficients give the corresponding radiation mean free paths as,

$$\ell_{\nu a} = \frac{1}{K_{\nu a}} \tag{4.7}$$

and $$\ell_{\nu s} = \frac{1}{K_{\nu s}}$$

The dimensionless quantity $d\tau_\nu = \mu_\nu dx$ in equation (4.5) is called the optical thickness of the layer.

(1.b) The radiative transfer equation:

It is shown [23] that the equation governing the variation in the radiation intensity I_ν, in space-time can be written as:

$$\frac{1}{c}\left(\frac{\partial I_\nu}{\partial t} + c\,\underline{s}\cdot\nabla I_\nu\right) = K'_\nu(I_{\nu p} - I_\nu) \tag{4.8}$$

where $$K'_\nu = K_\nu\left(1 - e^{-\frac{h\nu}{KT}}\right) \tag{4.9}$$

is the absorption coefficient modified for induced emission and $I_{\nu p}$ is the equilibrium radiation intensity. In quasi-steady state we can neglect the time derivative of I_ν in equation (4.8) so that

$$\underline{s}\cdot\nabla I_\nu = K'_\nu(I_{\nu p} - I_\nu) \tag{4.10}$$

The right hand side of the equation (4.10) gives the difference between the emission and absorption of radiation of frequency ν (per unit frequency interval) and in direction $\underline{s}$ (per unit solid angle) per unit time per unit volume. Integrating (4.10) over the entire solid angle gives the radiation energy of frequency ν lost by a unit volume of the medium per unit time.

$$\text{i.e.} \quad Q_\nu = \int_{4\pi} K_\nu(I_{\nu p} - I_\nu)\,d\omega = c\,K'_\nu(u_{\nu p} - u_\nu) \tag{4.11}$$

$$\text{where} \quad Q_\nu = \nabla\cdot\underline{S}_\nu \;, \quad \underline{S}_\nu = \int_{4\pi} \underline{s}\, I_\nu\, d\omega \tag{4.12}$$

$\underline{S}_\nu$ is the flux of radiation of frequency ν.

Equations (4.11) and (4.12) show that the radiant energy loss from the fluid can be calculated in terms of flux and energy density by

integrating the intensity over direction. However, the problem of angular distribution could be avoided, if it were possible to replace the direction - dependent radiative transfer equation by some other equation relating energy density and flux directly, such an equation is (4.11). A second equation to supplement (4.11) can only be derived in an approximate form:

The diffusion approximation:

It is shown [23] that multiplying (4.10) by a unit vector $\underline{s}$ and integrating over the entire solid angle, one gets for an isotropic radiation field

$$\underline{S}_\nu = -\left(\frac{\ell'_\nu c}{3}\right)\nabla u_\nu \qquad (4.13)$$

where $\ell_\nu = 1/k'_\nu$ is the absorption mean free path for photons of frequency ν corrected for induced emission. The above result can still be applied for a weakly anisotropic radiation field. Dividing (4.13) by the photon energy $h\nu$, we get

$$\underline{J}_\nu = -D_\nu \nabla N_\nu \qquad (4.14)$$

where J_ν is photon flux, N_ν is the photon number density and $D_\nu = \frac{\ell_\nu c}{3}$ is the photon diffusion coefficient. This is analogous to the diffusion coefficient of atoms or molecules, but in case of atom-atom collisions, the mean free path is the collisional mean free path, while in a photon-atom collision, the photon is absorbed by the atom. At the place of absorption, new photons are born with different frequencies and with random directions. In considering the diffusion of the photons of a given frequency ν, we look for the photons of that particular frequency among all the newly born photons.

Limitations:

The applicability of diffusion approximation requires that the radiation density should not change appreciably over a distance of the order of the radiation mean free path ℓ_ν: the gradients of the

radiation energy density in the medium should be small, which is true for an optically thick medium. If x denotes the characteristic scale length for the radiation energy density then the diffusion flux will be

$$S_\nu \sim \frac{\ell'_\nu}{x}(c U_\nu) \tag{4.15}$$

The quantity $c U_\nu$ is the maximum possible radiation flux which corresponds to the case when all the photons are travelling in the same direction. For an optically thick medium, $\frac{\ell_\nu}{x} < 1$ and correspondingly $S_\nu < (c U_\nu)$, the smaller the flux S_ν is in comparision to $c U_\nu$, the more applicable is the diffusion approximation. In an optically thin medium, $\frac{\ell_\nu}{x} > 1$, and the flux S_ν exceeds the upper limit $c U_\nu$, which merely indicates the inapplicability of the diffusion approximation, and in such a case the photon flux must be restricted by this upper limit.

Local equilibrium and radiation heat conduction approximation:

The intensity of a radiation field which is in thermodynamic equilibrium with the medium at a constant temperature, is independent of direction and is represented by Planck's distribution. The photons travel a distance of the order of a few mean free paths before they get absorbed in the medium. Therefore only those photons contribute in establishing the equilibrium intensity at a certain point in space which are born in the near vicinity of that point. Even if the temperature at a farthest distance is different from this region, there is no effect on the radiation intensity at the point under consideration. Therefore, in a sufficiently extended optically thick medium, if the temperature gradients are small, the intensity will still be close to the equilibrium corresponding to the local temperature. In such a case one can replace the non-equilibrium radiation energy density u_ν by equilibrium energy density $u_{\nu p}$ in equation (4.13) so that

$$S_\nu = -\frac{1}{3}\ell'_\nu c \nabla u_{\nu p} \tag{4.16}$$

The total radiation flux can be obtained by integrating equation (4.16) w.r.t. frequency.

$$\text{i.e. } \underline{S} = \int_0^\infty \underline{S}_\nu \, d\nu = -\frac{1}{3} c \int_0^\infty \ell_\nu' \nabla U_{\nu p} \, d\nu = -\left(\frac{16\sigma \ell_R T^3}{3}\right) \nabla T \quad (4.17)$$

$$\text{where} \quad \int_0^\infty U_{\nu p} \, d\nu = \frac{4\sigma T^4}{c} \quad (4.18)$$

$$\text{and} \quad \ell_R = \frac{\int_0^\infty \ell_\nu' \left(\frac{dU_{\nu p}}{dT}\right) d\nu}{\int_0^\infty \frac{dU_{\nu p}}{dT} \, d\nu} \quad (4.19)$$

is known as the Rosseland mean free path. The quantity $D_r = \frac{16\sigma \ell_R T^3}{3}$ is the radiation thermal conductivity where σ is Stefan's constant.

Non-equilibrium radiation transfer:

It is noted above that an optically thick medium with small temperature gradients, satisfies the conditions which simultaneously lead to a diffusional relationship between the radiation flux and radiation energy density as well as a local equilibrium situation between matter and the radiation field. In case of non-isotropic radiation fields, the diffusion approximation would lead to results with a limited accuracy, however, the qualitative picture of the phenomenon of radiative transfer is not altered and one can therefore still use this approximation to obtain approximate solutions involving non-equilibrium radiation fields. For example, in the case of maximum anisotropy of the radiation field, when all the photons are travelling in the same direction, the flux is given by $S_\nu = cU_\nu$. Such a situation can arise at the boundary between a hot and a cold body at temperatures T and T_o respectively where $T >> T_o$. In practice, no photons will be emitted from the surface of the cold body while those emitted from the surface of the hot body will be absorbed in the cold body over a distance of the order of a mean free path. This type of energy transfer is completely unlike the one for which we have local

equilibrium and radiation heat conduction. The diffusion equations (4.11) and (4.13) for the cold non-radiating medium are

$$\frac{dS_\nu}{dx} = -\frac{cU_\nu}{\ell'_\nu} \quad , \quad S_\nu = -\frac{\ell'_\nu c}{3}\frac{dU_\nu}{dx}$$

or in terms of optical thickness $\tau_x = \int_o^\infty K_\nu dx$ we get

$$\frac{dS_\nu}{d\tau_\nu} = -cU_\nu \quad , \quad S_\nu = -\frac{1}{3}c\frac{dU_\nu}{d\tau_\nu} \tag{4.20}$$

These equations lead to a solution:

$$S_\nu = \frac{cU_\nu}{\sqrt{3}} \sim e^{-\sqrt{3}\,\tau_\nu} \tag{4.21}$$

Using $S_\nu = cU_\nu$ instead of that given in equation (4.20) we get

$$S_\nu = cU_\nu \sim e^{-\tau_\nu} \tag{4.22}$$

which differs from the diffusion approximation solution (4.21) by a factor of $\sqrt{3}$ in the exponent and by a factor $\frac{1}{\sqrt{3}}$ in relation between energy flux and radiation density gradient, which is a reasonably good result.

Integrating time dependent radiative transfer equation (4.8) over the entire solid angle we get:

$$\frac{\partial U_\nu}{\partial t} + \nabla\cdot\underline{S}_\nu = cK'_\nu(U_{\nu p} - U_\nu)$$

This equation expresses conservation of radiation energy of frequency ν. Substituting expression for diffusion flux from equation (4.13),

$$\frac{\partial U_\nu}{\partial t} - \nabla\cdot\left(\frac{\ell'_\nu c}{3}\nabla U_\nu\right) = cK'_\nu(U_{\nu p} - U_\nu)$$

Integrating this equation w.r. to frequency gives the energy transport due to radiative transfer over the entire spectrum so that,

$$\frac{\partial}{\partial t}\int_o^\infty U_\nu d\nu - \frac{c}{3}\nabla\cdot\int_o^\infty \ell'_\nu \nabla U_\nu d\nu = c\int_o^\infty K'_\nu(U_{\nu p} - U_\nu)d\nu \tag{4.22a}$$

In section (4.2) we will use this equation to include the transport of

continuum radiation into MEDUSA.

(1.c) Opacity of the medium: (23)

To evaluate total radiative energy transport using radiative transfer equation, one has to calculate the Rosseland mean opacity which requires a detailed knowledge of atomic absorption cross sections as a function of frequency. The photons can interact with matter in many ways including free-free, free-bound, bound-bound and scattering processes. In the present work, however, we are only interested in the continuum radiation which is the result of free-free and free-bound transitions. A simple treatment for the evaluation of absorption coefficients for these two processes is presented in the following.

Free-free transitions:

From classical electrodynamics, one can calculate the emission coefficient for free-free transitions (bremsstrahlung), and by applying the principle of detailed balancing, the corresponding absorption coefficient can be evaluated. It is shown (23) that the bremsstrahlung absorption coefficient averaged over Maxwell velocity distribution, for a gas at temperature T is:

$$K_\nu = \frac{4}{3}\left(\frac{2\pi}{3m_e KT}\right)^{1/2} \frac{z^2 e^6}{hcm\nu^3} N_i N_e \qquad (4.23)$$

where N_i is the ion number density, N_e is the electron number density and z is the atomic number of the ion. The rest of the symbols have their usual meaning. Substituting the values of the quantities in MKS units the above equation reduces to,

$$K_\nu = 4.1 \times 10^{-9} \frac{z^2 N_i N_e}{x^3 T^{7/2}} \quad m^{-1} \qquad (4.24)$$

where $x = \frac{h\nu}{KT}$, N_i and, N_e are in m^{-3}. One can evaluate the Rosseland mean free path for bremsstrahlung absorption as,

$$\ell_R = \int_0^{\infty} \frac{1}{K_\nu} G(x)\, dx \qquad (4.25)$$

where $G(x) = \dfrac{15\, x^4\, e^{-x}}{4\pi^4 (1 - e^{-x})^3}$

such that

$$(\ell_R)_{ff} = 4.8 \times 10^{34} \frac{T_e^{7/2}}{Z^2 N_i N_e} \quad m \qquad (4.26)$$

It can be seen from (4.26) that the elements with higher z are more opaque to bremsstrahlung radiation.

Bound-free transitions

It is shown (23) that the cross section for the absorption of a photon of energy $h\nu$ by a hydrogen-like atom whose atomic remainder charge is z and which is in the nth quantum state, is,

$$\sigma_{\nu n} = \frac{64\pi^4}{3\sqrt{3}} \cdot \frac{e^{10} m_e Z^4}{h^6 c \nu^3 n^5} \qquad (4.27)$$

using $h\nu_n = \dfrac{I_H z^2}{n^2}$, where I_H is the ionization potential of hydrogen atom, and thus ν_n is the minimum energy of the photon capable of knocking out an electron from quantum level n,

$$\sigma_{\nu n} = 7.9 \times 10^{-14} \frac{n}{Z^2} \left(\frac{\nu_n}{\nu}\right)^3 \quad m^2 \qquad (4.28)$$

It can be seen from equation (4.28) that the cross section $\sigma_{\nu n}$ is proportional to $\dfrac{1}{\nu^3}$ and has a maximum value at $\nu = \nu_n$. Equation (4.27) is derived on semi-classical assumption and is valid only for strongly excited states $n \gg 1$, still gives good results even when applied to photo-ionization from ground state, n = 1. Quantum mechanical treatment of cross section from ground state of the hydrogen like atom gives (23):

$$\sigma_{\nu 1} \simeq \frac{6.34 \times 10^{-14}}{Z^2} \left(\frac{\nu_1}{\nu}\right)^{8/3} \quad m^2 \quad \nu - \nu_1 \ll \nu_1 \qquad (4.29)$$

$$\sigma_{\nu_1} \simeq \frac{8.32 \times 10^{-14}}{Z^2} \left(\frac{\nu_1}{\nu}\right)^3 \quad m^2 \qquad \nu - \nu_1 \sim \nu_1 \tag{4.30}$$

$$\sigma_{\nu_1} \simeq \frac{5.42 \times 10^{-13}}{Z^2} \left(\frac{\nu_1}{\nu}\right)^3 \quad m^2 \qquad \nu >> \nu_1 \tag{4.31}$$

Setting n = 1 in equation (4.28), for $\nu = \nu_1$ we get

$$\sigma_{\nu_1} = 7.9 \times 10^{-14}/Z^2 \qquad m^2 \tag{4.32}$$

which exceeds the quantum-mechanical cross section (4.29) by only 25%. A comparison of equation (4.32) with (4.30) shows that the two agree to within 5%. However a marked difference exists between (4.32) and (4.31) which is the case when the photon energy is very large as compared to the ionization potential.

At a given temperature the gas contains atoms with all possible excited levels. The total absorption coefficient for bound-free absorption is given by

$$K'_\nu = \sum_{n^*}^{\infty} N_n \sigma_{\nu n} \tag{4.33}$$

where N_n is the number density of atoms in quantum state n. The lower limit in the summation is determined by the condition that the photon energy is greater than the binding energy of the electron in the atom, otherwise the atom will not be ionized. It is shown [23] that using the Boltzmann equation to evaluate N_n, and substituting $\sigma_{\nu n}$ from equation (4.27), the above equation, for a hydrogen-like atom, leads to

$$K'_\nu = \frac{64\pi^4}{3\sqrt{3}} \cdot \frac{e^{10} m_e Z^4 N}{h^6 c \nu^3} \sum_{n^*}^{\infty} \frac{1}{n^3} e^{-(x_1 - x_n)} \tag{4.34}$$

where
$$x_1 = \frac{I_H}{KT} Z^2$$
and
$$x_n = \frac{x_1}{n^2} \tag{4.35}$$

It is to be noted that if the photon energy is small compared to the ionization potential of the atom, then the ionization will only take place from a highly excited level, where the electron moves in a very large orbit. In such a case, the field experienced by the electron due to the remainder charge of the atom is close to the coulomb field of a point charge. Therefore the structure of the highly excited states of any atom or ion is close to that of hydrogen, and the approximation of hydrogen-like atoms used in the derivation of (4.34) is valid.

Continuous absorption coefficient (singly ionized mono-atomic gas):-

All sources of opacity mentioned above contribute to the attenuation of radiation simultaneously, any of which may dominate depending upon the thermodynamic state of the medium. It is to be noted from (4.19) that the sum of Rosseland mean opacities of each component is not equal to the Rosseland mean of the sum. The Rosseland mean of individual components therefore has little importance in radiative transfer unless that opacity is the dominant one. Hence one must sum all the frequency dependent opacities, correcting the true absorption for induced emission, and then evaluate the Rosseland mean. However in the present case we are only interested in the absorption of the continuum radiation, and we would therefore evaluate total continuum absorption coefficient for the radiation of frequency ν as:

$$K_\nu = K'_\nu + K''_\nu \tag{4.36}$$

It is shown (23) that substituting K'_ν and K''_ν the above equation reduces to

$$K_\nu = \frac{64\pi^4}{3\sqrt{3}} \frac{e^{10} m_e Z^4 N_i}{h^6 c \nu^3} \left[\sum_{n^*}^{\infty} \frac{1}{n^3} e^{-(x_1 - x_n)} + \frac{e^{-x}}{2x_1} \right] \tag{4.37}$$

Case I: $h\nu \ll I$ (Photon energy << Ionization potential):

In this case the absorption of photons takes place only from

excited levels and the number density of these levels increases rapidly with increasing values of n. Therefore one can replace the summation on R.H.S. of (4.37) by integration. From (4.35)

$$\frac{dx_n}{dn} = -\frac{2x_1}{n^3} \tag{4.38}$$

or $$\frac{dn}{n^3} = -\frac{1}{2}\frac{dx_n}{x_1}$$

So $$\sum_{n^*} \frac{1}{n^3} e^{-(x_1 - x_n)} \approx -\frac{e^{-x_1}}{2x_1}\int_x^0 e^{x_n} dx_n = \frac{e^{-x_1}}{2x_1}(e^x - 1)$$

From (4.37) we get

$$K_\nu = \frac{16\pi^2}{3\sqrt{3}} \cdot \frac{e^6 Z^2 KT N_i}{h^4 c \nu^3} e^{-\left(\frac{I - h\nu}{KT}\right)} \tag{4.39}$$

Case II: $h\nu > I$

When the photon energy exceeds the ionization potential of the atom, all the atoms including those in the ground state, absorb radiation and the summation in equation (4.37) includes all values of n from o to ∞. A dominant role in the absorption of these photons is played by the atoms in the ground state, so that only the first term is retained in the sum, that is, unity. This gives the approximate equation

$$K_\nu = \frac{32\pi^2}{3\sqrt{3}} \frac{e^6 Z^2 N_i}{h^4 c \nu^3} I \tag{4.40}$$

where $I = I_H z^2$.

Continuous absorption coefficient (multiply ionized mono-atomic gas:-

At very high temperatures, of the order of several thousand electron volts encountered in laser produced plasmas, the atoms of a medium z element will be multiply ionized. Each of these ions contributes to the continuous absorption and participates in the bound-free and free-free transitions. It is shown [23] that the continuous absorption coefficient for an m-times ionized hydrogen-like ion is,

$$K_{\nu m} = \frac{a\, N_m (m+1)^2}{T}\, e^{-x_{1m}}\, F_m(x) \qquad (4.41)$$

where $$a = \frac{16\pi^2}{3\sqrt{3}} \cdot \frac{e^6}{hc\,k^2}$$

$$x_{1m} = \frac{I_{m+1}}{kT}\,, \qquad x = \frac{h\nu}{kT}$$

N_m is the number density and I_{m+1} is the ionization potential of the m-times ionized ion. The function $F_m(x)$ depends on the frequency according to

$$F_m(x) = \frac{e^x}{x^3} \quad \text{for} \quad x < x_{1m} \qquad (4.42)$$

and

$$F_m(x) = 2x_{1m} \cdot \frac{e^{x_{1m}}}{x^3} \quad \text{for} \quad x > x_{1m}$$

To obtain the total absorption coefficient at a frequency ν we must sum the partial absorption coefficient $K_{\nu m}$ over all species of ions i.e. over m

$$K_\nu = \sum_m K_{\nu m} \qquad (4.43)$$

Mean opacity of the medium:-

(i) Rosseland mean free path:

The Rosseland mean free path as defined by equation (4.25), can be written as [23]:

$$\ell_R = \int_0^\infty \frac{T^2\, G(x)\, dx}{a \sum_m N_m (x+1)^2\, e^{-x_{1m}} F_m(x)} \qquad (4.44)$$

where $G(x) = \frac{15}{4\pi^4} \cdot \frac{x^4 e^{-x}}{(1-e^{-x})^3}$

Case I Low energy photons:

It is shown [23] that when the photon energy is small compared to the ion with smaller value of m, the Rosseland mean free path becomes

$$\ell_R = \frac{0.87\, T^2}{a} \cdot \frac{1}{\sum_m N_m (m+1)^2\, e^{-x_{1m}}} \qquad (4.45)$$

Case II High energy photons:

In this case one can show that

$$\ell_R = 98\cdot 2\frac{T^2}{a}\cdot\frac{1}{\sum_m N_m(m+1)^2 e^{-x_{1m}}} \tag{4.46}$$

(ii) Planck Mean:

This represents the integrated emission coefficient of the gas and is defined as

$$K_p = \frac{\int_0^\infty K'_\nu u_{\nu p}\,d\nu}{\int_0^\infty u_{\nu p}\,d\nu} = \int_0^\infty K'_\nu G_1(x)\,dx \tag{4.47}$$

where the weighting factor $G_1(x) = \frac{15}{\pi^4}\cdot\frac{x^3}{e^x-1}$ (4.48)

For low energy photons we have (23)

$$K_p = \frac{45\,a}{\pi^4 T^2}\sum_m N_m(m+1)^2\,\frac{e^{-x_{1m}}}{x^3} \tag{4.49}$$

On the other hand, for high energy photons one can write

$$K_p = \frac{30\,a}{\pi^4 T^2}\cdot\sum_m N_m(m+1)^2\,x_{1m} \tag{4.50}$$

(4.2) Incorporation of Radiative Transfer Into MEDUSA:-

In this section, we discuss the numerical details of the incorporation of the radiation diffusion model, described in section (4.1b), into MEDUSA. At present, we are interested in the transport of the continuum radiation only. Consider equation (4.22a), which governs the radiative energy transfer for an isotropic radiation field, i.e.

$$\frac{\partial}{\partial t}\int_0^\infty u_\nu\,d\nu - \frac{c}{3}\nabla\cdot\int_0^\infty \ell_\nu\nabla u_\nu\,d\nu = c\int_0^\infty K'_\nu(u_{\nu p}-u_\nu)\,d\nu$$

This equation can be greatly simplified if we assume that the photons achieve a Planckian equilibrium characterized by a radiation temperature T_r, at a rate much faster than their equilibrium rate

with the electrons. Then we have

$$\int_0^\infty U_\nu \, d\nu = \frac{4\sigma T_r^4}{c} \tag{4.51}$$

and also we can define a Rosseland mean and a Planck mean so that

$$\frac{\partial}{\partial t}\left(\frac{4\sigma T_r^4}{c}\right) - \frac{c}{3}\nabla\cdot l_R \nabla\left(\frac{4\sigma T_r^4}{c}\right) = 4\sigma K_p (T_e^4 - T_r^4) \tag{4.52}$$

$$\text{i.e.} \left(\frac{16\sigma T_r^3}{\rho c}\right)\frac{\partial T_r}{\partial t} = \frac{1}{\rho}\nabla\cdot\left(\frac{16\sigma l_R T_r^3}{3}\right)\nabla T_r + \frac{4\sigma K_e}{\rho}(T_e^2 + T_r^2)(T_e + T_r)(T_e - T_r) \tag{4.53}$$

where we have divided the above equation by mass density ρ to convert the energy / unit mass. This equation can be written as

$$(C_v)_r \frac{\partial T_r}{\partial t} = \frac{1}{\rho}\nabla\cdot(D_r \nabla T_r) + K_{re} \tag{4.54}$$

where $(Cv)_r = \dfrac{16\sigma T_r^3}{\rho c}$: Radiation specific heat.

$D_r = \dfrac{16\sigma l_R T_r^3}{3}$: Radiation thermal conductivity.

$K_{re} = (Cv)_e \omega_{re} (T_e - T_r)$: Electron-radiation energy exchange rate.

$\omega_{re} = \dfrac{4 K_p (T_e^2 + T_r^2)(T_e + T_r)}{(Cv)_e \rho}$ is the electron-photon collision frequency (4.55)

and $(Cv)_e$ is the specific heat of the electrons.

In a laser produced plasma, the radiation field is in equilibrium with matter in the core region and therefore the radiation temperature is nearly equal to the electron temperature. In such a case one can take K_p out of the brackets in equation (4.53). On the other hand in the corona region the radiation temperature is much less than the electron temperature and therefore the last term in equation (4.53) is not valid. However, in the corona region the plasma is fully ionized and the free-free transitions dominate the opacity. One can therefore substitute K_ν for free-free transitions from equation (4.34) and integrate w.r. to frequency so that (appendix 5)

$$\omega_{re} = 8.5 \times 10^{-14} \left(\frac{\bar{Z}^2 \bar{Z} N_i}{M T_e^{1/2} (C_v)_e} \right) I_g \qquad (4.56)$$

where M is the molecular weight of the element and I_g is an integral defined by

$$I_g = \int_0^\infty \frac{\xi (e^{\xi u} - e^u)}{(\xi - 1)(e^u - 1)(e^{\xi u} - 1)} du \qquad (4.57)$$

where $\xi = T_e / T_r$ and $u = \frac{h\nu}{KT}$.

The integral I_g is evaluated numerically and a set of values is calculated for different values of ξ. We then interpolate between appropriate values of this table to obtain I_g in the given temperature range.

Equation (4.54) is suitable to study the radiation thermal conduction problems, however, to include the effects of compression and expansion of the plasma we need to modify this equation (as shown in appendix 2) so that,

$$(C_v)_r \frac{\partial T_r}{\partial t} + B_r \frac{\partial \rho}{\partial t} + P_r \frac{\partial V}{\partial t} = S_r \qquad (4.58)$$

where

$$P_r = \frac{1}{3} U_r = \frac{4\sigma T_r^4}{3c} \qquad (4.59)$$

is the radiation pressure for an isotropic radiation field and

$$B_r = \left(\frac{\partial U_r}{\partial \rho} \right)_{T_r} = -3 P_r \left(\frac{1}{\rho^2} \right) \qquad (4.60)$$

The source term on the R.H.S. of equation (4.58) is given by

$$S_r = H_r + K_{re}$$

where H_r is the radiation heat conduction rate and K_{re} is the electron-radiation energy exchange rate. Using equation (4.59) and (4.60), equation (4.58) reduces to

$$(C_v)_r \frac{\partial T}{\partial t} + 4 P_r \frac{\partial V}{\partial t} = S_r \qquad (4.61)$$

To solve equation (4.61) for radiation temperature, we need to know

the coefficients $(Cv)_r$, P_r and the source term S_r. One can calculate $(Cv)_r$ and P_r from equations (4.55) and (4.59) respectively. The evaluation of radiation heat conduction is discussed in the following while the electron-radiation energy exchange rate will be treated later.

Radiation heat conduction

We have $H_r = \frac{1}{\rho} \nabla \cdot (D_r \nabla T_r)$ where the radiation thermal conductivity, D_r, is given by equation (4.55). However, evaluation of the Rosseland mean free path, necessary in the calculation of D_r (equation (4.45)), requires a knowledge of N_m, the number density of ions which are m-times ionized. It was shown in chapter 3, that the atomic physics package TRIP (4), calculates the fractional populations of ions with different degrees of ionization, f_m, related to N_m as, $N_m = f_m N_i$. One can then calculate the Rosseland mean free path as a function of local plasma density and local electron temperature. It is to be noted that in the low density, and the high temperature corona region, the plasma is fully ionized and therefore the opacity in that region is dominated by free-free transitions. From equation (4.24), one can see that the absorption coefficient for the free-free transitions is $\propto \frac{N_i N_e}{T_e^{\frac{1}{2}}}$, whereas the Thomson scattering coefficient (scattering by free electrons), K_s, is proportional to N_e. Therefore at very low densities ($\sim 10^{20}$ m^{-3}) and at high temperature ($\sim 10^7$ K), this scattering process will dominate the absorption process. In such a case the absorption coefficient in equation (4.25) must be replaced by the Thomson scattering coefficient.

It was mentioned in section (4.1b) that the diffusion approximation breaks down in an optically thin medium. The diffusion flux predicted by equation (4.13), in such a case, can easily exceed the photon free streaming limit, $\int_0^\infty c U_\nu d\nu$. It is therefore necessary

to limit the radiation flux in the optically thin corona region of a laser produced plasma as,

$$F_r' = \frac{F_r F_f}{F_r + F_f} \tag{4.62}$$

where $F_r = D_r|\nabla T_r|$ and $F_f = b\int_0^\infty cu_\nu d\nu = 4b\sigma T_r^4$, where $0 < b \leq 1$. (4.63)

The modified thermal conductivity is

$$D_r' = D_r\left(1 + \frac{4}{3b}\frac{l_R}{T_r}|\nabla T_r|\right)^{-1} \tag{4.64}$$

Boundary conditions:

For the inner boundary of the target we simply choose zero radiation flux. However, at the moving outer boundary, either of the following two boundary conditions can be applied.

(a) Perfect reflector:

Under this option, flux at the boundary is taken to be zero, so no radiation escapes.

(b) Emission option:

In this case the radiation is allowed to escape from the outer boundary of the plasma and the outward flux is given by,

$$\text{Fout} = D_b \nabla_b T_r$$

where D_b is the radiation thermal conductivity and $\nabla_b T_r$ is the temperature gradient at the target boundary.

Solution of radiation energy equation:

The radiation energy equation is solved for the radiation temperature numerically, using an implicit difference scheme, as described in chapter 2. The quantities labelled with a subscript are evaluated at the cell centres while those labelled with a subscript j are evaluated at the cell boundary. For simplicity we drop the subscript r from the variables representing the radiation field. Equation (4.61) can be written in finite difference form as:

$$(C_v)_\ell^{n-1/2} \frac{T_\ell^n - T_\ell^{n-1}}{\Delta t^{n-1/2}} + 4\, P_\ell^{n-1/2} \frac{V_\ell^n - V_\ell^{n-1}}{\Delta t^{n-1/2}} = S_\ell^{n-1/2} \qquad (4.65)$$

where $$S_\ell^{n-1/2} = H_\ell^{n-1/2} + K_{\ell e}^{n-1/2}$$

The quantities $(Cv)_e^{n-\frac{1}{2}}$ and $p_e^{n-\frac{1}{2}}$ are calculated by taking simple averages of the corresponding quantities at time levels n and n-1, as given by equations (4.55) and (4.59) respectively. The two source terms are treated as follows:

Heat conduction term

The heat conduction term can be written as

$$H_\ell^{n-1/2} = \frac{1}{2}\left(H_\ell^n + H_\ell^{n-1}\right)$$

The quantity H_e^n, the rate of energy absorbed in the coll due to thermal conduction is calculated as shown below:

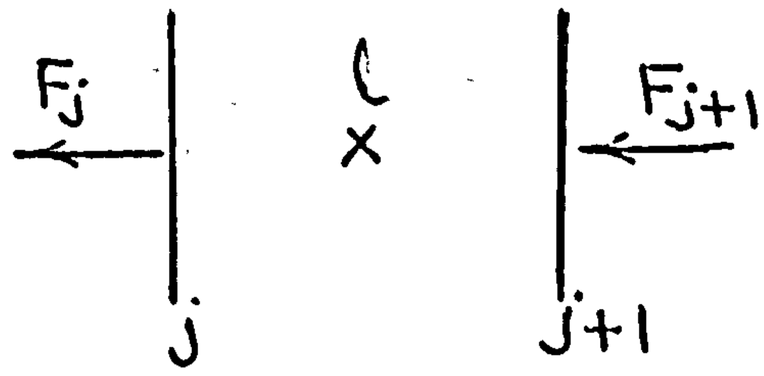

where the flux out of the boundary j is given by

$$F_j^n = (R_j^n)^2 D_j^n \frac{T_\ell^n - T_{\ell-1}^n}{R_\ell^n - R_{\ell-1}^n} \qquad (4.66)$$

and $$H_\ell^n = \frac{1}{dM_\ell}\left(F_{j+1}^n - F_j^n\right) \qquad (4.67)$$

as shown in appendix (6).

Energy exchange term

It has been discussed in chapter 2 that for reasons of accuracy, MEDUSA employs a special technique to evaluate rapid electron-ion energy exchange rate in a two-component plasma. In the present work we have extended that method to evaluate electron-ion and electron-radiation energy exchange rates in a three-component plasma

(electrons, ions and radiation). It is shown in appendix (7) that the following results are obtained.

$$\xi_i^{n-1/2}(t) = C_i\left[\frac{1.0}{X\cdot\Delta t^{n-1/2}}\left(e^{X\cdot\Delta t^{n-1/2}}-1\right)-\frac{1.0}{Y\cdot\Delta t^{n-1/2}}\left(e^{Y\cdot\Delta t^{n-1/2}}-1\right)\right]$$
$$+\left(\xi_i^{n-1}-\left(\frac{\alpha_i}{\gamma}\right)^{n-1/2}\right)\frac{1.0}{Y\cdot\Delta t^{n-1/2}}\left(e^{Y\cdot\Delta t^{n-1/2}}-1\right)+\left(\frac{\alpha_i}{\gamma}\right)^{n-1/2} \quad (4.68)$$

$$\xi_r^{n-1/2}(t) = C_r\left[\frac{1.0}{X\cdot\Delta t^{n-1/2}}\left(e^{X\cdot\Delta t^{n-1/2}}-1\right)-\frac{1.0}{Y\cdot\Delta t^{n-1/2}}\left(e^{Y\cdot\Delta t^{n-1/2}}-1\right)\right]$$
$$+\left(\xi_r^{n-1}-\left(\frac{\alpha_r}{\gamma}\right)^{n-1/2}\right)\frac{1.0}{Y\cdot\Delta t^{n-1/2}}\left(e^{Y\cdot\Delta t^{n-1/2}}-1\right)+\left(\frac{\alpha_r}{\gamma}\right)^{n-1/2} \quad (4.69)$$

where

$$X = -\lambda/2+\frac{\sqrt{\lambda^2-4\gamma}}{2}$$
$$Y = -\lambda/2-\frac{\sqrt{\lambda^2-4\gamma}}{2}$$
$$\lambda = \beta_i\omega_{ie}+\beta_r\omega_{re}$$
$$\gamma = (\beta_i\beta_r-G)\,\omega_{ie}\omega_{re}$$
$$\alpha_i = (\Phi_r+\beta_r\Phi_i)\,\omega_{re}$$
$$\alpha_r = (G\,\Phi_i+\beta_i\Phi_r)\,\omega_{ie} \quad (4.70)$$

In the above set of equations

$$\beta_i = 1+\frac{(Cv)_i}{(Cv)_e}$$

$$\beta_r = 1+\frac{(Cv)_e}{(Cv)_r}$$

and $$G = \frac{(Cv)_i}{(Cv)_e}$$

The integration constants c_i and c_r used in equations (4.68) and (4.69) are as follows:

$$C_i = \frac{1}{\sqrt{\lambda^2-4\gamma}}\left[\Phi_i-\beta_i\omega_{ie}\xi_{io}+\omega_{re}\xi_{ro}+\lambda/2\left(\xi_{io}-\frac{\alpha_i}{\gamma}\right)\right]+\frac{1}{2}\left(\xi_{io}-\frac{\alpha_i}{\gamma}\right) \quad (4.71)$$

$$C_2 = \frac{1}{\sqrt{\lambda^2 - 4\gamma}}\left[\Phi_2 - \beta_2 \omega_{2e} \xi_{20} + G\omega_{ie}\xi_{10} + \lambda_2\left(\xi_{10} - \frac{\alpha_2}{\gamma}\right)\right] + \frac{1}{2}\left(\xi_{20} - \frac{\alpha_2}{\gamma}\right) \quad (4.72)$$

where $\Phi_i = \frac{W_i}{(C_v)_i} - \frac{W_e}{(C_v)_e}$ and $\Phi_2 = \frac{W_e}{(C_v)_e} - \frac{W_2}{(C_v)_2}$

the terms W_i, W_e and W_r are defined in the appendix (7) and are evaluated as:

$$\Phi_i = \frac{\xi_i^n - \xi_i^{n-1}}{\Delta t^{n-1/2}} + \beta_i \xi_i^{n-1/2} \omega_{ie}^{n-1/2} - \omega_{2e}^{n-1/2} \xi_2^{n-1/2} \quad (4.73)$$

$$\Phi_2 = \frac{\xi_2^n - \xi_2^{n-1}}{\Delta t^{n-1/2}} + \beta_2 \xi_2^{n-1/2} \omega_{2e}^{n-1/2} - G\,\omega_{ie}^{n-1/2} \xi_i^{n-1/2} \quad (4.74)$$

After evaluating Φ_i and Φ_r from above equations we can calculate the two integration constants from (4.71) and (4.72), which are then used to evaluate $\xi_i^{n-\frac{1}{2}}$ and $\xi_r^{n-\frac{1}{2}}$ from equations (4.68) and (4.69) respectively. The energy exchange rates can be calculated as

$$K_{ie}^{n-1/2} = (C_v)_i \cdot \xi_i^{n-1/2}\, \omega_{ie}^{n-1/2} \quad (4.75)$$

$$K_{2e}^{n-1/2} = (C_v)_e \cdot \xi_2^{n-1/2}\, \omega_{2e}^{n-1/2} \quad (4.76)$$

where $\omega_{ie}^{n-1/2} = \frac{1}{2}\left(\omega_{ie}^n + \omega_{ie}^{n-1}\right)$

and $\omega_{2e}^{n-1/2} = \frac{1}{2}\left(\omega_{2e}^n + \omega_{2e}^{n-1}\right)$

The electron-ion collision frequency is given by (11)

$$\omega_{ie} = \frac{Z^2 e^4 N_i \log\Lambda\, m_e^{1/2}}{3\sqrt{2}\,\pi\,\varepsilon_0^2 m_H M}(KT_e)^{-3/2} \quad (4.77)$$

where the symbols have their usual meaning.

Special cases of energy exchange

I - (Electron-ion energy exchange rate dominates):

So $\beta_i \omega_{ie} \gg \beta_r \omega_{re}$

In such a case equations (4.68) and (4.69) reduce to

$$\xi_i^{n-1/2}(t) = \frac{1}{\beta_i \omega_{ie} \Delta t^{n-1/2}}\left(\frac{\Phi_i}{\beta_i \omega_{ie}} - \xi_i^{n-1}\right)\left(e^{-\beta_i \omega_{ie} \Delta t^{n-1/2}} - 1\right) + \left(\frac{\alpha_i}{\gamma}\right)^{n-1/2}$$

$$\xi_r^{n-1/2}(t) = \frac{1}{\beta_i \omega_{ie} \Delta t^{n-1/2}}\left(\frac{\Phi_r}{\beta_i \omega_{ie}} + \frac{G}{\beta_i}\xi_i^{n-1}\right)\left(e^{-\beta_i \omega_{ie} \Delta t^{n-1/2}} - 1\right) + \left(\frac{\alpha_r}{\gamma}\right)^{n-1/2}$$

II - (Electron-radiation energy exchange rate dominates):

So $\beta_r \omega_{re} \gg \beta_i \omega_{ie}$

Equations (4.68) and (4.69) become

$$\xi_i^{n-1/2}(t) = \frac{1}{\beta_r \omega_{re} \Delta t^{n-1/2}}\left(\frac{\Phi_i}{\beta_r \omega_{re}} + \frac{1}{\beta_r}\xi_r^{n-1/2}\right)\left(e^{-\beta_r \omega_{re} \Delta t^{n-1/2}} - 1\right) + \left(\frac{\alpha_i}{\gamma}\right)^{n-1/2}$$

$$\xi_r^{n-1/2}(t) = \frac{1}{\beta_r \omega_{re} \Delta t^{n-1/2}}\left(\frac{\Phi_r}{\beta_r \omega_{re}} - \xi_r^{n-1/2}\right)\left(e^{-\beta_r \omega_{re} \Delta t^{n-1/2}} - 1\right) + \left(\frac{\alpha_r}{\gamma}\right)^{n-1/2}$$

III - (Very slow exchange rates):

When both energy exchange rates are very slow such that $\left|K_{ie}^{n-\frac{1}{2}} \Delta t^{n-\frac{1}{2}}\right| \leqslant 10^{-3}$ and $\left|K_{re}^{n-\frac{1}{2}} \cdot \Delta t^{n-\frac{1}{2}}\right| \leqslant 10^{-3}$, the equations (4.68) and (4.69) reduce to

$$\xi_i^{n-\frac{1}{2}}(t) = \xi_i^{n-1}$$

$$\xi_r^{n-\frac{1}{2}}(t) = \xi_r^{n-1}$$

Substituting in equation (4.65) the quantities, calculated above, and arranging the coefficients of $T_{\ell-1}^n$, T_ℓ^n and $T_{\ell+1}^n$ we get

$$A_\ell^n T_{\ell-1}^n + B_\ell^n T_\ell^n + C_\ell^n T_{\ell+1}^n = D_\ell^n + G_\ell^{n-1} \qquad (4.78)$$

as shown in appendix (8). The coefficients in the above equation are:

$$A_\ell^n = -\frac{1}{dM_\ell} \cdot \frac{(R_j^n)^2 D_j^n}{(R_{j+1}^n - R_{j-1}^n)} \Delta t^{n-1/2}$$

$$C_\ell^n = -\frac{1}{dM_\ell} \cdot \frac{(R_{j+1}^n)^2 D_{j+1}^n}{(R_{j+2}^n - R_j^n)} \Delta t^{n-1/2}$$

$$B_\ell^n = \frac{1}{2}\left[(C_v)_\ell^n + (C_v)_\ell^{n-1}\right] - A_\ell^n - C_\ell^n$$

$$D_\ell^n = \frac{1}{2}\left[(K_{re})_\ell^{n-1/2} \cdot \Delta t^{n-1/2} + T_\ell^{n-1}\left((C_v)_\ell^n + (C_v)_\ell^{n-1}\right) - 4\left(P_\ell^n + P_\ell^{n-1}\right) \cdot \left(V_\ell^n - V_\ell^{n-1}\right)\right]$$

$$G_\ell^{n-1} = A_\ell^{n-1}\left(T_\ell^{n-1} - T_{\ell-1}^{n-1}\right) - C_\ell^{n-1}\left(T_{\ell+1}^{n-1} - T_\ell^{n-1}\right)$$

It can be seen that the coefficients A^n, B^n, C^n and D^n are functions of T^n and equation (4.78) is therefore solved iteratively using Gauss's elimination scheme (2.4), for the two cases of boundary conditions. For case I we set $A_1^n = C_N^n = 0$ while for case II we have $A_1^n = 0$. The set of equations obtained from (4.78) can be written as

$$E_1 = \frac{C_1}{B_1}, \quad F_1 = \frac{D_1 + G_1}{B_1}$$

$$E_\ell = \frac{C_\ell}{B_1 - A_\ell E_{\ell-1}}, \quad F_\ell = \frac{D_\ell + G_\ell - A_\ell F_{\ell-1}}{B_\ell - A_\ell F_{\ell-1}}, \quad \ell = 2,N.$$

The temperature can then be obtained from the above equations as:

$$T_N = F_N$$

$$T_\ell = F_\ell - E_\ell T_{\ell+1}, \quad \ell = N-1, N-2, \ldots\ldots 2,1$$

Time step control, convergence of iterations:

The time variation of T_r can be controlled by imposing a restriction on Δt as

$$\Delta t^{n+1/2} \leq a_5 \, \text{Min} \left| \frac{T_\ell^{n+1} - T_\ell^n}{T_{\ell+1/2}^{n+1} + T_{\ell+1/2}^n} \right| \cdot \Delta t^{n-1/2} \qquad (4.79)$$

where a_5 is a real +ve number < 1.

To check the convergence of iterations on T_r we evaluate quantity

$$\delta T_{\ell+1/2} = \text{Max} \left| \frac{T^m - T^{m-1}}{T_{\ell+1/2}^m + T^{m-1}} \right| \qquad (4.80)$$

where T_r^m denotes the value of T_r after the mth iteration. If δT_r is less than a certain specified value $(\delta T_r)_{max}$ the convergence is achieved and we can prepare for the next step. However, in a high density ($\sim$ solid density) and low temperature ($\sim 10^4$ K) plasma, the energy in the radiation field is negligible compared to the electron thermal energy. In such a case, it is not important to check the convergence of iterations on T_r and the restriction enforced

on the time step by equation (4.79) is not considered.

Energy calculations

The energy stored in the radiation field is given by

$$E_r = \sum_i \frac{4\sigma T_r^4}{\rho c} dM_i \qquad (4.81)$$

and must be added to the total energy of the system. The energy loss depends upon the boundary condition.

Case I:

In this case no energy is lost and all the energy absorbed from the laser is converted into kinetic and thermal energy of the plasma.

Case II:

In this case the outward radiation flux at the target boundary is:

$$F_{out} = R^3_{N+1} D^n_{j+1} \left(\frac{T_r(N+1) - T_r(N)}{R(N+2) - R(N)} \right) \qquad (4.82)$$

and $T_r(n+1) = 0$, so Fout is -ve which implies a radiation loss.

Modifications in MEDUSA:-

(i) Equation of motion:

$$\rho \frac{du}{dt} = -\nabla (P_e + P_i + P_r + Q) \qquad (4.83)$$

The radiation pressure P_r is added to the fluid pressure. It can be seen from equation (4.59) that the radiation pressure $\propto T_r^4$. At low temperatures ($\sim 10^5$ K) the radiation pressure is negligible, however, at high temperature ($\sim 10^7$ K) it becomes comparable to the fluid pressure.

(i) Electron energy equation:

The radiation loss term is replaced by the electron-radiation coupling term ($-K_{re}$).

Limitations:

(1) As mentioned before, the radiation diffusion approximation is

not valid in the corona region of the laser produced plasma. Nevertheless, it gives approximate results if the radiation flux limitation is used. In one-dimensional computer simulations, we are mainly interested in the physics of the core region, where the diffusion approximation is valid. We can therefore overlook this deficiency of the model for the present case.

(2) The analytic expressions used for the evaluation of opacities in the calculation of the Rosseland mean free path have a limited accuracy. However, this problem can be overcome by using more accurate tabulated values of opacities [25].

CHAPTER 5

Results: Atomic Physics

In this chapter we present laser-compression simulation results showing some important atomic physics effects which cannot be observed by using MEDUSA alone. In section (5.1) we deal with compression of solid micro-spheres, in section (5.2) we treat gas filled micro-balloons while in section (5.3) we present some results with layered targets.

(5.1) Solid Micro-Spheres:

(5.1a) Degree of ionization:-

Results for 10^4 - fold compression of 1 - μg solid carbon and silicon micro-spheres are presented in this section. An ideal laser-fusion pulse with total energy 70 J/steradian is used. In fig. (5.1) we plot $\log T_e{}_{10}$, $\log \rho_{10}$ and $\langle z \rangle$ along the radius of the carbon pellet at the time when the compression has reached its maximum value. These results are obtained by use of MEDUSAT, a modified version of MEDUSA which contains a steady state density and temperature dependent atomic physics model, TRIP (4). It can be seen from fig. (5.1) that the carbon plasma gets fully ionized in the low density and high temperature corona region, while in the high density core region the degree of ionization is very low, although the temperature is appreciably high. This drop in ionization in the target core is because of the 3-body recombination rate which dominates in the high density region. For comparison, fig. (5.2) shows results obtained by using the steady state corona model which is only temperature dependent. One can see that the interesting feature of low degree of ionization in the compressed core disappears and instead we get a fully ionized carbon plasma. Figures (5.3) and (5.4) show the same behaviour for a silicon micro-sphere, however, as silicon ions are not fully stripped at that temperature.

From the above considerations we conclude that in the medium z laser-plasmas, the degree of ionization exhibits a large spatial variation and therefore must be evaluated by an appropriate atomic physics model.

(5.1b) - Radiation loss rates:-

In fig. (5.5) we plot the total radiation rate (free-free + free-bound + bound-bound) and the corresponding black body radiation rate (at that temperature) vs the radius of the pellet when compression has achieved its maximum value. In the corona region the total radiation rate is much less than the black body rate while in the core region the former exceeds the black body limit. This is because the expressions we use for the radiation loss rates are valid only for an optically thin plasma. Radiation re-absorption becomes important when the medium is optically thick. This deficiency of the model is overcome by limiting the radiation loss rates with the black body rate in the core region. Also we see from fig. (5.6) that in corona region where the plasma is fully ionized, the bremsstrahlung rate dominates over the recombination and line radiation rates, as expected.

(5.1c) Comparison with no atomic physics case:-

In the following we give a comparison between the two models, MEDUSA and MEDUSAT for a 10^4-fold compression of a 1 -μg carbon microsphere with initial radius 49.2 μm and initial density 2×10^3 kg/m^3.

TABLE (5.1)

	MEDUSA	MEDUSAT
Initial Power: P_o (W/steradian)	7×10^8	2.1×10^9
Initial Temperature	6×10^4	6×10^4
Initial Pressure (J/m^3)	5.75×10^{11}	1.2×10^{11}

Initial ionization level z	6	0.45
Final temperature	3×10^7	1.2×10^7
Final Pressure: (J/m^3)	10^{18}	2×10^{17}

If the initial temperature of the plasma, T_o, is chosen to be less than 6×10^4 K, mean ionization in the plasma evaluated by MEDUSAT is so small that we do not get a critical density surface, where the laser energy could be dumped.

From table (5.1) it is seen that the initial power level, P_o, required in MEDUSAT, is 3-times larger than that in MEDUSA. The reason for this increase in power requirement is that in the initial stages of compression, most of the laser energy is used to ionize the atoms* and more power is required to get good compression and heating at the same time. We note also that the maximum electron temperature achieved in MEDUSAT is lower than that in MEDUSA, because the electrons bring about ionization by electron-ion collisions and partly lose their energy, resulting in lower electron temperature. In case of the silicon micro-sphere, the required initial power is even higher (3.5×10^9 $W/_{steradian}$).

* Energy required to ionize 1 - μg of carbon 8.2J, while that for 1 μ-g of silicon is 26.5J.

1 - μg Solid Carbon Micro-sphere

$z = f(n_e, T_e)$

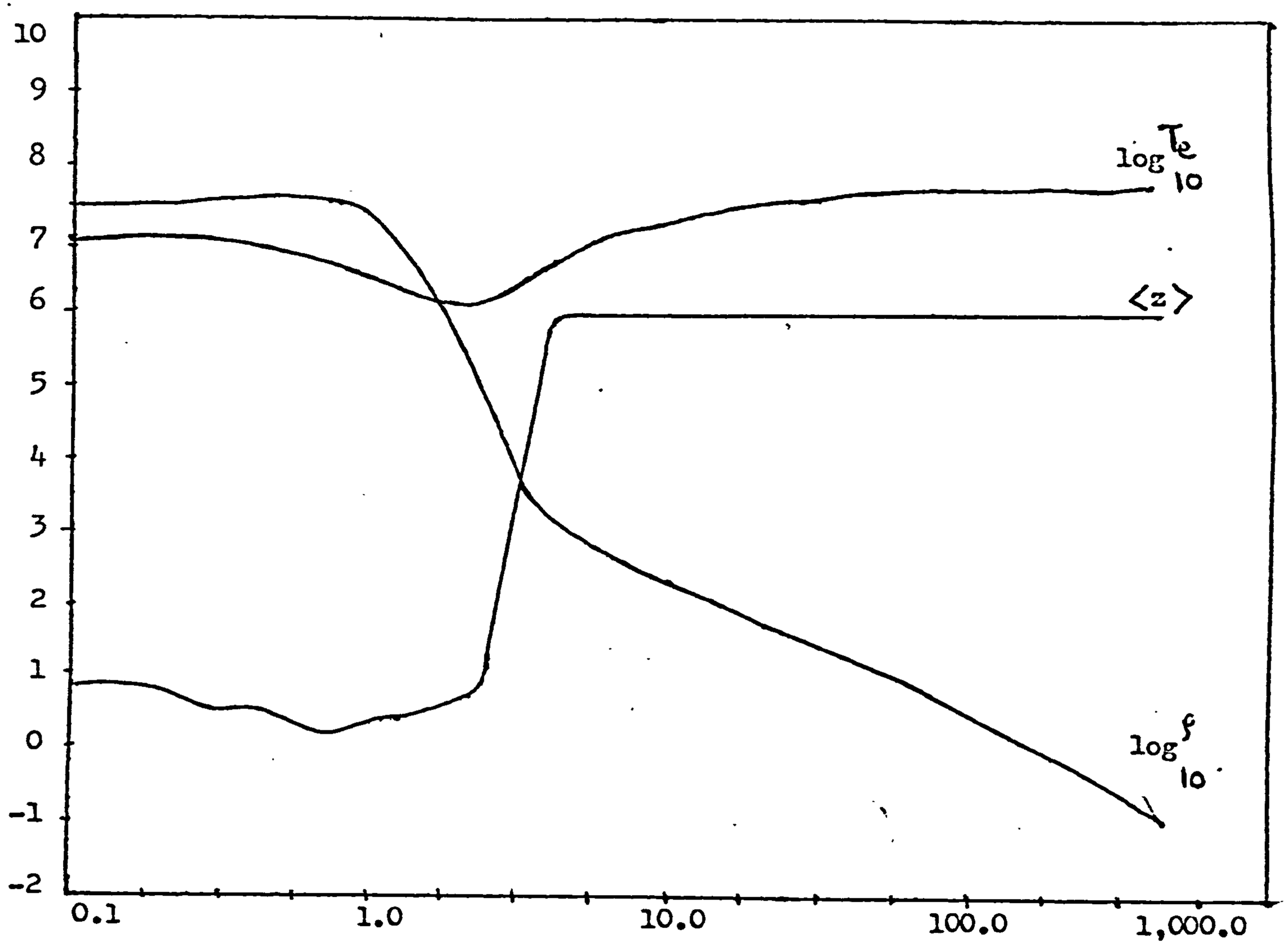

Fig. (5.1)

1 - μg Solid Carbon Micro-sphere

$\langle z \rangle = f(T_e)$

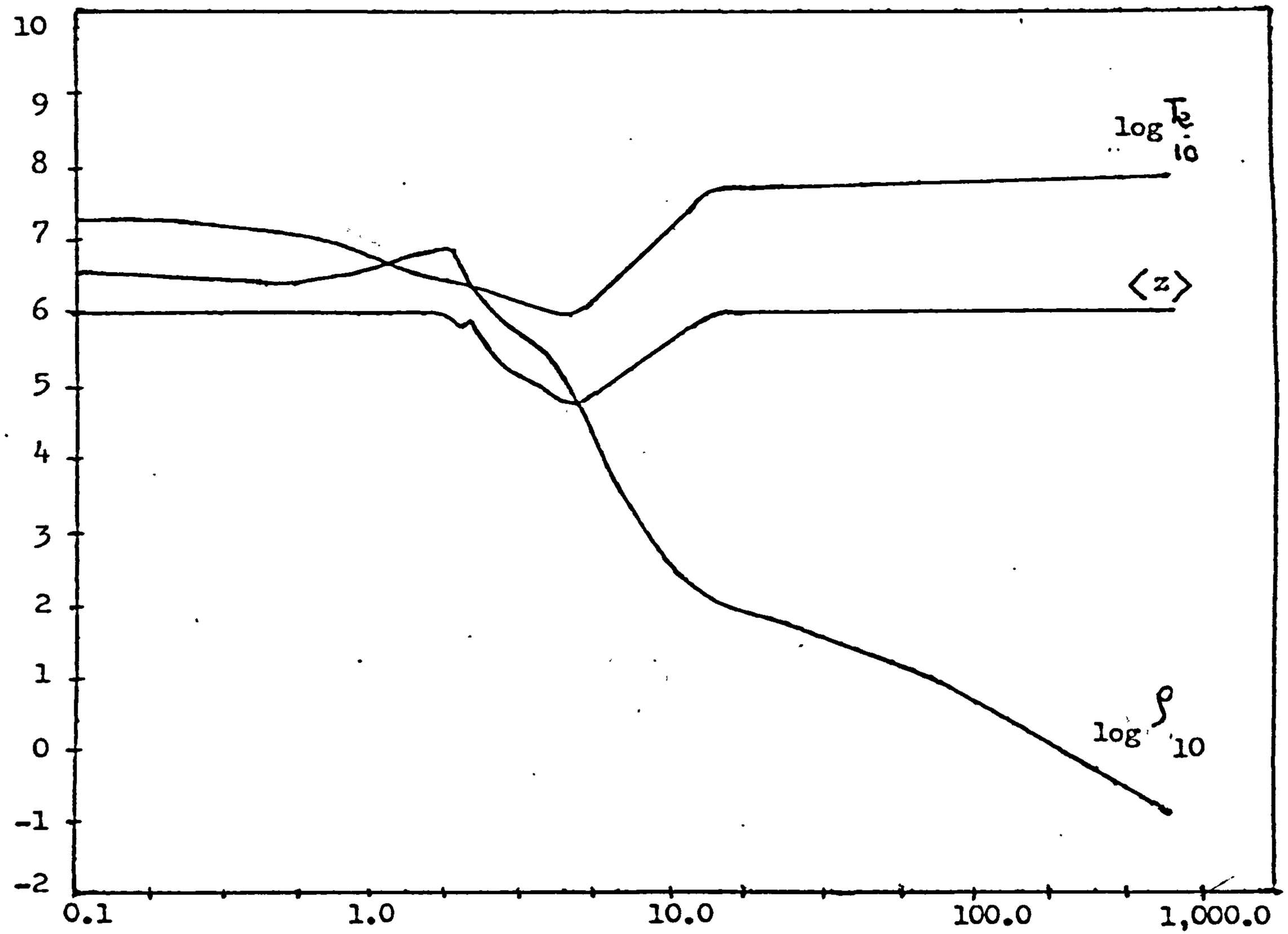

Fig. (5.2)

1 - μg Solid Silicon Micro-sphere

$\langle z \rangle = f(n_e, T_e)$

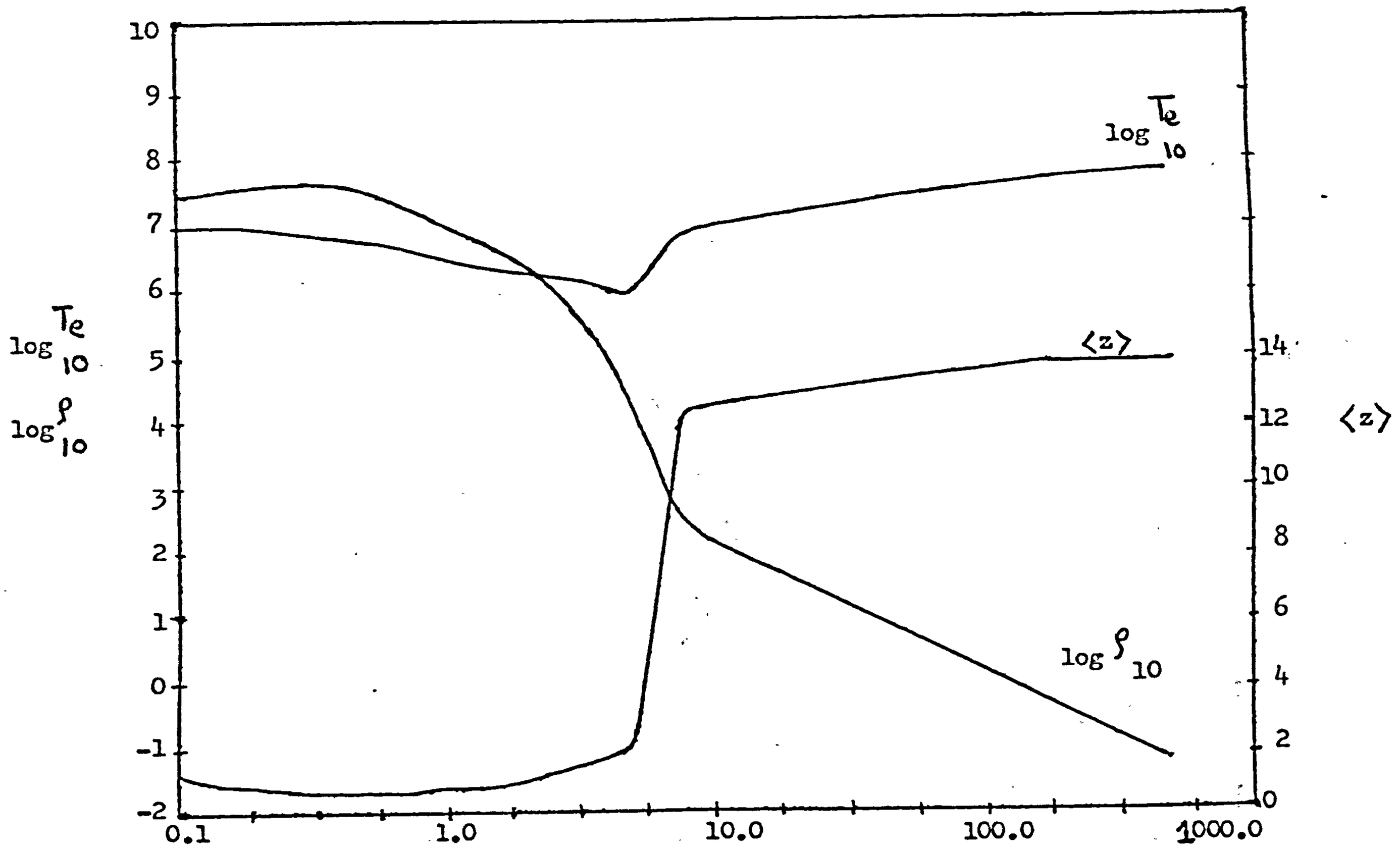

Fig. (5.3)

$1 - \mu g$ Solid Silicon Micro-sphere

$\langle z \rangle = f(T_e)$

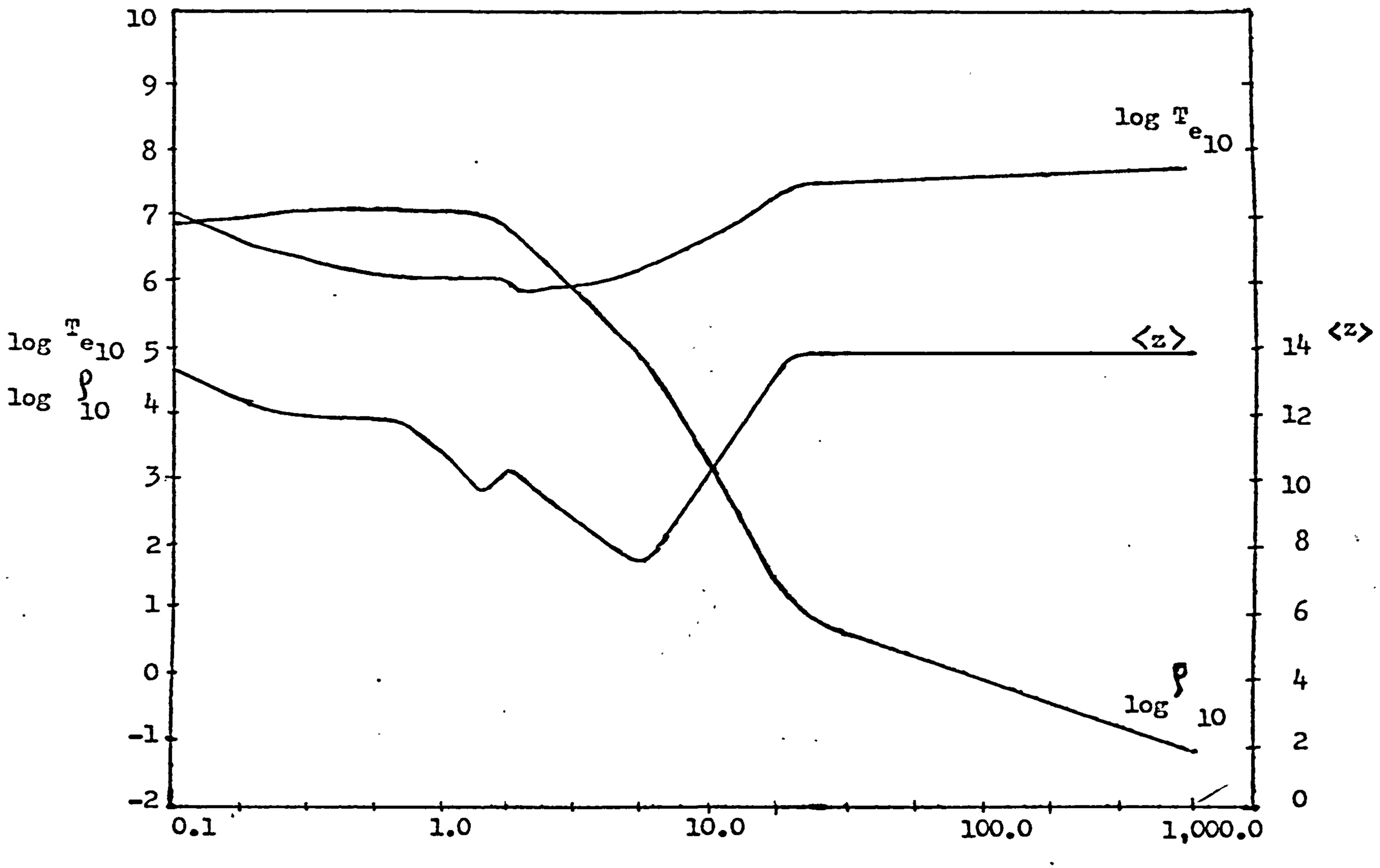

Fig. (5.4)

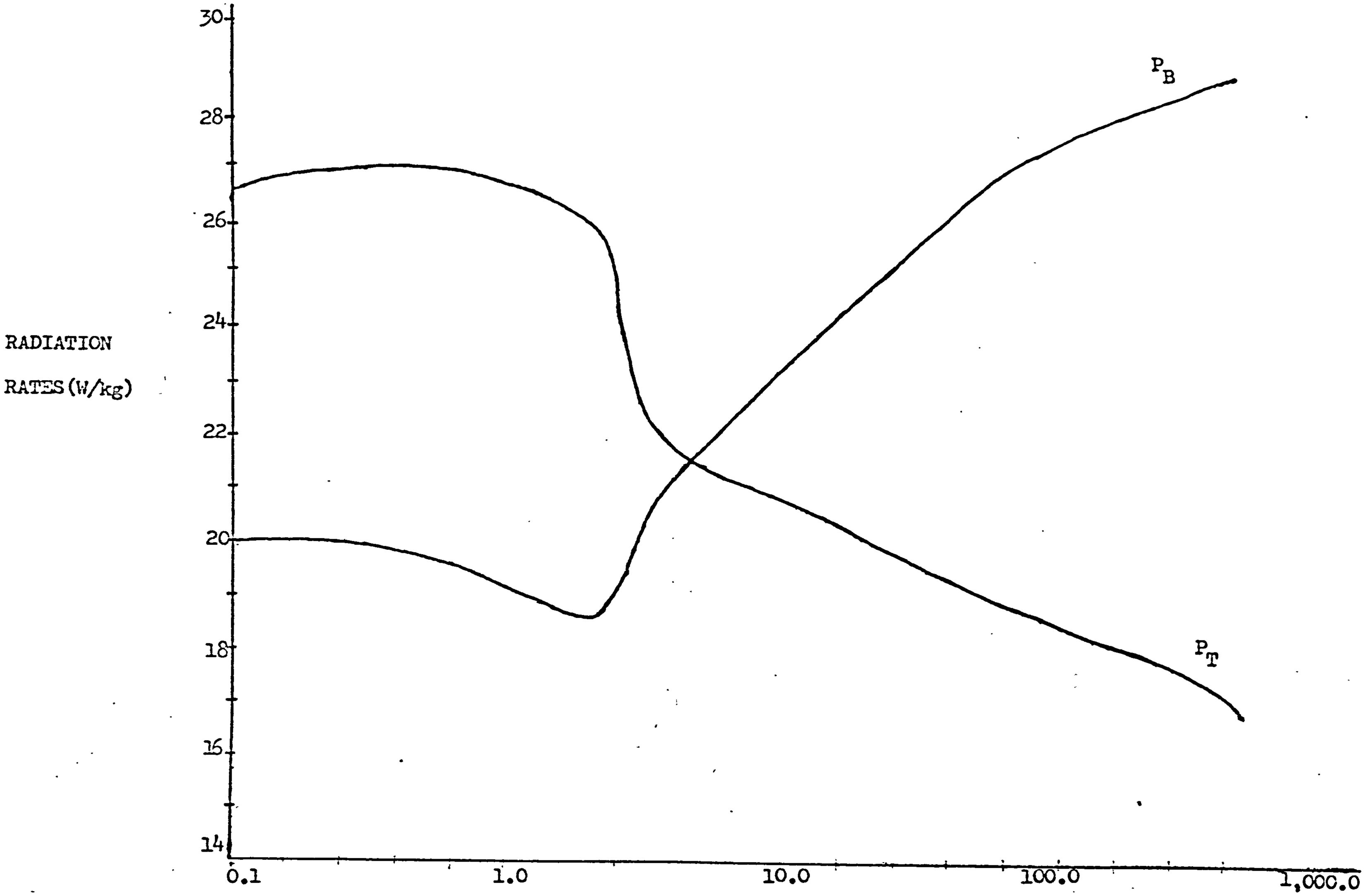
30
28
26
24
22
20
18
16
14
RADIATION
RATES (W/kg)
P_B
P_T
0.1
1.0
10.0
100.0
1,000.0
RADIUS (μ)

Fig. (5.5)

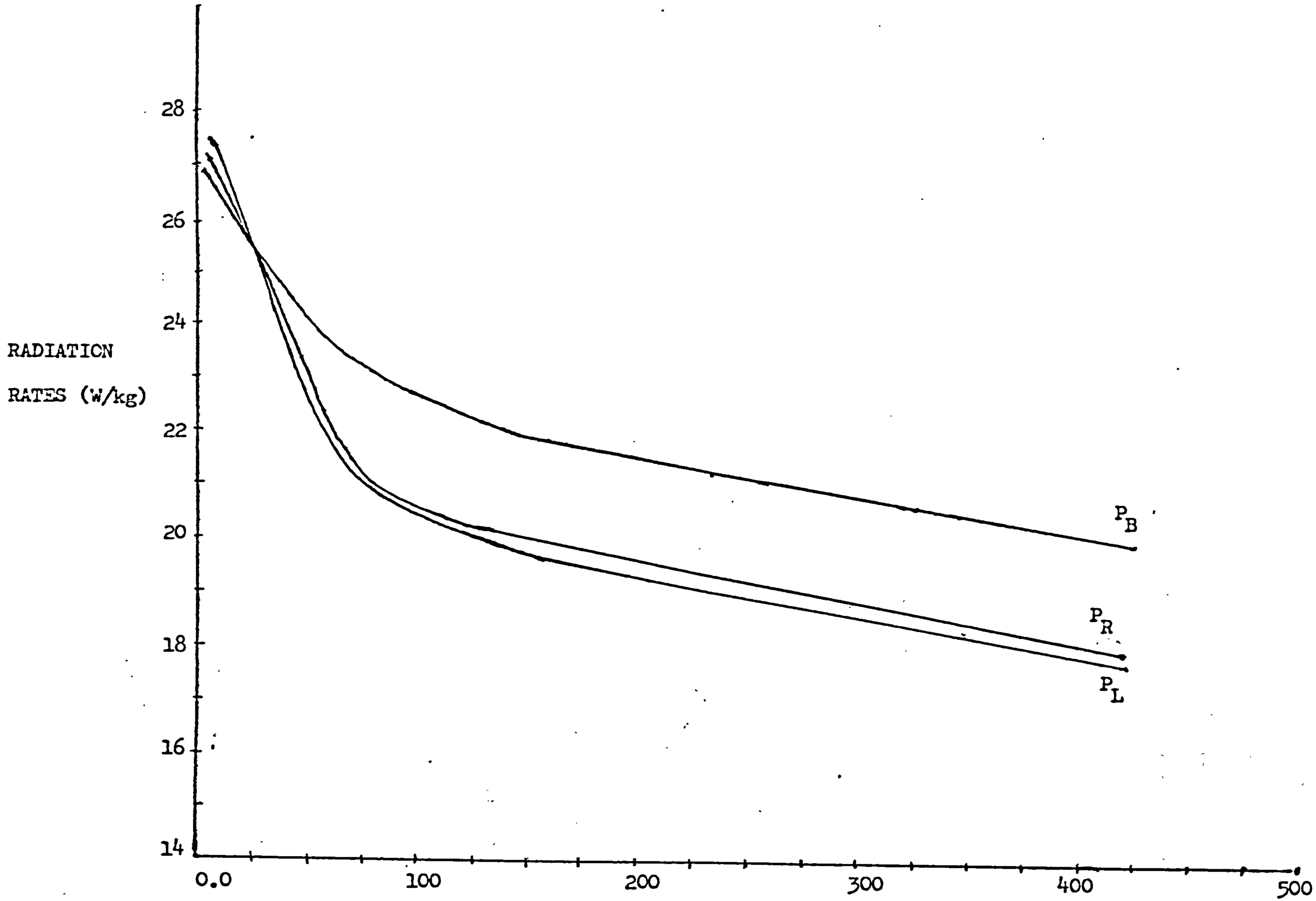
RADIATION
RATES (W/kg)
28
26
24
22
20
18
16
14
0.0
100
200
300
400
500
P_B
P_R
P_L
RADIUS (μ)

Fig. (5.6)

(5.2) Gas filled micro-balloons:

In practice, a glass micro-balloon coated with a low z material and filled with a gas (say Ne) is used as a laser target. Inclusion of the atomic physics package TRIP in the computer code to simulate the compression of such a system gives rise to computational problems. However, in the case of thin micro-balloons with wall thickness ~ 1 or 2 μm and with moderate laser powers $\sim$ few GW, the micro-balloon gets ionized very quickly, as we show below.

We simulate compression of carbon and silicon micro-balloons. For computational simplicity, we consider the carbon micro-balloons filled with carbon at a low density (~ 5 kg/$_m^3$) and the silicon micro-balloons filled with silicon at a density = 5 kg/$_m^3$. The target and pulse parameters are shown in table (5.2).

TABLE (5.2)

	R = 35 μm	
ΔR (μm)	1	2
P_o (^{W}/steradian)	2×10^9	3×10^9
τ (ps)	90	100
E (^{J}/steradian)	2.5	5.0
Gas density ($kg/_m^3$)	5	5

In fig. (5.7) and fig. (5.8) we plot log $T_{e_{10}}$, log ρ_{10} and $\langle z \rangle$ Vs target radius for 1-μm and 2-μm thick carbon micro-shells respectively, when the compression has reached the centre of the target. Fig. (5.9) and (5.10) represent corresponding quantities for 1-μm and 2-μm thick silicon shells. We see that the gas is compressed to solid density and even the silicon plasma gets almost fully ionized. Therefore, to a good approximation, we can ignore the atomic physics effects in simulating compression of thin micro-balloons. However, in case of thick

micro-shells with wall thickness $\sim 5 - 10 \mu m$, where the implosion is ablative in type, inclusion of atomic physics is essential.

In the next section, we present some interesting features of laser-compression using layered targets, excluding atomic physics.

CARBON SHELL, $\Delta R = 1 \mu m$

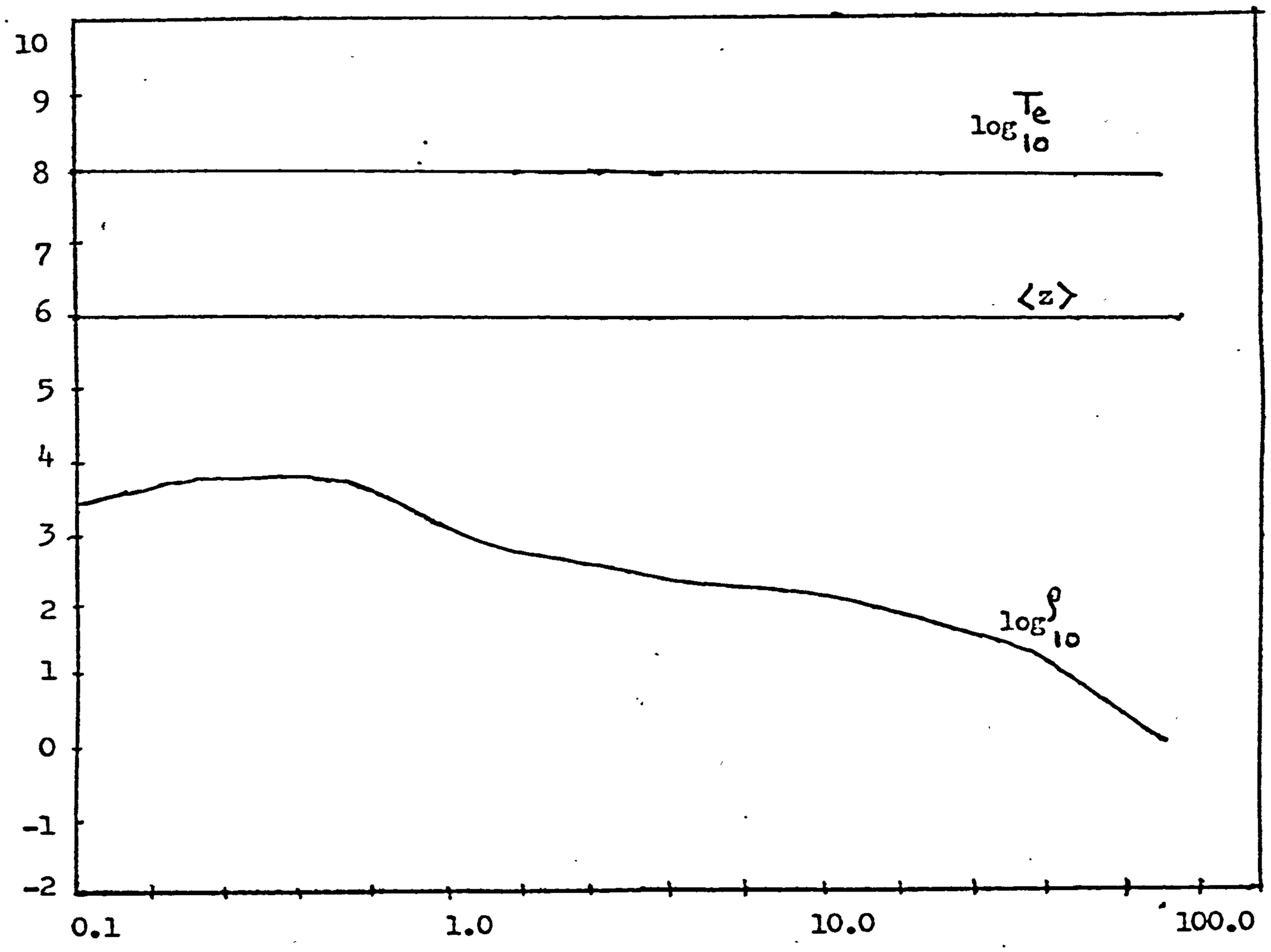

Fig. (5.7)

CARBON SHELL, $\Delta R = \cdot 2 \mu m$

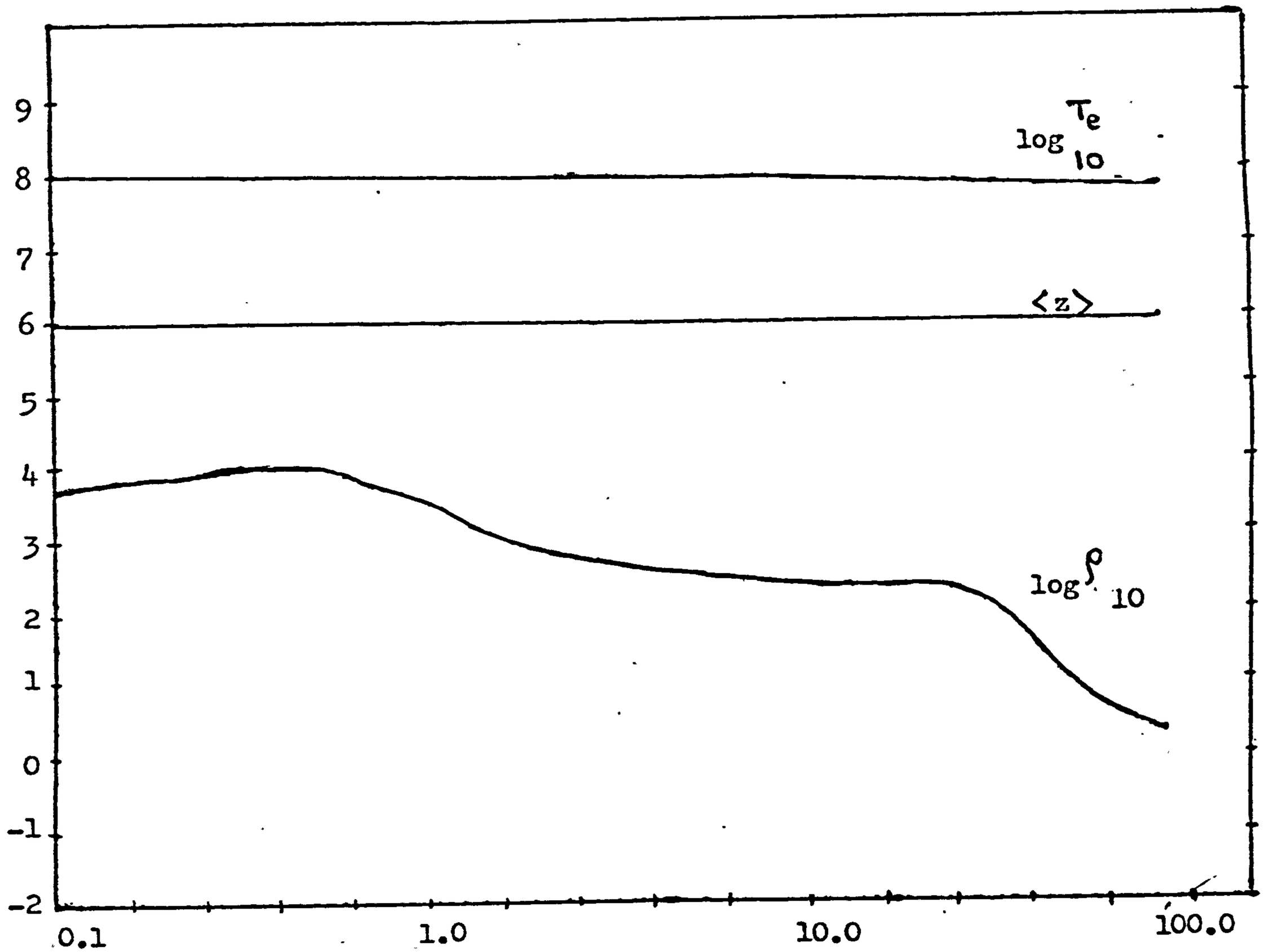

RADIUS (μ)

Fig. (5.8)

SILICON SHELL, $\Delta R = 1 \mu m$

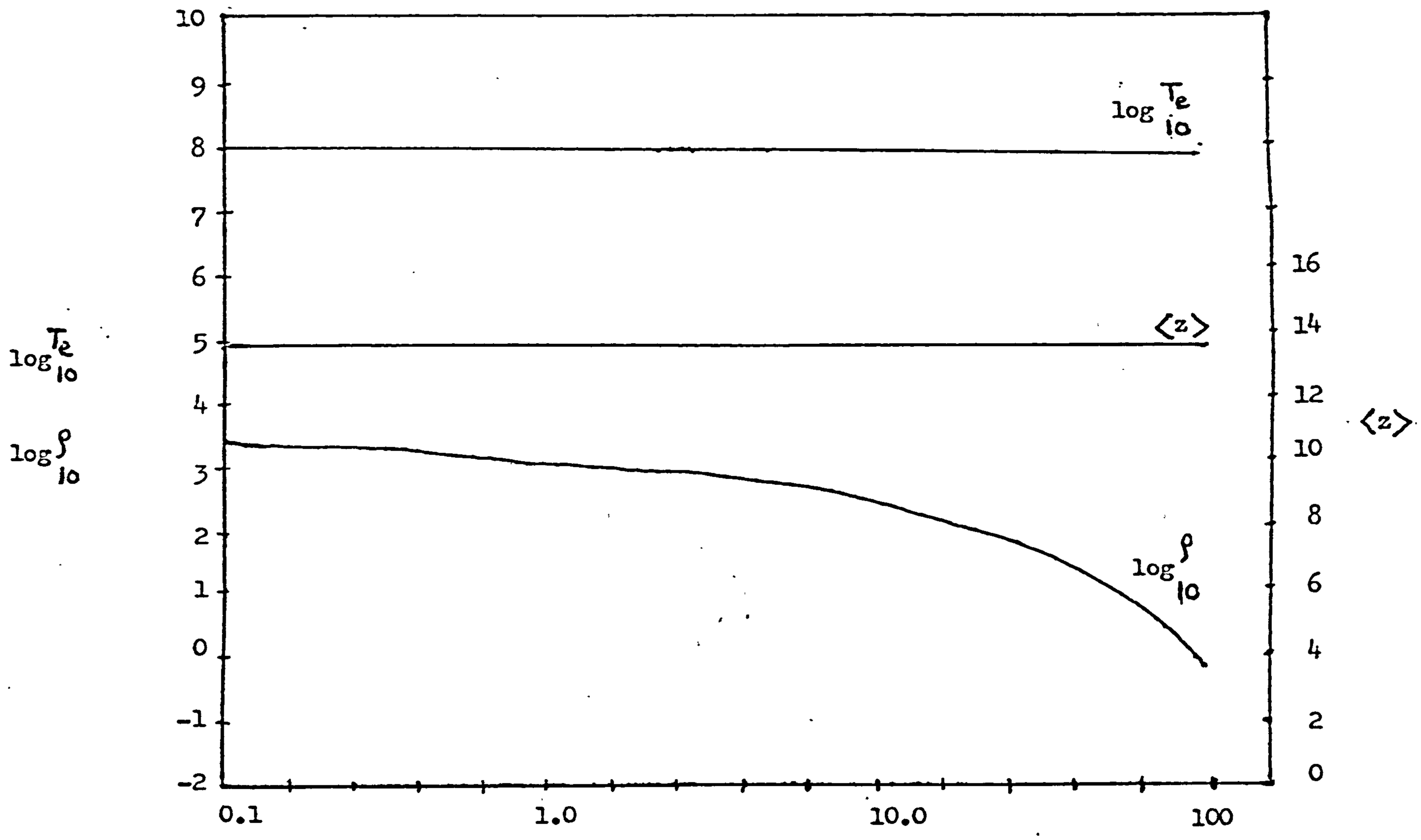

Fig. (5.9)

SILICON SHELL $\Delta R = 2\,\mu m$

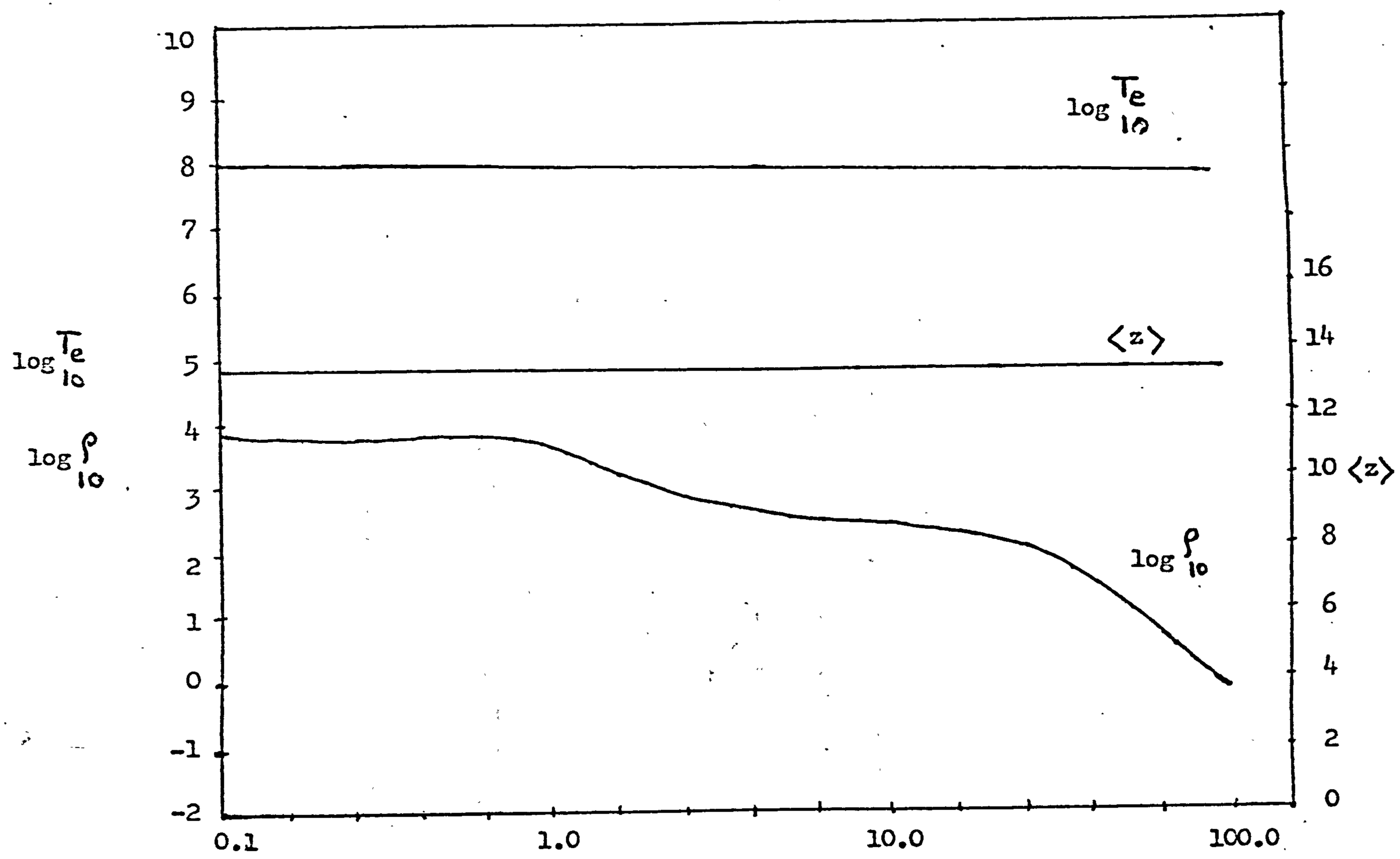

Fig. (5.10)

(5.3) Layered Targets:

In this case, results are obtained using a modified version of MEDUSA which can handle layered targets (as described in appendix 4). These results are simulated by compressing D-T filled glass (S_iO_2) micro-balloons using a laser pulse which is Gaussian in time and the pulse parameters are within the capability of the Rutherford Laboratory laser system. In the present work, however, our aim is not to simulate any particular experiment but to show the effect of various phenomena on compression and neutron yield.

(5.3a) Yield Vs pulse length τ :

Initial Radius of the shell: $R = 35\mu m$

Wall thickness : $\Delta R = 0.9\mu m$

Energy in the laser pulse : $E = 17$ J

Initial density of D-T gas : $\rho_g = 2\ kg/m^3$

Initial Temperature : $T_o = 10^4$ K

For constant laser pulse energy, the yield Y for various values of τ is shown in fig. (5.11), and maximum temperature and density of the D-T as a function of τ in table (5.3).

TABLE (5.3)

τ(ps)	P_m (GW)	$(\rho_g)_m$ (kg/m^3)	$(T_i)_m$ (K)
40	20.5	3×10^4	9.2×10^7
50	16.4	3.9×10^4	6.6×10^7
60	13.6	5×10^4	5.5×10^7
80	10.0	8.8×10^4	4×10^7
100	8.19	5.3×10^4	3.1×10^7

We see that with shorter laser pulses, the maximum gas density is lower, due to more shock heating, the maximum ion temperature is larger. Since the cross-section for a D-T reaction varies strongly with temperature in the range 5 Kev to 100 Kev, the shorter laser

* τ is the $\frac{1}{e}$ width of the Gaussian.

pulses give better yield.

(5.3b) Yield Vs Initial gas density:

In fig. (5.12) we show thermonuclear yield against the initial gas density, ρ_g, from 2 - 5 kg/m^3 using pulse parameters, τ = 60 ps, P_m = 13.6 $GW/steradian$. In this case the compression ratio drops by a factor of 2.5 while the temperature remains almost constant. The yield is thus rather insensitive to the change in the initial gas density in this range.

TABLE (5.4)

$S_g (kg/m^3)$	$(S_g)_m$ (kg/m^3)	T_m (K°)
2.0	5×10^4	6.6×10^7
2.5	3.38×10^4	5.5×10^7
3.0	2.6×10^4	5.1×10^7
3.5	2.5×10^4	5×10^7
4.0	2.1×10^4	4.6×10^7
5.0	1.9×10^4	4.3×10^7

(5.3c) Effect of a medium A impurity on yield:

It is to be noted that the shock heating rate Q in the ion energy equation used in MEDUSA is $\propto$ the atomic weight of the element, A. The addition of an impurity gas like Ne into D-T would enhance the shock heating rate, thereby increasing the ion temperature. The increase in the ion temperature would make the yield better, however, if the percentage of impurity is increased too much, the yield drops down because of decrease in the D-T mass available for reaction. In fig. (5.13), we plot yield for 20% N and Ne in the D-T mixture respectively. It can be seen that yield increases with increasing A.

(5.3d) Effect of wall thickness on Yield:

We have investigated the effect of increasing the wall thickness

of the micro-balloon from 0.9 - 2μm on the compression and heating of the gas. The pulse parameters are kept constant.

TABLE (5.5)

ΔR (μm)	ρ_m (kg/m^3)	T_i (K^0)
0.9	5×10^4	5.5×10^7
1.0	1.6×10^5	5×10^7
1.2	5×10^5	3.3×10^7
1.4	3.5×10^5	2.8×10^7
1.6	2×10^5	2.3×10^7
1.8	10^5	1.6×10^7
2.0	5×10^4	10^7

where τ = 60 ps, P_m = 13.6 GW/steradian and ρ_g = 2 kg/m^3.

From table (5.5) we see that final density of the gas increases with the shell thickness while the final temperature decreases, because, in thinner shells the laser energy quickly burns through the shell, heating the gas to higher temperature. The momentum of the shell in this case is not enough to compress the gas highly. On the other hand, in the case of thicker shells the transport of energy to the gas is slowed down while the larger momentum of the shell compresses the gas to higher densities at relatively low temperature. However, sufficient increase in the shell thickness causes the compression to drop, since the laser energy is not enough to compress the target. A Scenario of 0.9 and 2.0μm thick shells is plotted in fig. (5.14), line with + represents the ion temperature whereas that with - represents electron temperature. The neutron yield Vs ΔR is shown in fig. (5.15).

(5.3c) Y vs Z of the coated layer

It is of interest to investigate the effect of coating the outer surface of the glass micro-balloon with a layer of low z element, on the D-T compression. Table (5.6) shows the maximum gas density and

temperature for a 1 - μm thick glass micro-shell coated with a 1 -μm thick layer of 4 B_e^9, $6C^{12}$ and CF_2 (with effective z$\sim$8) respectively. The initial density of the outer layer is taken to be the same as that of the glass (2.3×10^3 kg/$_m^3$) to keep the mass of the target constant. The initial density of D-T is 2 kg/$_m^3$. Since the electron thermal conduction is $\propto \frac{1}{z}$, a lower z would lead to a better thermal conduction. Table (5.6) shows that as z of the outer layer increases the compression and heating of D-T is degraded and consequently the neutron yield is affected, as shown in fig. (5.16). Also, in fig. (5.15) we show the implosion history of a 2 -μm thick glass micro-balloon Vs that of 1 - μm glass micro-balloon coated with 1 - μm thickness of $_4B_e^9$. The implosion in the latter case is more efficient as a result of good thermal conduction.

R = 35 μm, = 60 ps, P_m = 13.6 W/steradian

Table 5.6

Material	ρ_g (kg/$_m^3$)	T_i (K)
$_4B_e^9$	3×10^5	4.1×10^7
$_6C^{12}$	1.58×10^5	2.2×10^7
CF_2	10^5	1.86×10^7

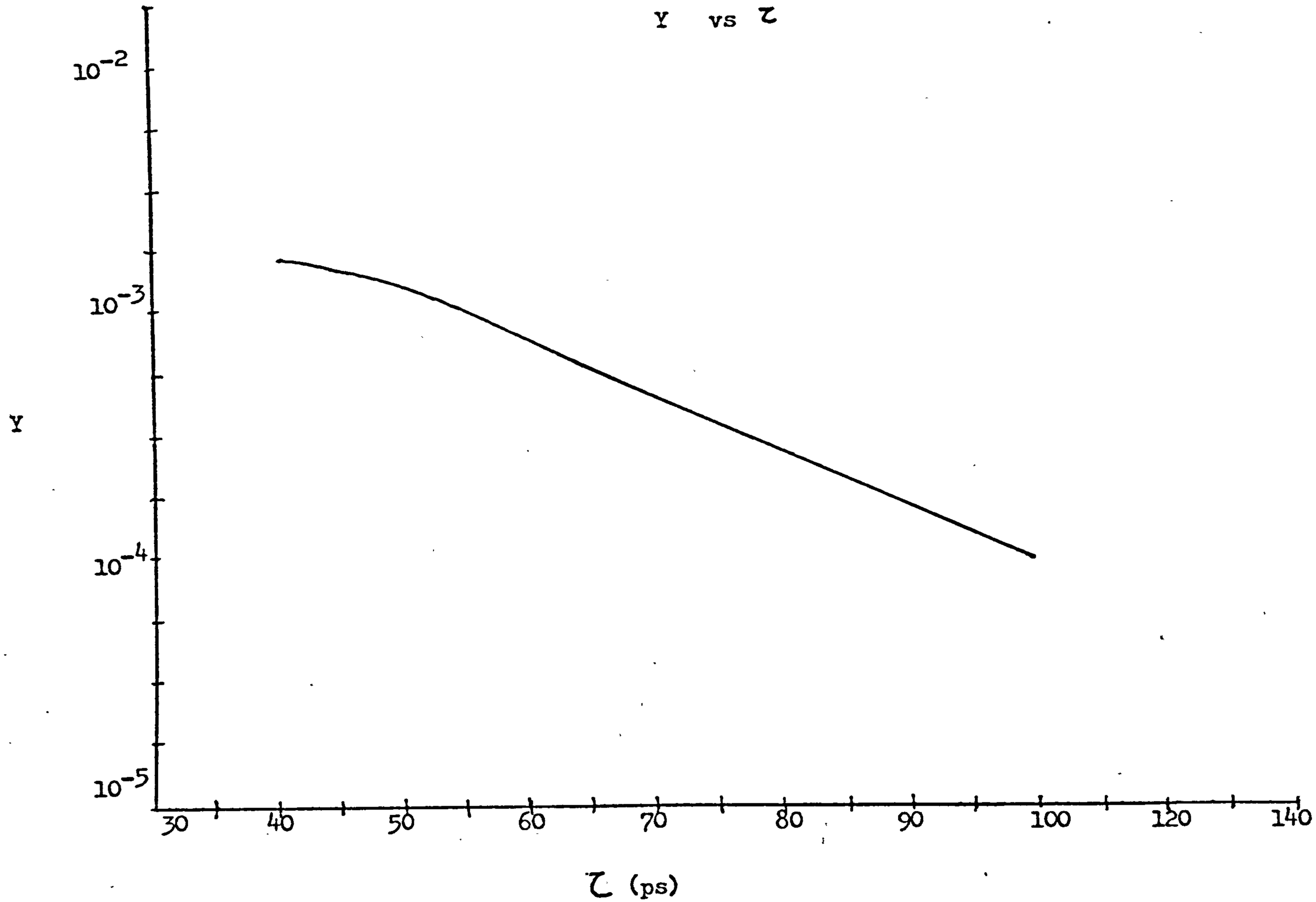

Fig. (5.11)

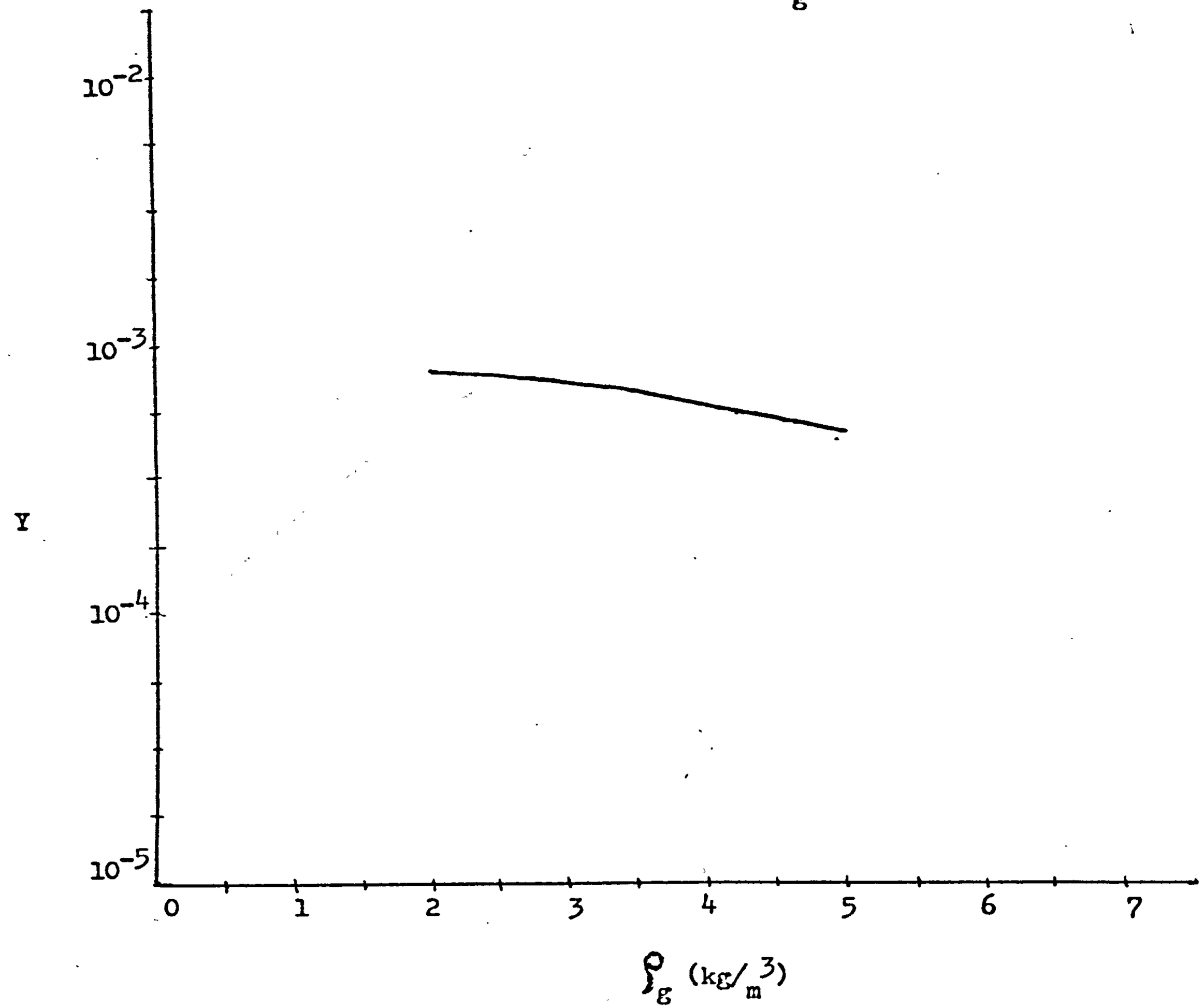

Fig. (5.12)

Y vs A

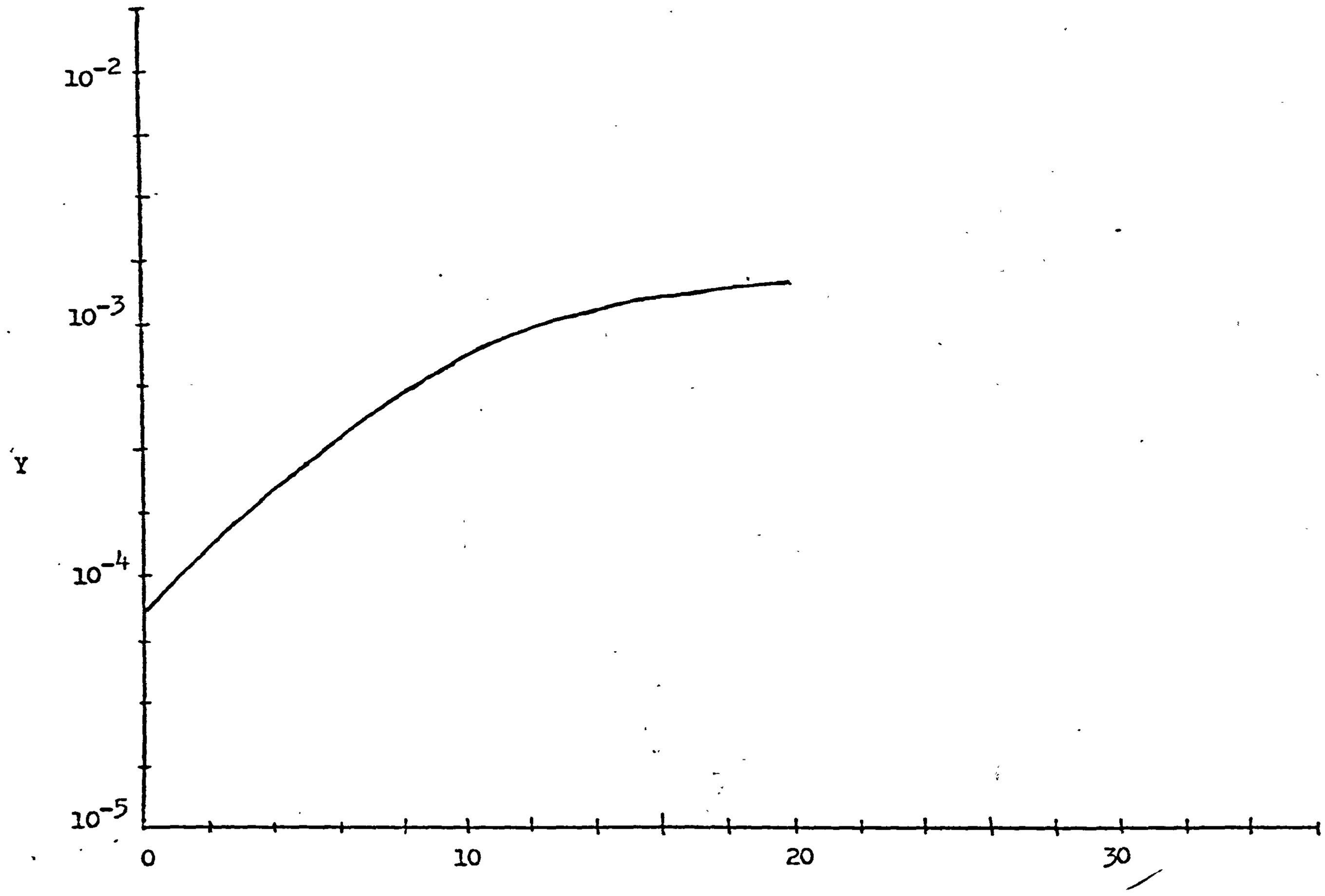

Fig. (5.13)

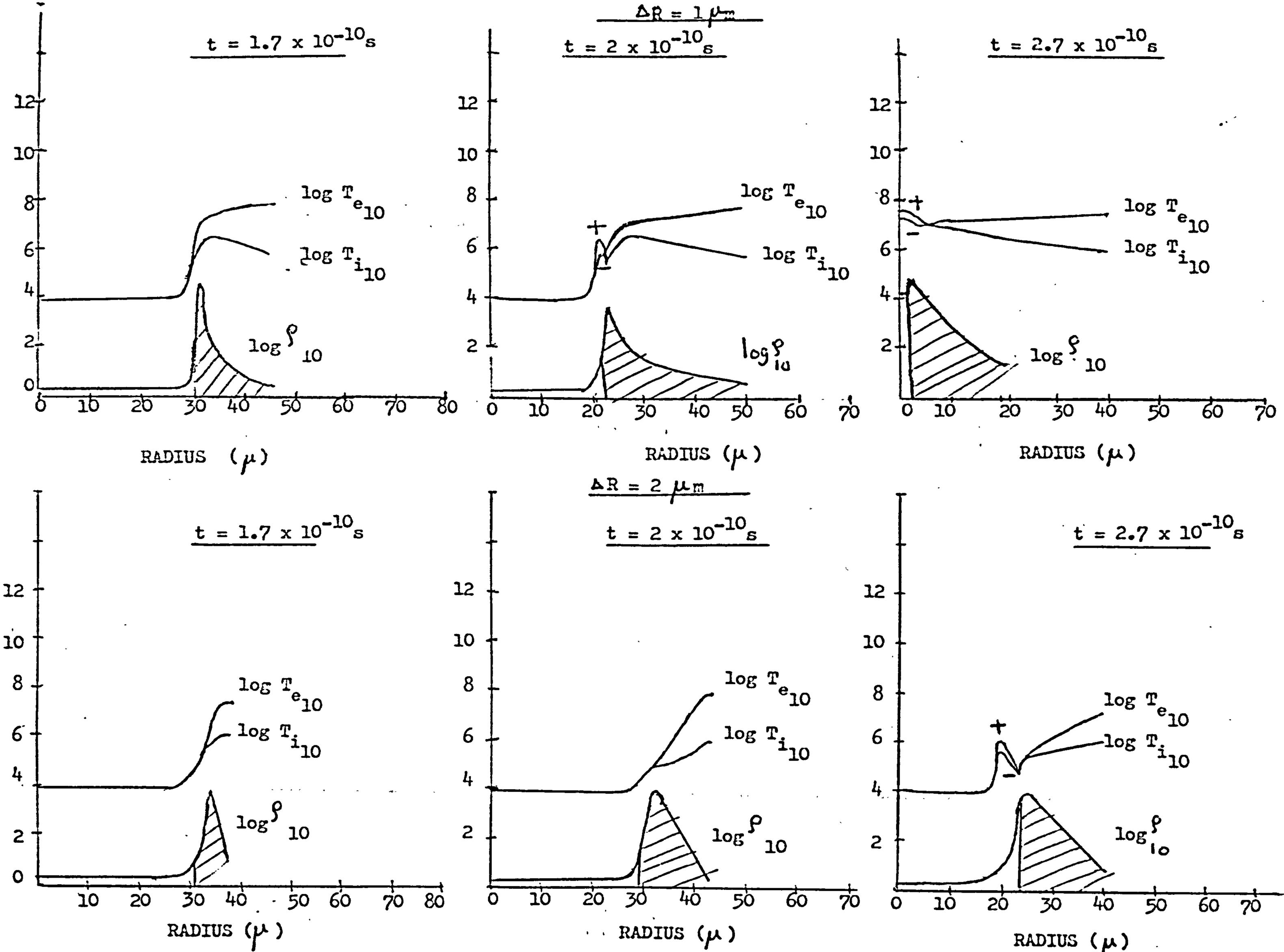
ΔR = 1 μm
t = 1.7 x 10^-10 s
t = 2 x 10^-10 s
t = 2.7 x 10^-10 s
log T_e10
log T_i10
log ρ_10
RADIUS (μ)
ΔR = 2 μm
t = 1.7 x 10^-10 s
t = 2 x 10^-10 s
t = 2.7 x 10^-10 s
log T_e10
log T_i10
log ρ_10
RADIUS (μ)

Fig. (5.14)

Y vs Δ R

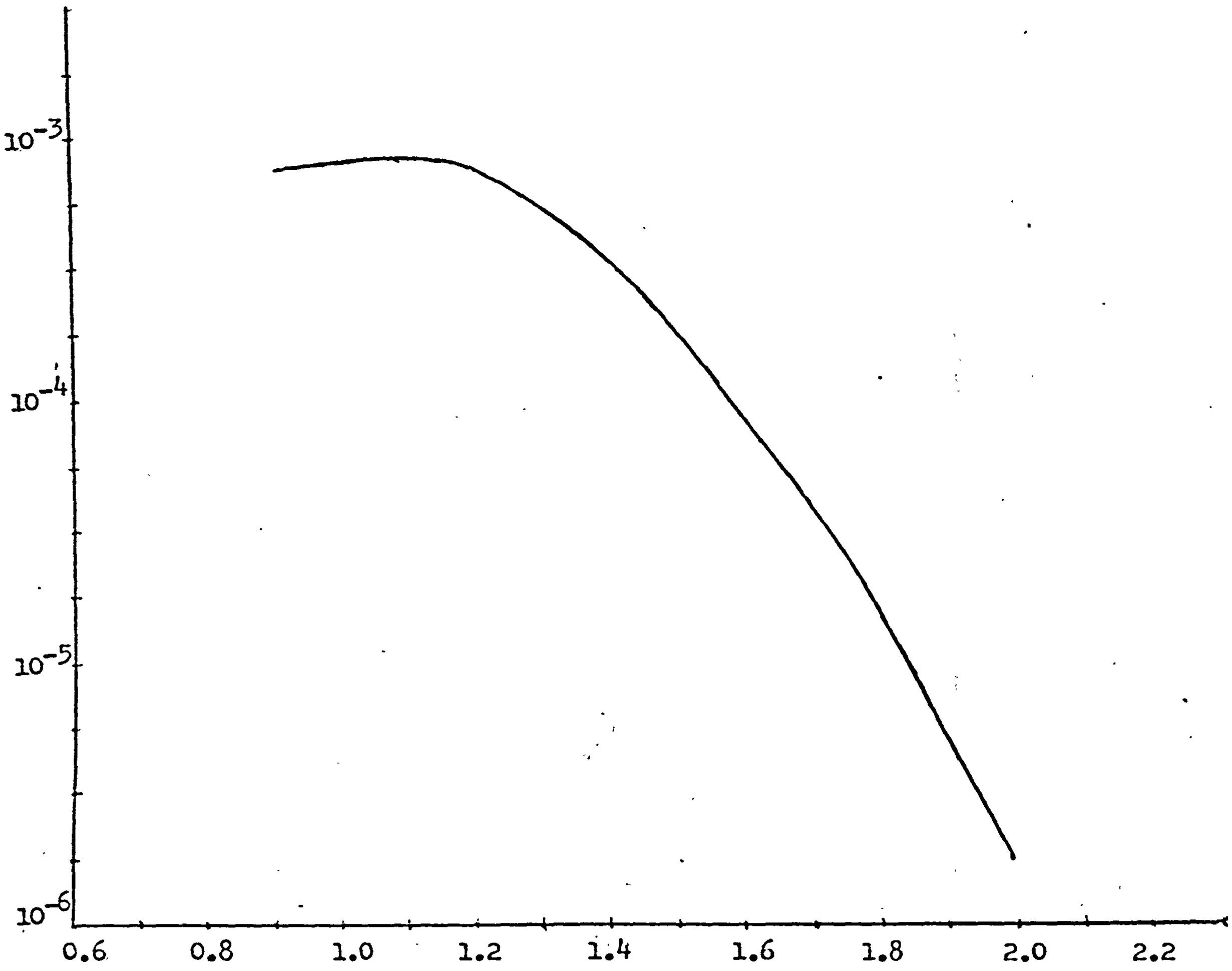

Fig. (5.15)

$\Delta R = 2\mu m$ ($1\mu m$ $S_i O_2$ + $1\mu m$ B_e)

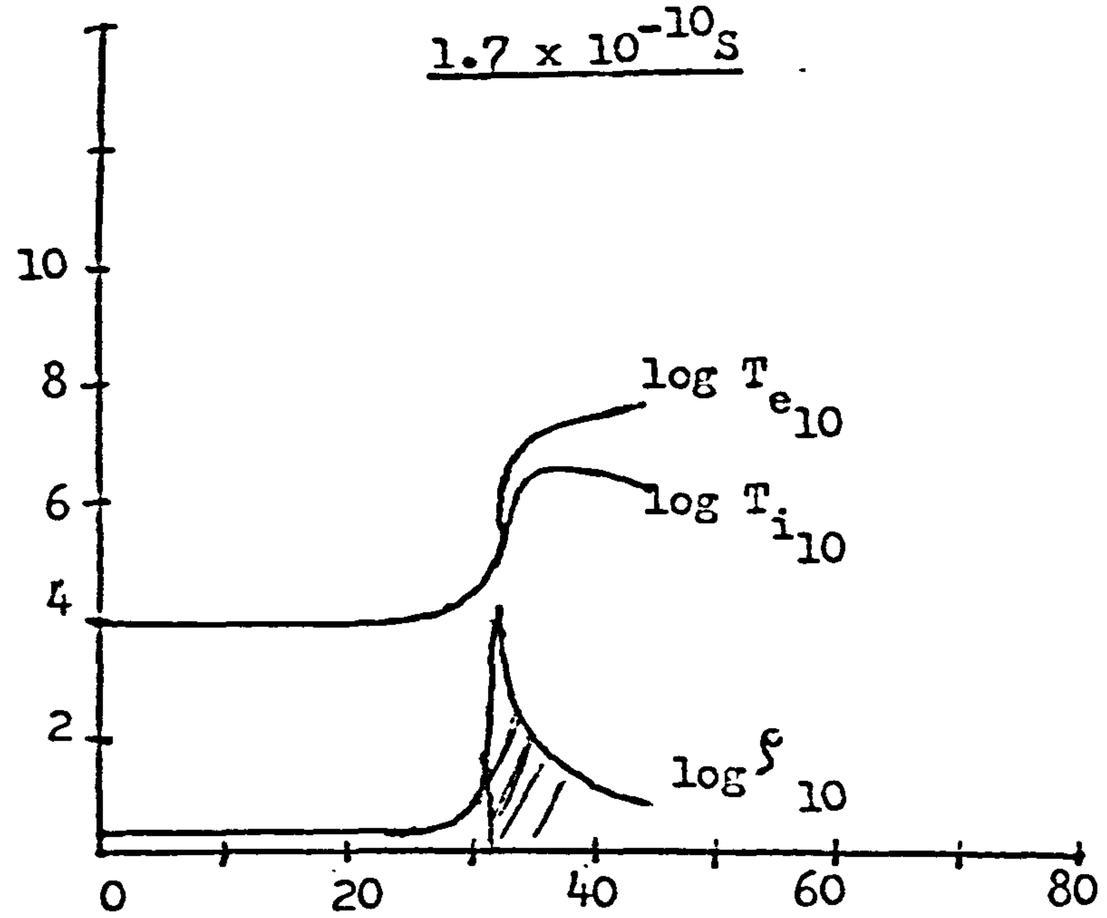

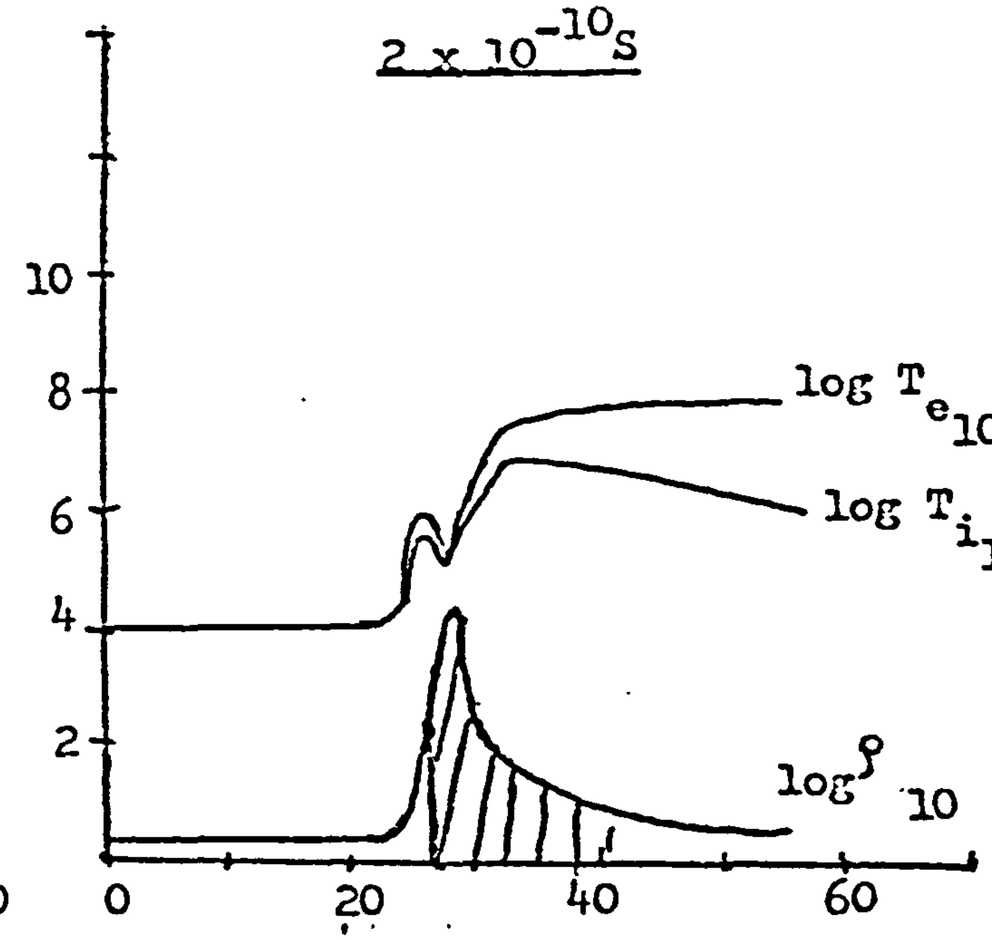

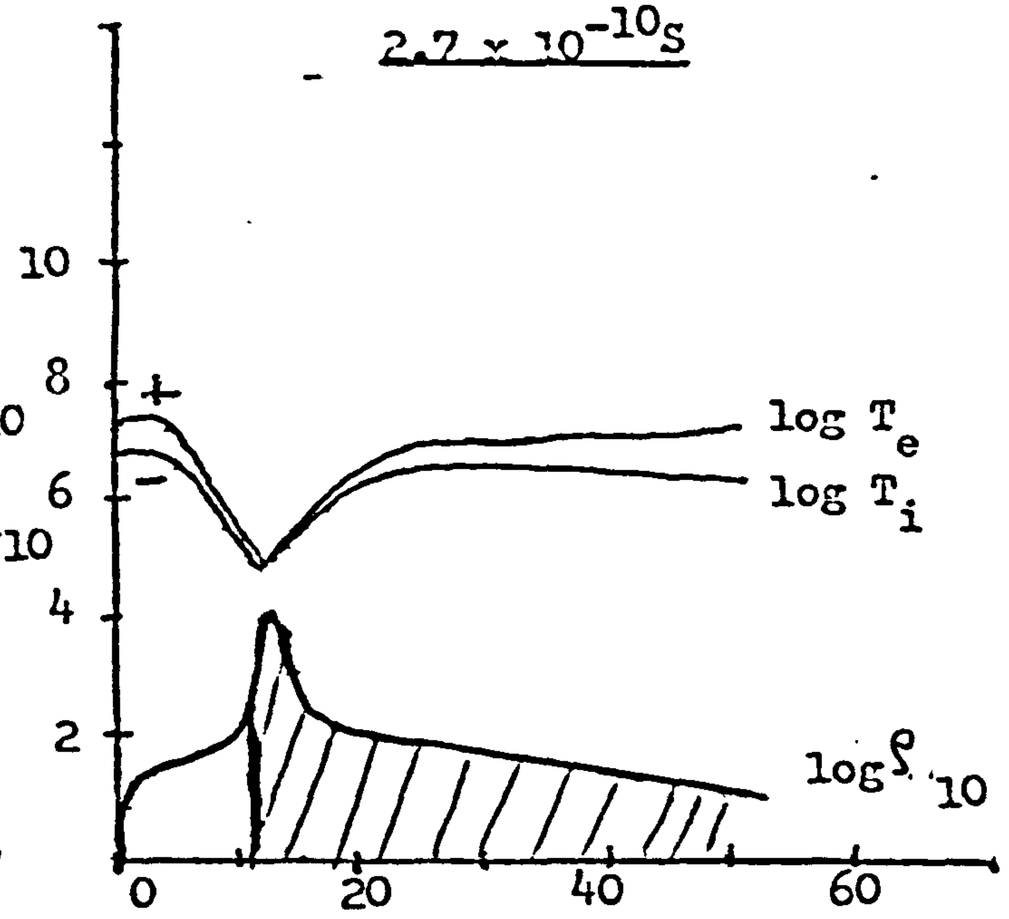

$\Delta R = 2\mu m$ $S_i O_2$

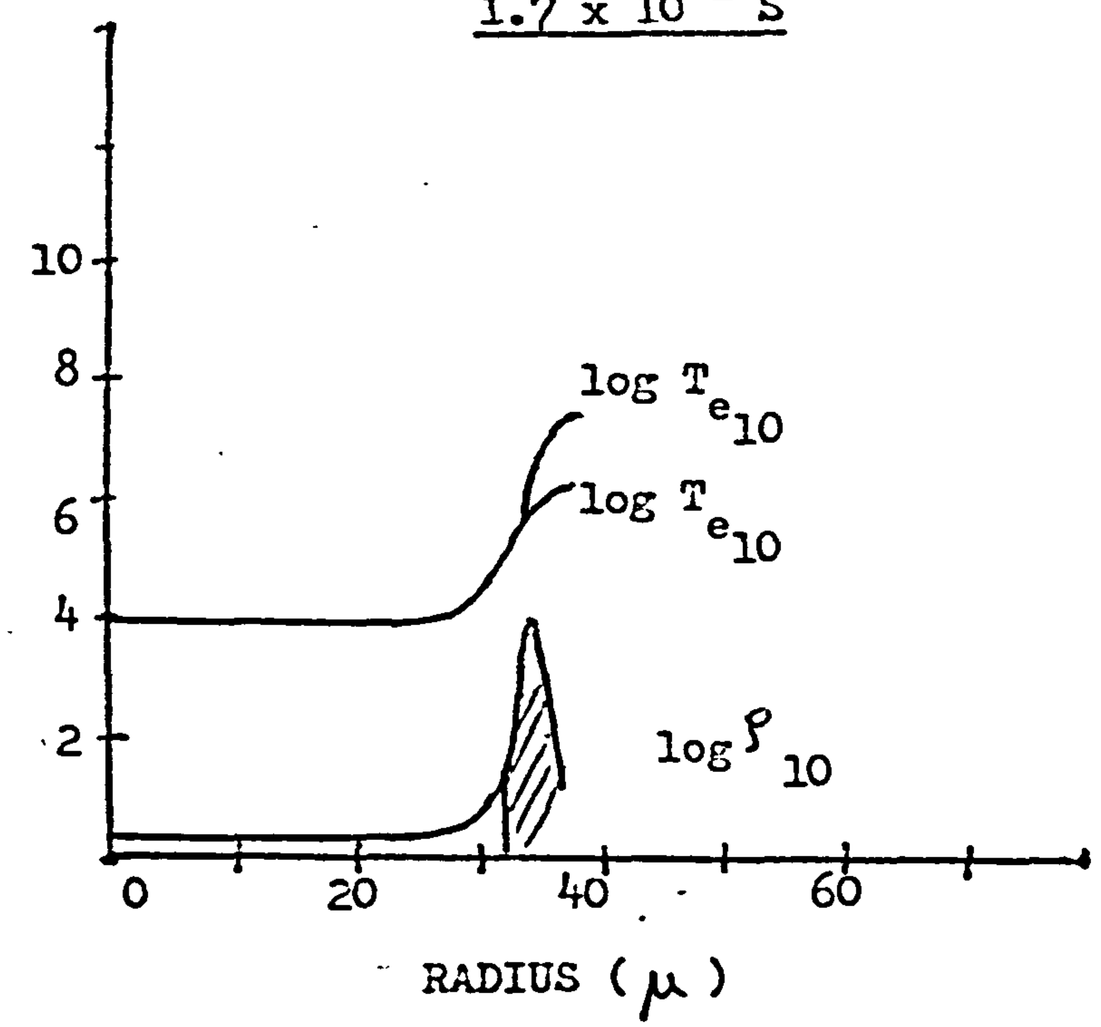

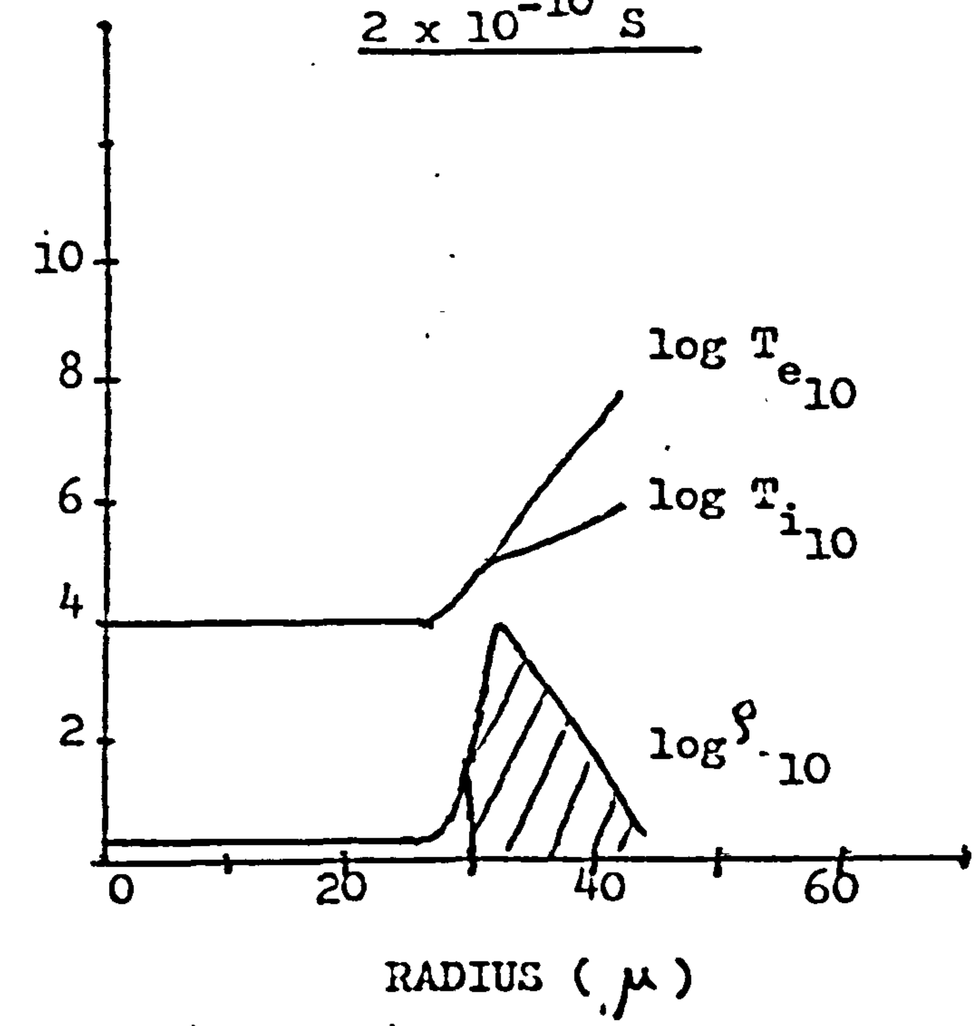

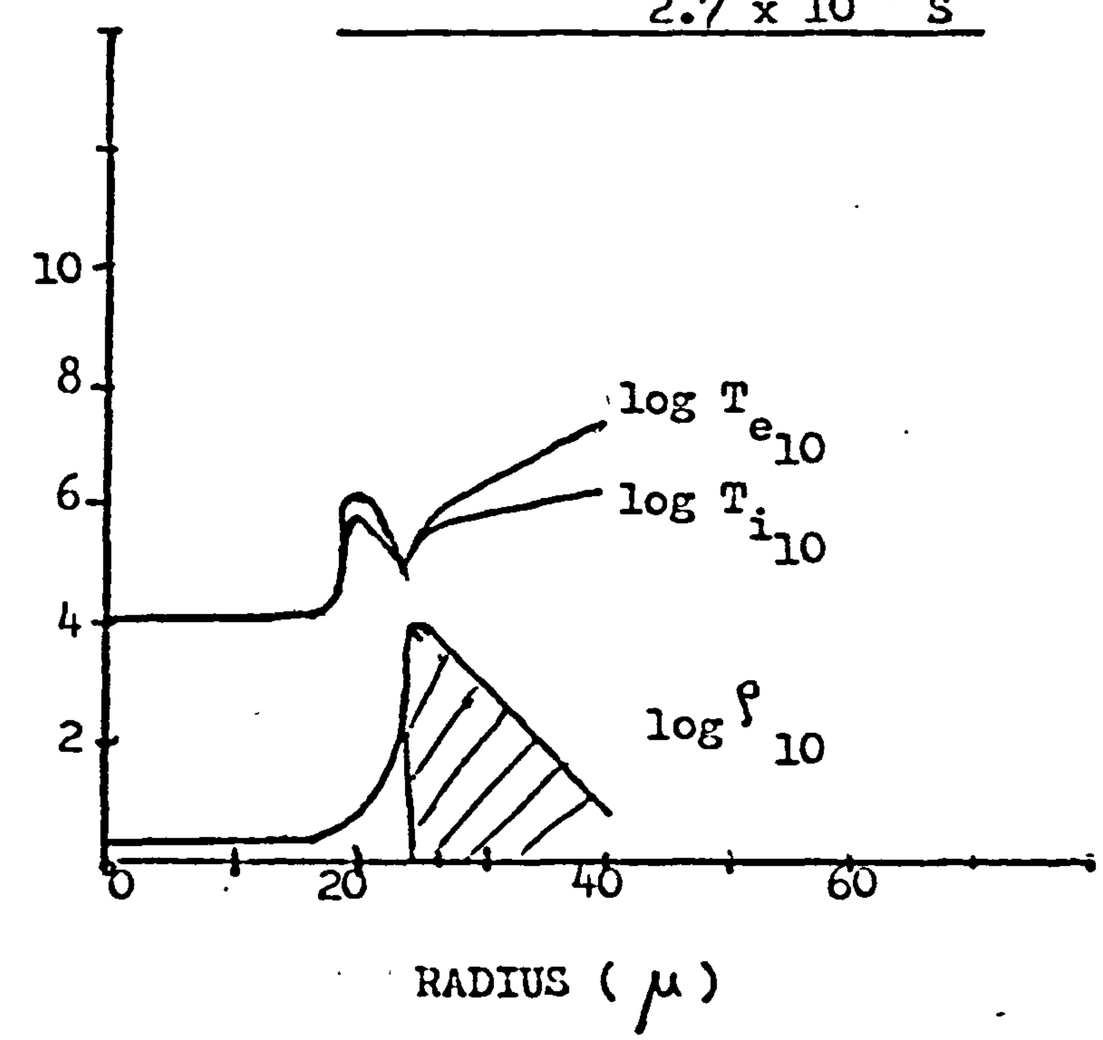

FIG. (5.15)

Y vs Z

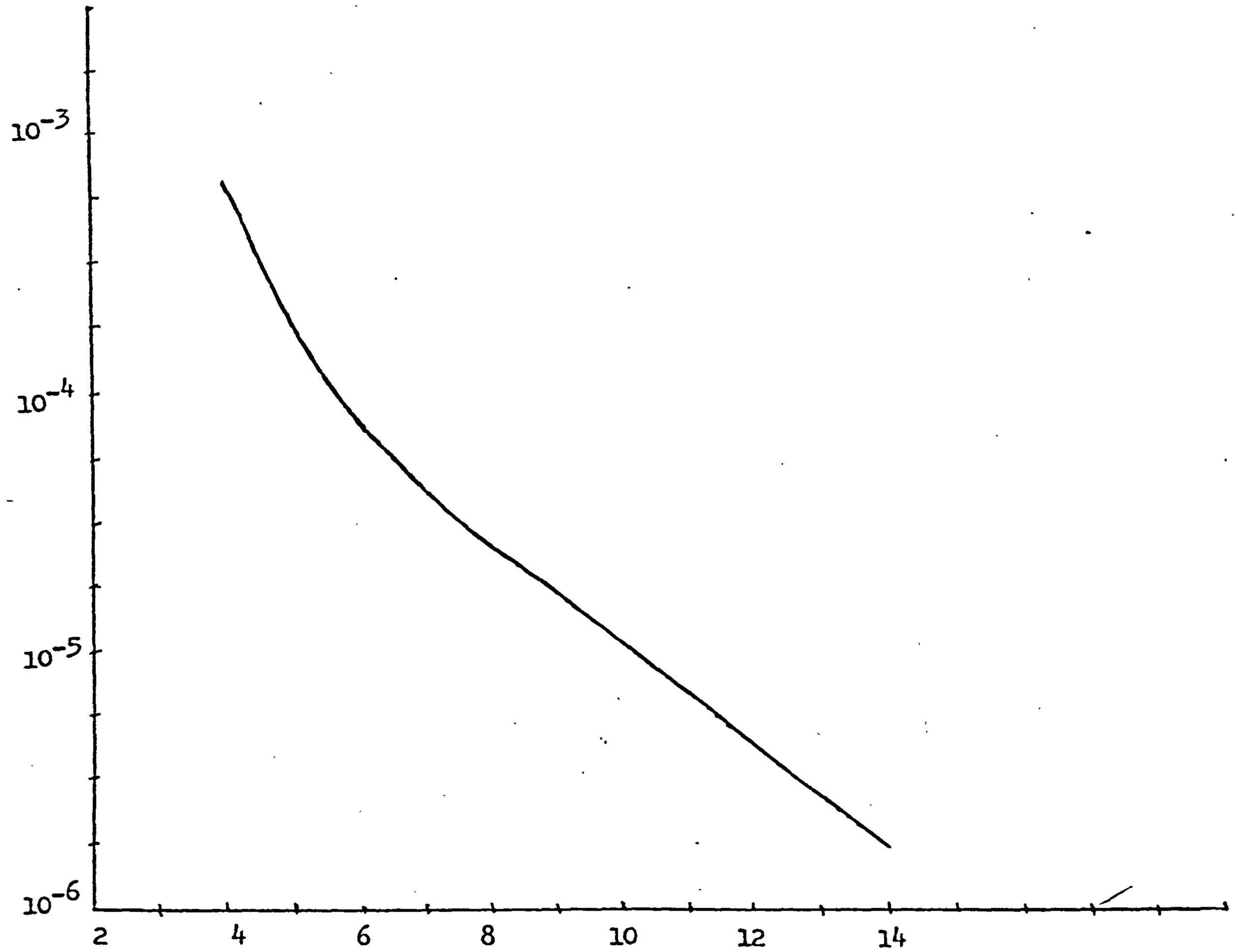

CHAPTER 6

Results: Radiative Pre-heat Effects

We have done extensive computer runs using the modified version of MEDUSA, described in chapter 4, to investigate pre-heat effects due to continuum radiation in laser-compression simulations. In section (6.1) we deal with solid carbon micro-spheres while in section (6.2) we treat carbon micro-balloons filled with carbon at a low density (~ 10 kg/$_m^3$).

(6.1) Solid Micro-spheres:

We consider a 10 - μg solid carbon micro-sphere with initial conditions

Initial Radius: $R_o = 106 \mu m$

Initial Density: $\rho_o = 2 \times 10^3$ kg/$_m^3$

Initial Temperature: $T_o = 6 \times 10^4$ K

An ideal laser-fusion pulse with total energy 600 J/$_{steradian}$ is used to compress this target. For comparison, we optimize the results not including the radiative transport and obtain a 10^4-fold compression. In this case, maximum density $\sim 3 \times 10^7$ kg/$_m^3$ is achieved corresponding to the initial laser power, $P_o = 10$ GW/$_{steradian}$ and pulse length, $\tau = 4$ nS. We find, however, that the maximum density falls to 5×10^6 kg/$_m^3$ when radiative transport is included. The reason for this marked decrease in compression is that the photons, because of their larger mean free path, penetrate the target faster than the thermal electrons, thereby pre-heating the uncompressed material, and as a result the final compression is degraded. To study this effect in detail, we plot in figs. (6.1) - (6.4) the implosion histories of the compression runs for the two above mentioned cases. Graphs (a) correspond to the case when the radiative transport is included while graphs (b) correspond to no radiative transport case. Fig.(6.1a) shows that the radiation temperature is higher than the

electron temperature ahead of the shocked material. Consequently, the electrons in this region are heated by the radiation field and the shock front spreads into the material at a faster rate. In fig. (6.2a), we see that the shock front has moved into the pellet, to a point, 25 -μm away from the centre whereas in fig. (6.2b) the shock front is at a distance of 40μm from the centre. From fig. (6.3a) we see that the disturbance has reached the centre, heating and compressing the matter to a temperature $\sim 5 \times 10^5$ K and density $\sim 4.5 \times 10^4$ kg/$_m^3$. However, in fig. (6.3b), the compression front is still at a distance of 12μm from the centre of the pellet. Figs. (6.4a) and (6.4b) are plotted at the time when the laser pulse is switched off and the compression has reached its maximum value. We see that in the former case, as a result of pre-compression and pre-heating of the target core, the final compression has dropped by a factor of 6.

In the following we discuss the effects of the variation in the initial laser power and pulse length on the radiative pre-heat.

$t = 8.53 \times 10^{10}$s

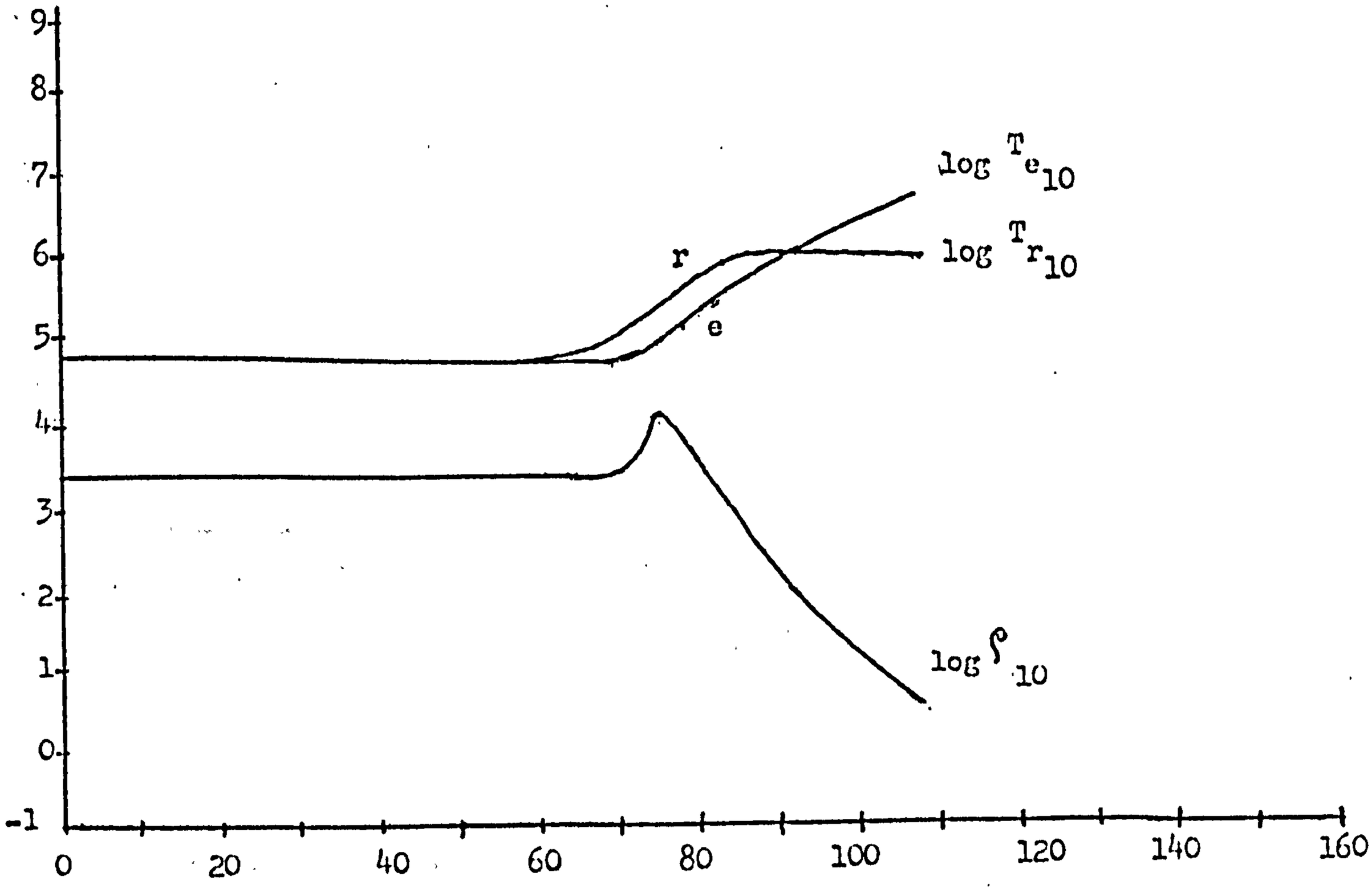

RADIUS (μ) Fig. (6.1a)

8.6×10^{-10}s

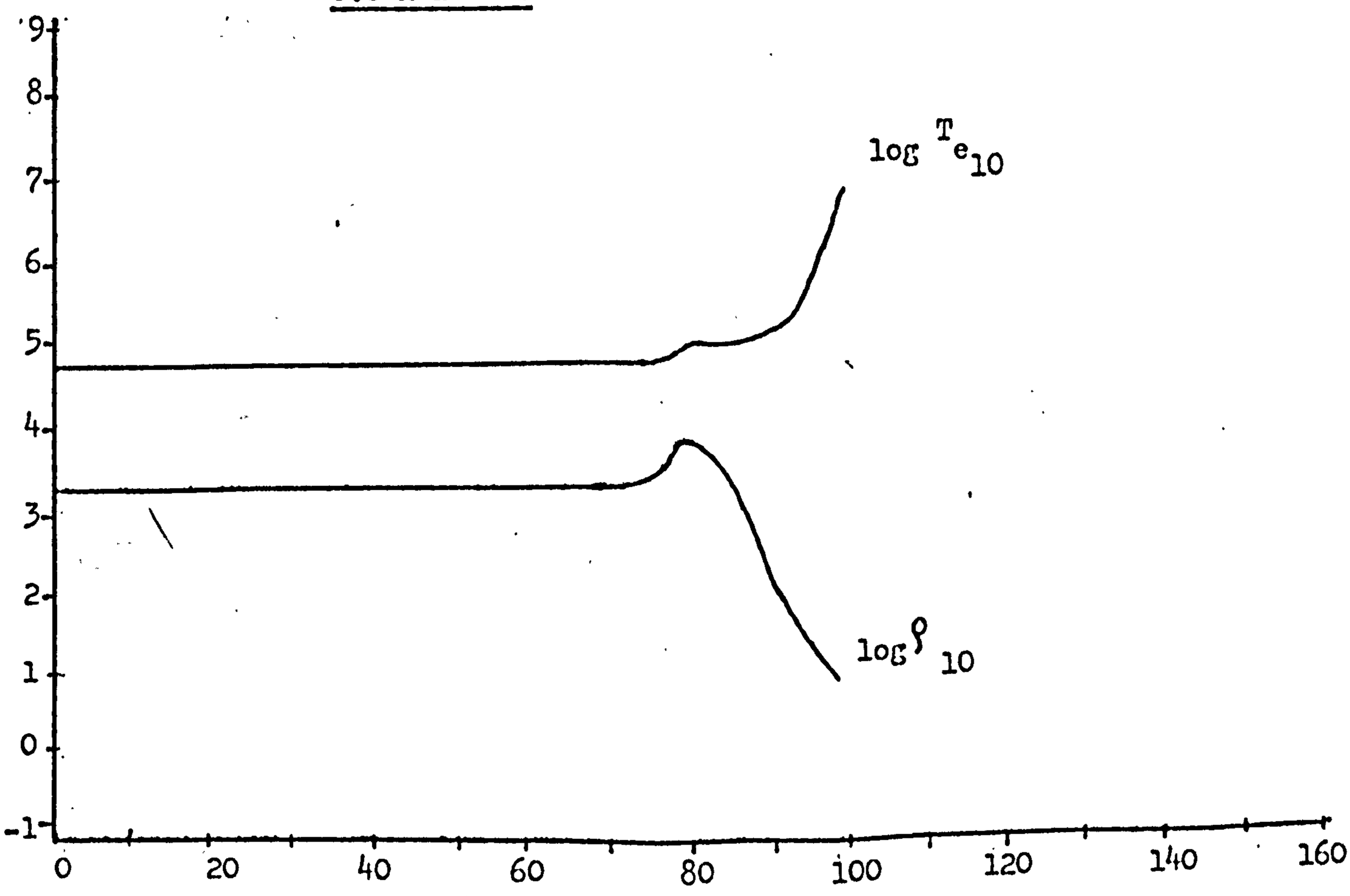

RADIUS (μ) Fig. (6.1b)

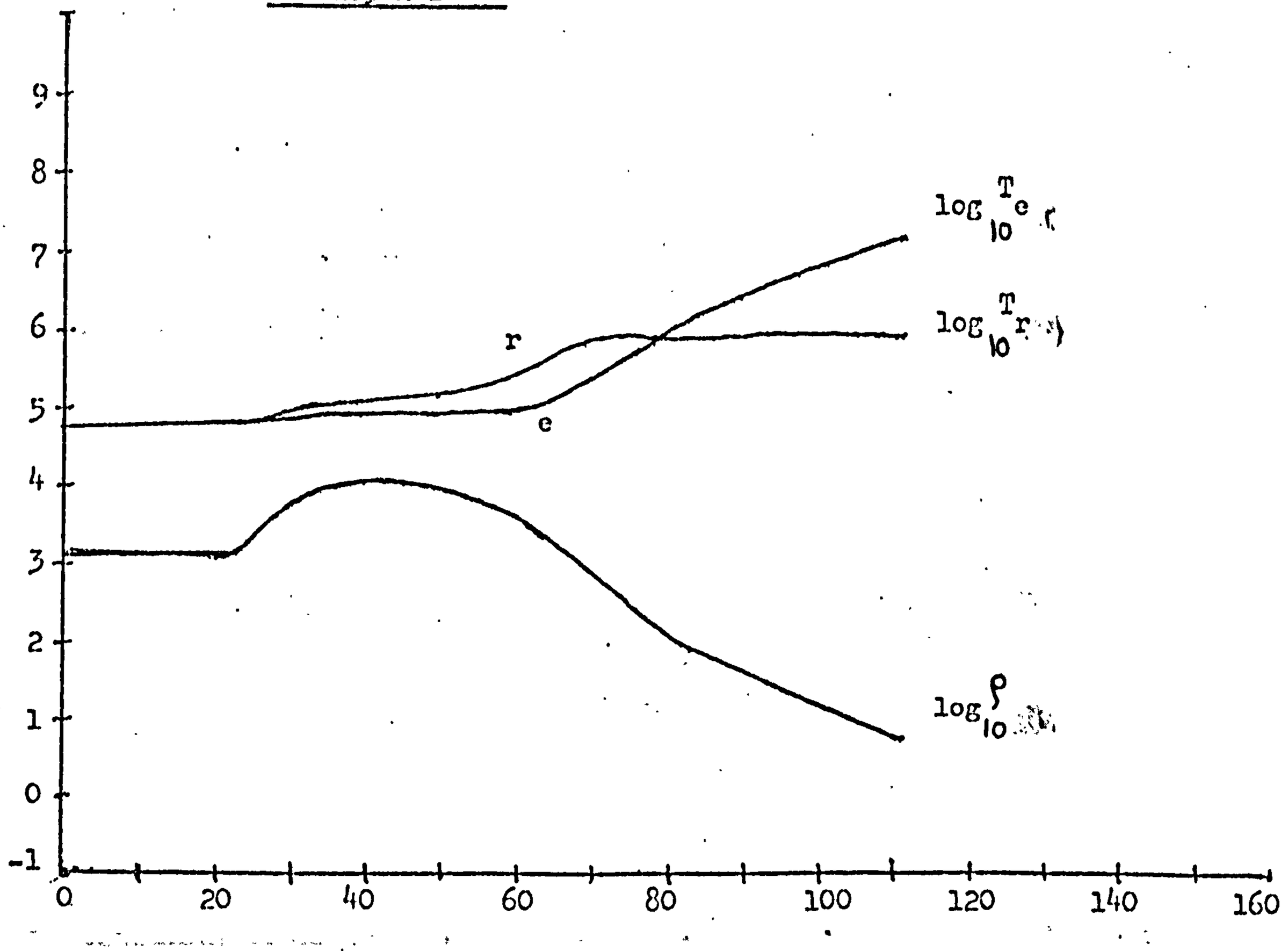

Fig. (6.2a)

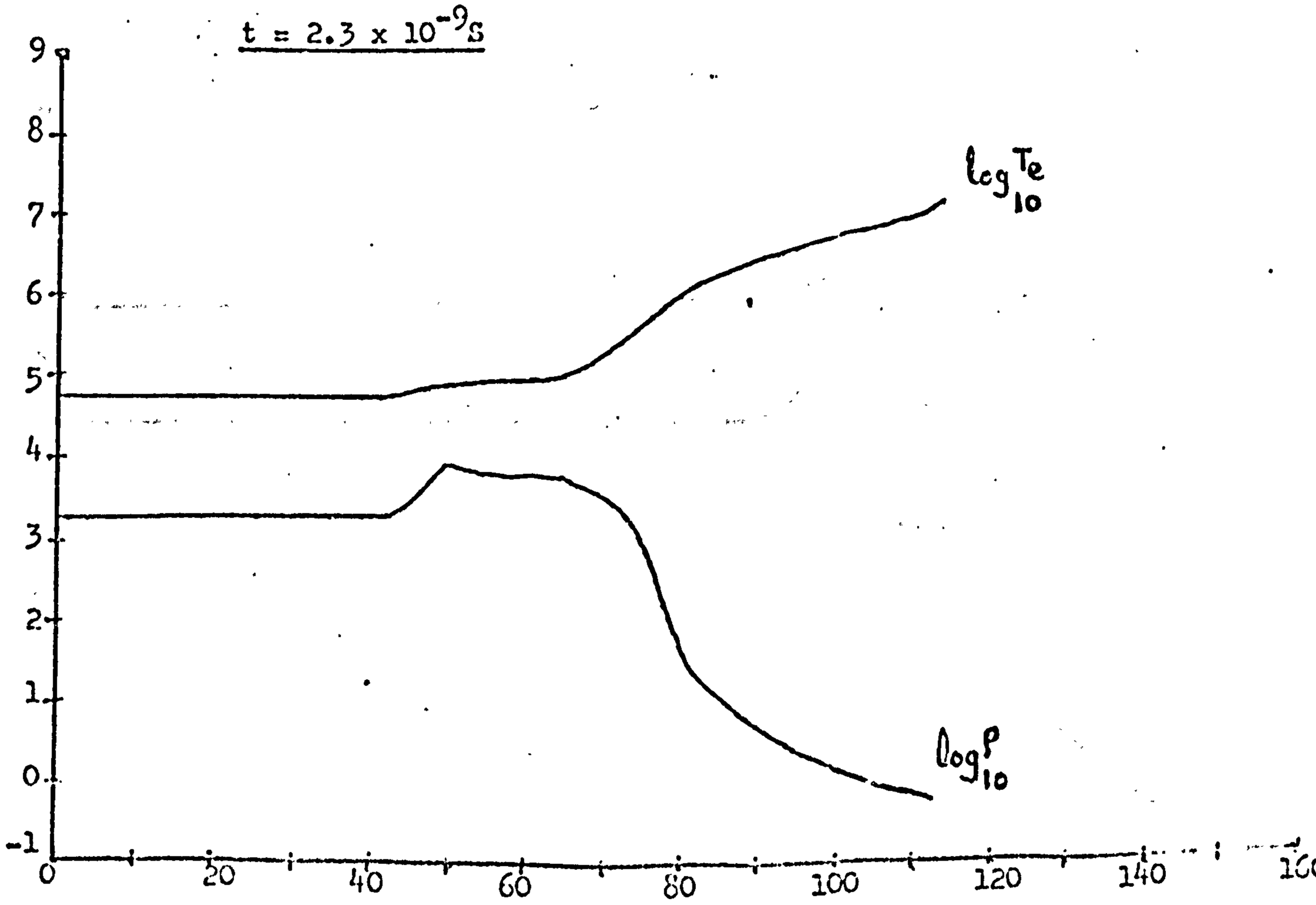

Fig. (6.2b)

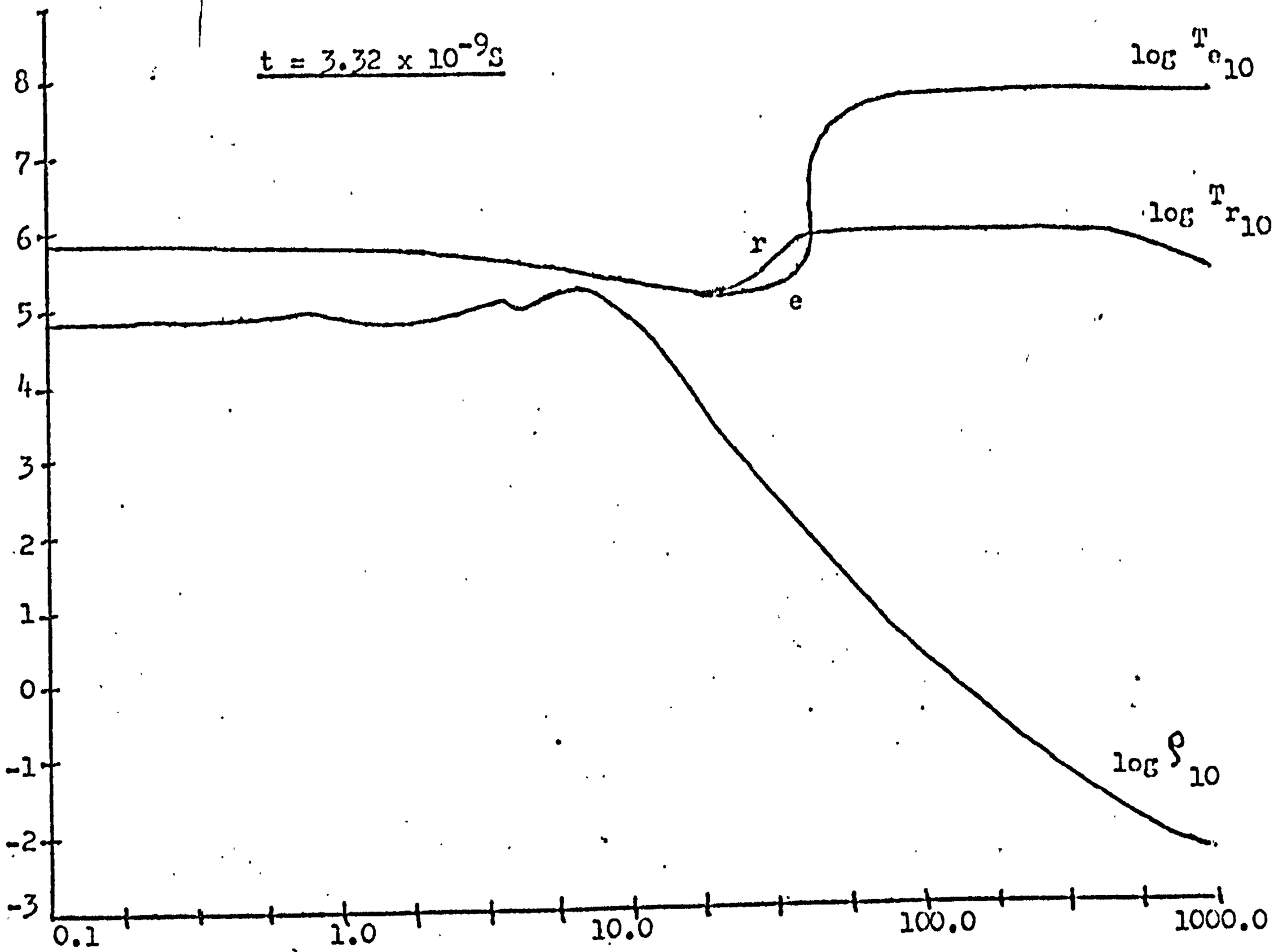

Fig. (6.3a)

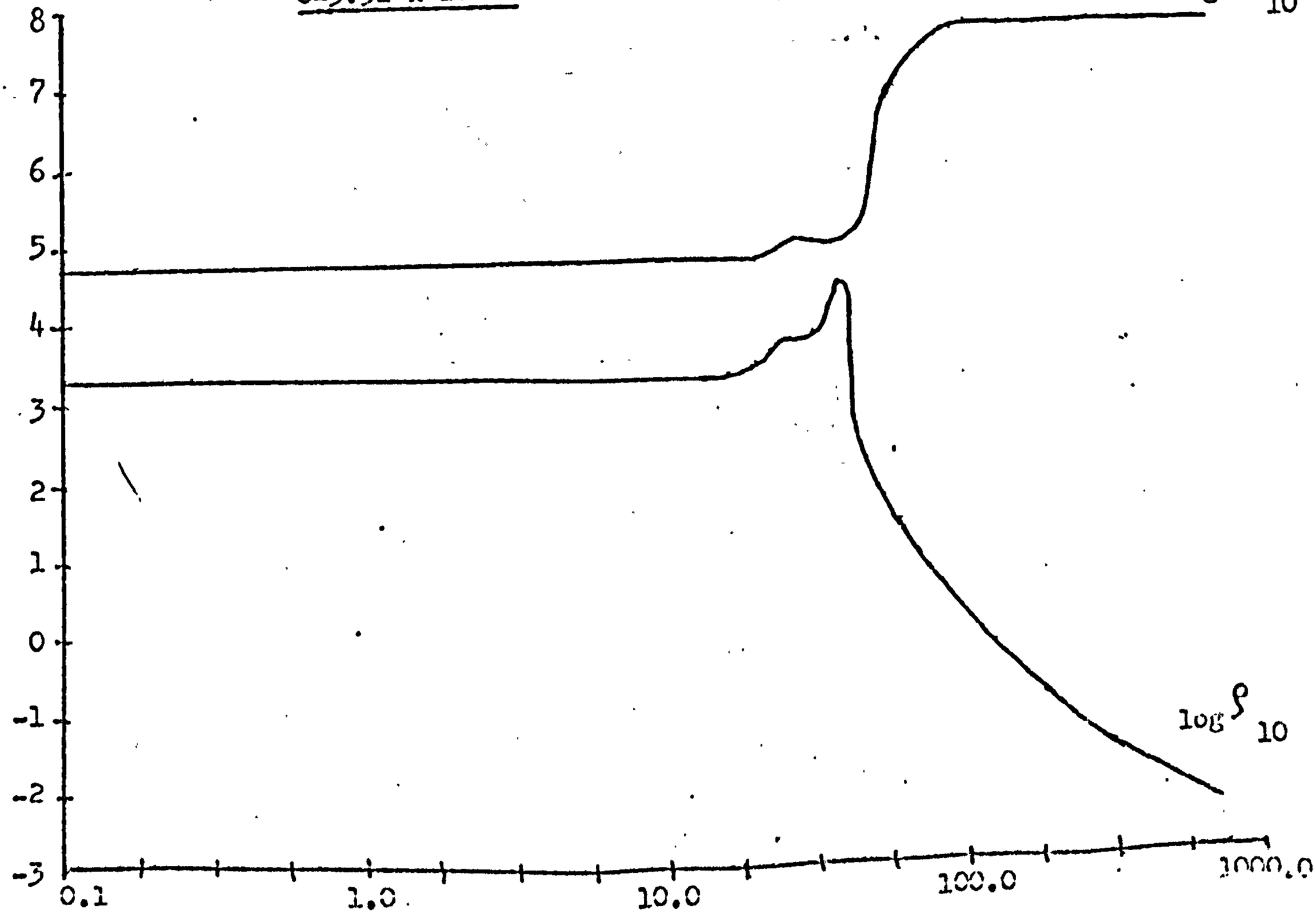

Fig. (6.3b)

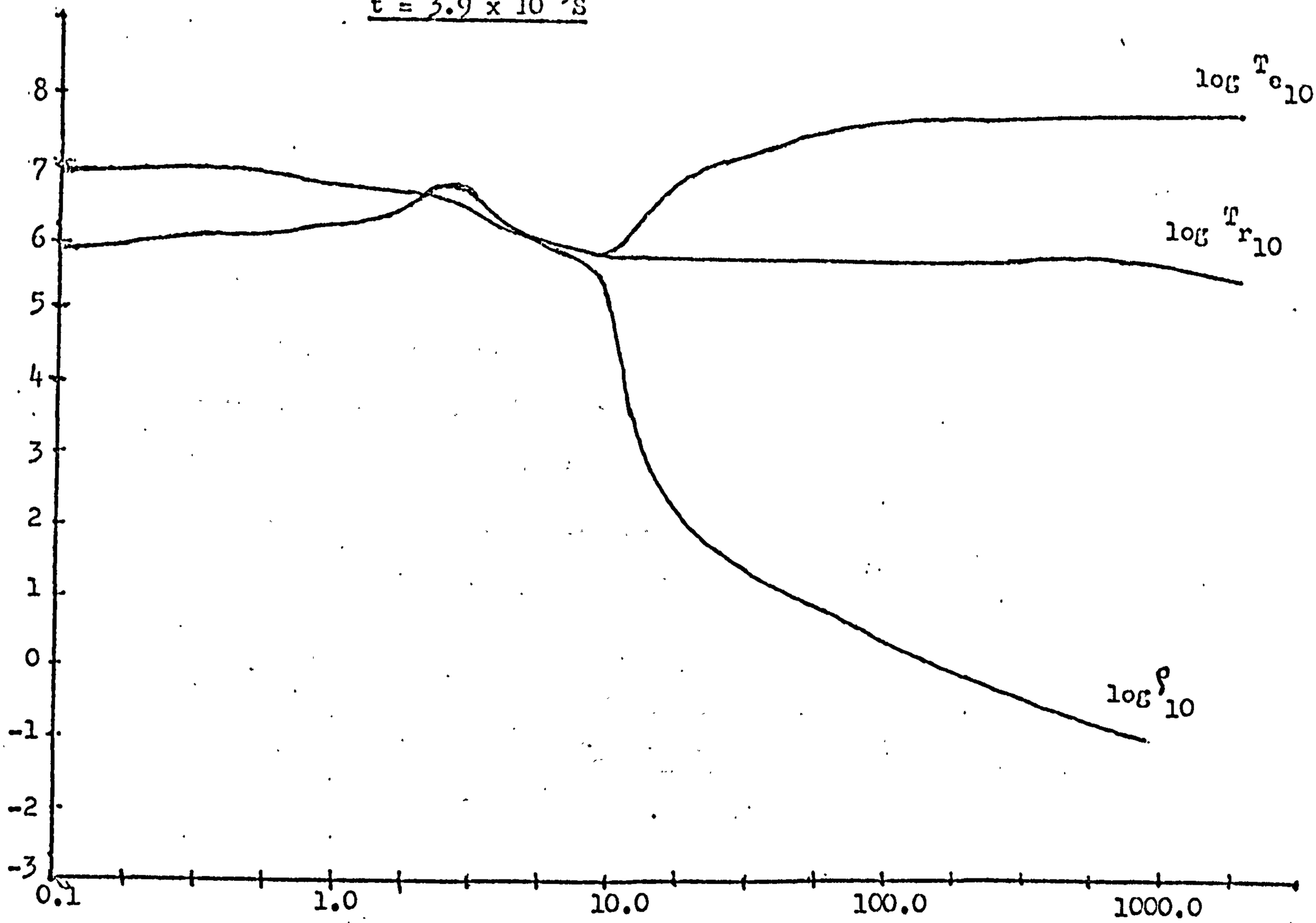

Fig. (6.4a)

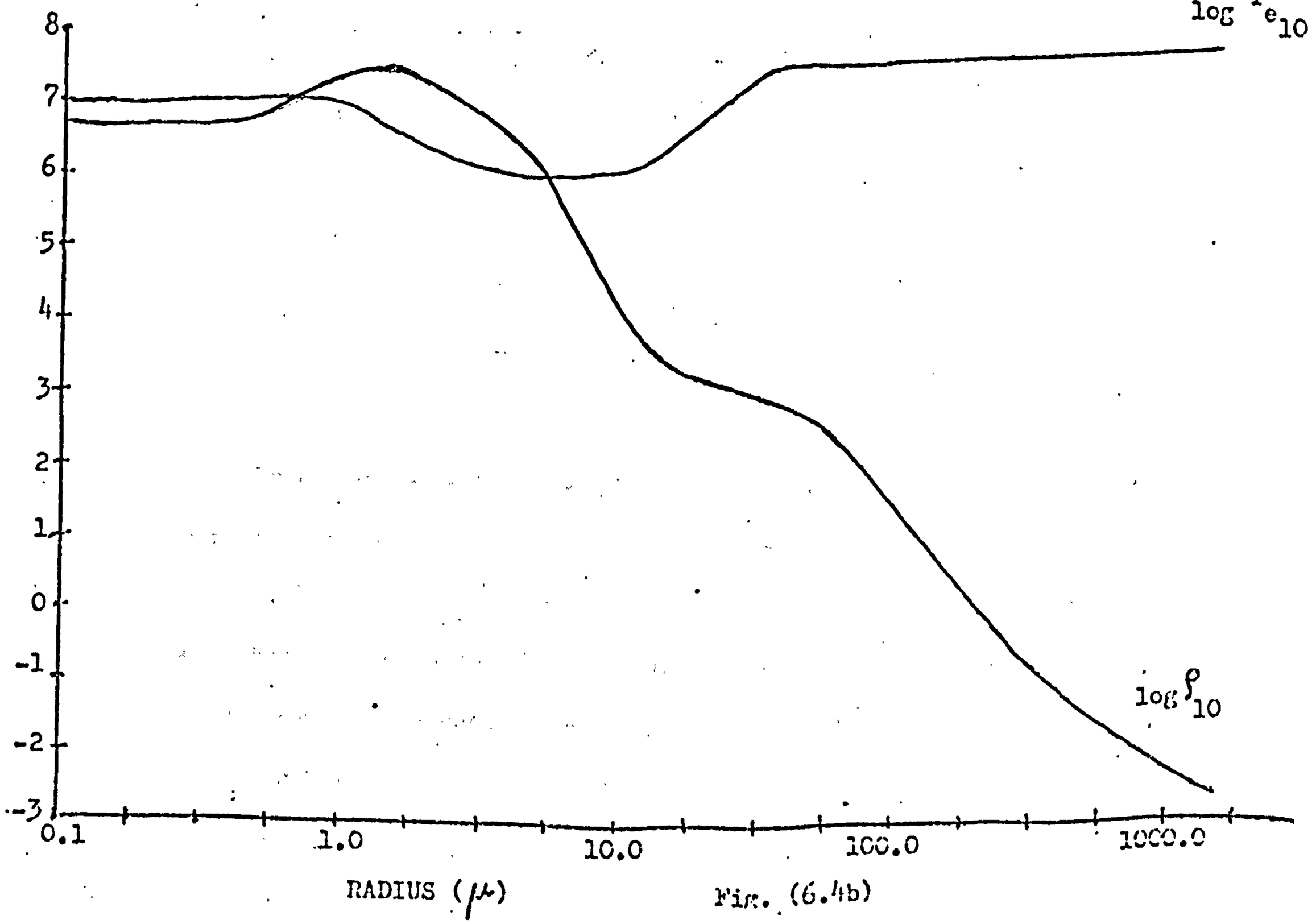

Fig. (6.4b)

(6.1a) Compression vs P_0 (τ constant):

We have investigated the effect of the initial laser power on the radiative pre-heat, keeping the pulse length and the total laser energy constant. The maximum densities achieved without radiative transport and with radiative transport, for various values of P_0 are given in table 6.1. The decrease in the compression, ρ_d, which is the ratio between the maximum densities achieved without radiative transport and with radiative transport respectively, is plotted in fig. (6.5).

Table (6.1)

τ = 4 ns

P_0 (GW/steradian)	No Radiative Transport ρ_m (kg/m^3)	Radiative Transport Case ρ_m (kg/m^3)
6	5×10^6	3.9×10^6
8	1.8×10^7	6×10^6
9	2.4×10^7	6×10^6
10	3×10^7	5×10^6
15	9.4×10^6	1.3×10^6
20	3.5×10^6	6.3×10^5

From the above table we see that the radiative pre-heat becomes more effective as the initial laser power is increased. However, fig.(6.5) shows that ρ_d increases with P_0 up to a value, $P_0 = 15$ GW and then starts to decrease again. This is because when the initial laser power is increased too much from its optimum value, shock heating dominates, as can be seen from fig. (6.6a) and (6.6b) where we plot $\log \rho_{10}$ and $\log T_{e_{10}}$ for P_0 = 10 GW/steradian and P_0 = 20 GW/steradian

without radiative transport at a time ~ 3.32 ns, respectively. In the former case, the compression is still at a distance of 30 μm from the pellet centre whereas in the latter case it has reached the target centre, pre-heating and pre-compressing the material. Thus with an appreciably higher initial laser power, shock heating competes with radiative pre-heat.

ρ_d Vs P_o

$\tau = 4$ ns

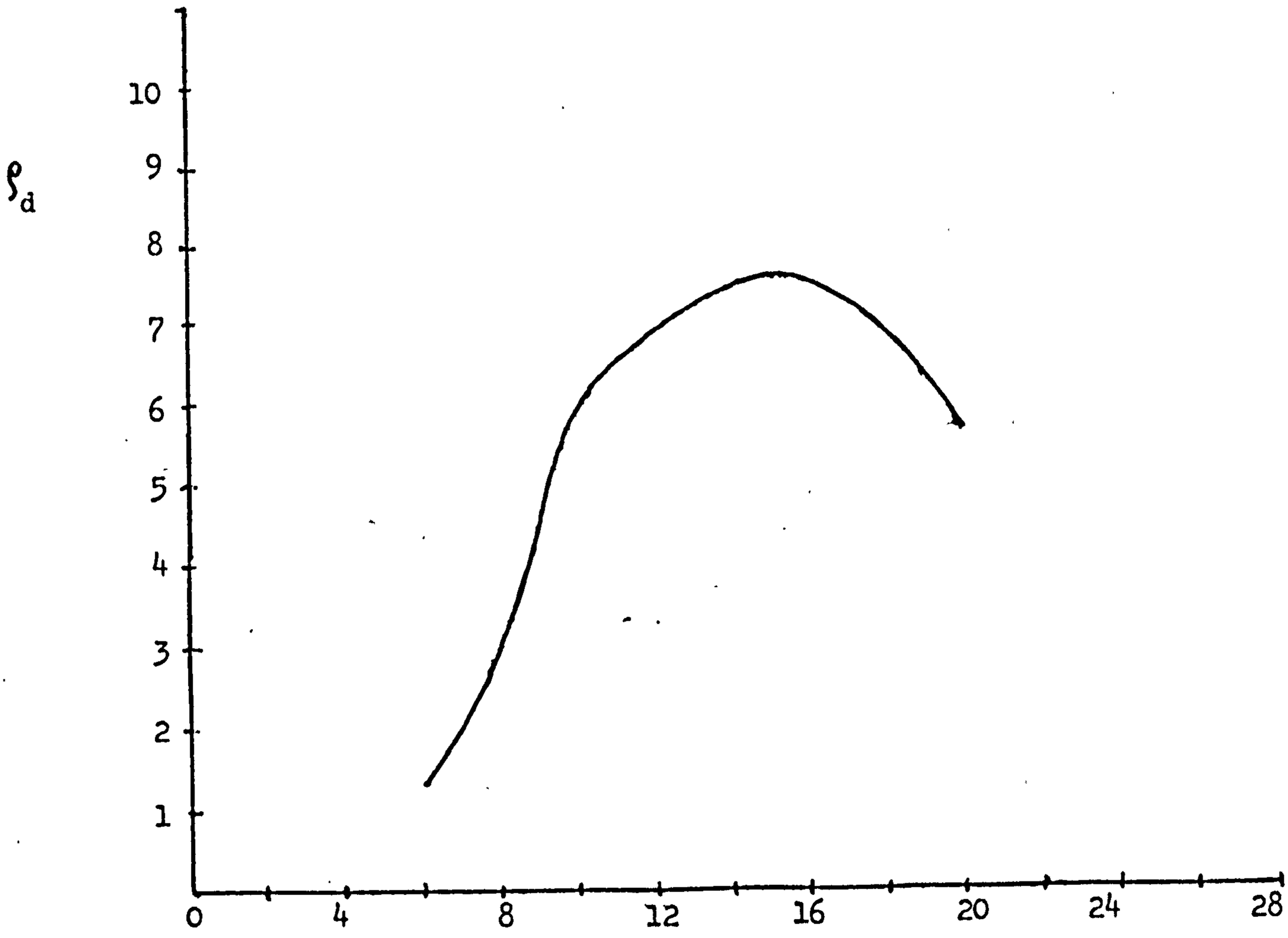

Fig. (6.5)

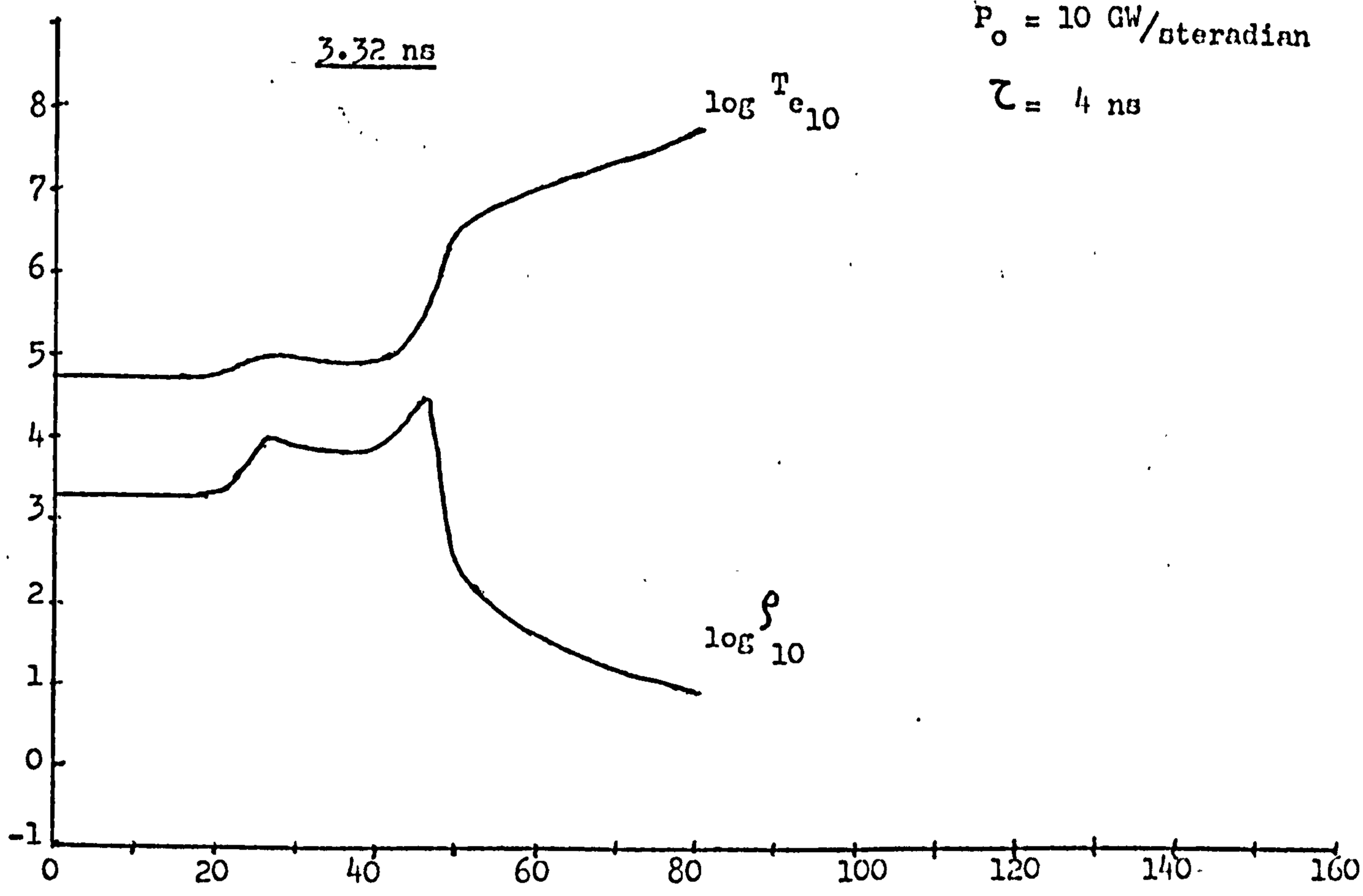

P_o = 10 GW/steradian

τ = 4 ns

Fig. (6.6a)

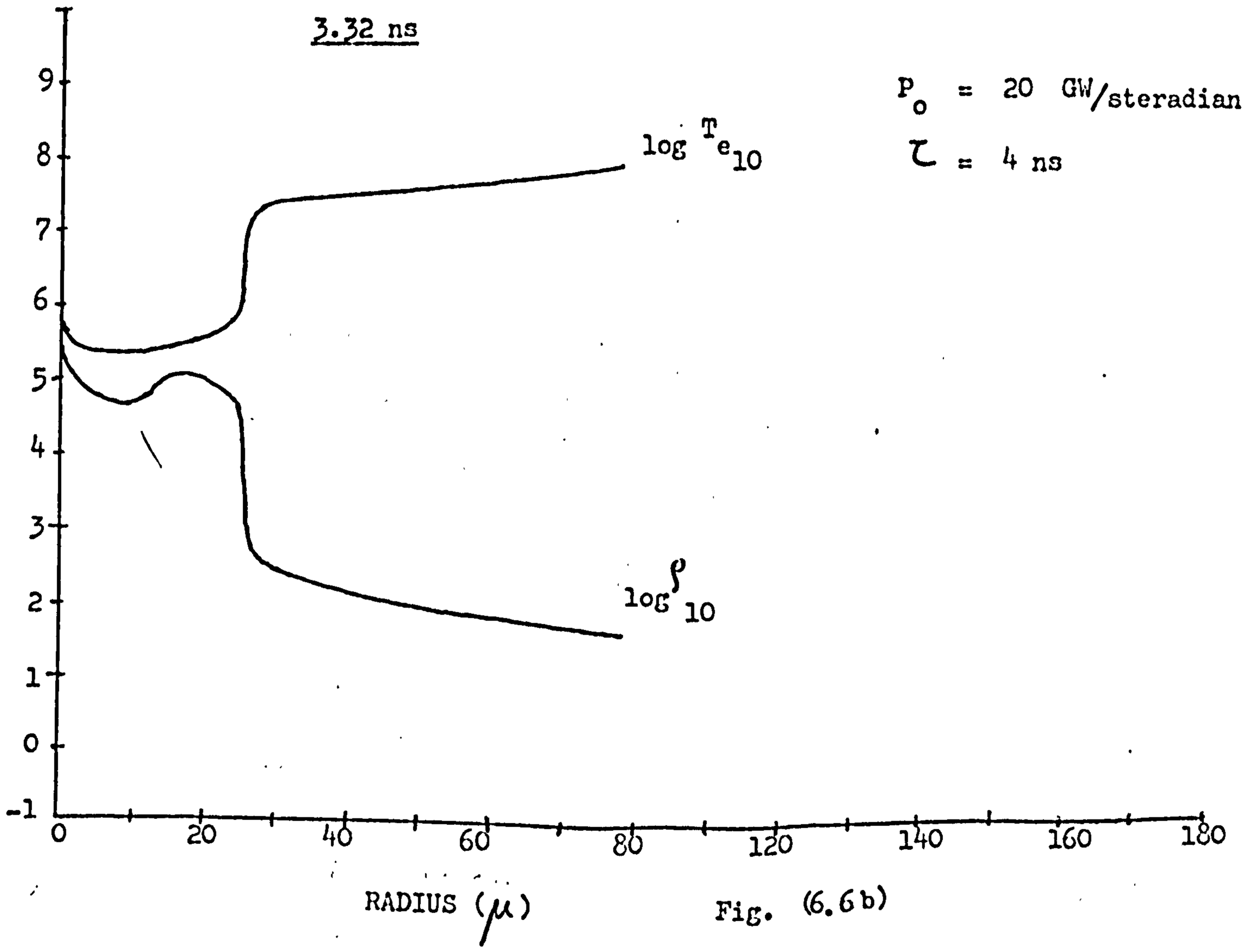

P_o = 20 GW/steradian

τ = 4 ns

Fig. (6.6b)

(6.1b) Compression vs τ (P_o constant):

We now discuss the effect of varying the laser pulse length, on radiative pre-heat, keeping the initial power, P_o and the total energy in the laser pulse constant. The maximum densities achieved with and without radiative transport for various values of τ, are given in table (6.2) and ρ_d vs τ is plotted in fig. (6.7).

Table (6.2)

P_o = 10 GW/Steradian

	No Radiative Transport	Radiative Transport Case
(ns)	ρ_m (kg/m^3)	ρ_m (kg/m^3)
3	5×10^6	3.5×10^6
3.6	3×10^7	5.6×10^6
3.8	3×10^7	5.1×10^6
4.0	3×10^7	5×10^6
4.5	1.6×10^7	2.5×10^6

Table (6.2) shows that the compression is insensitive to τ, in the range 3.6 to 4 ns. Also fig. (6.7) shows that ρ_d is constant in this range. For shorter laser pulses, ρ_d decreases rapidly. We thus conclude that the radiative pre-heat is less effective for shorter laser pulses.

$$\frac{\rho_d \; v_s \; \tau}{P_o = 10 \text{ GW/steradian}}$$

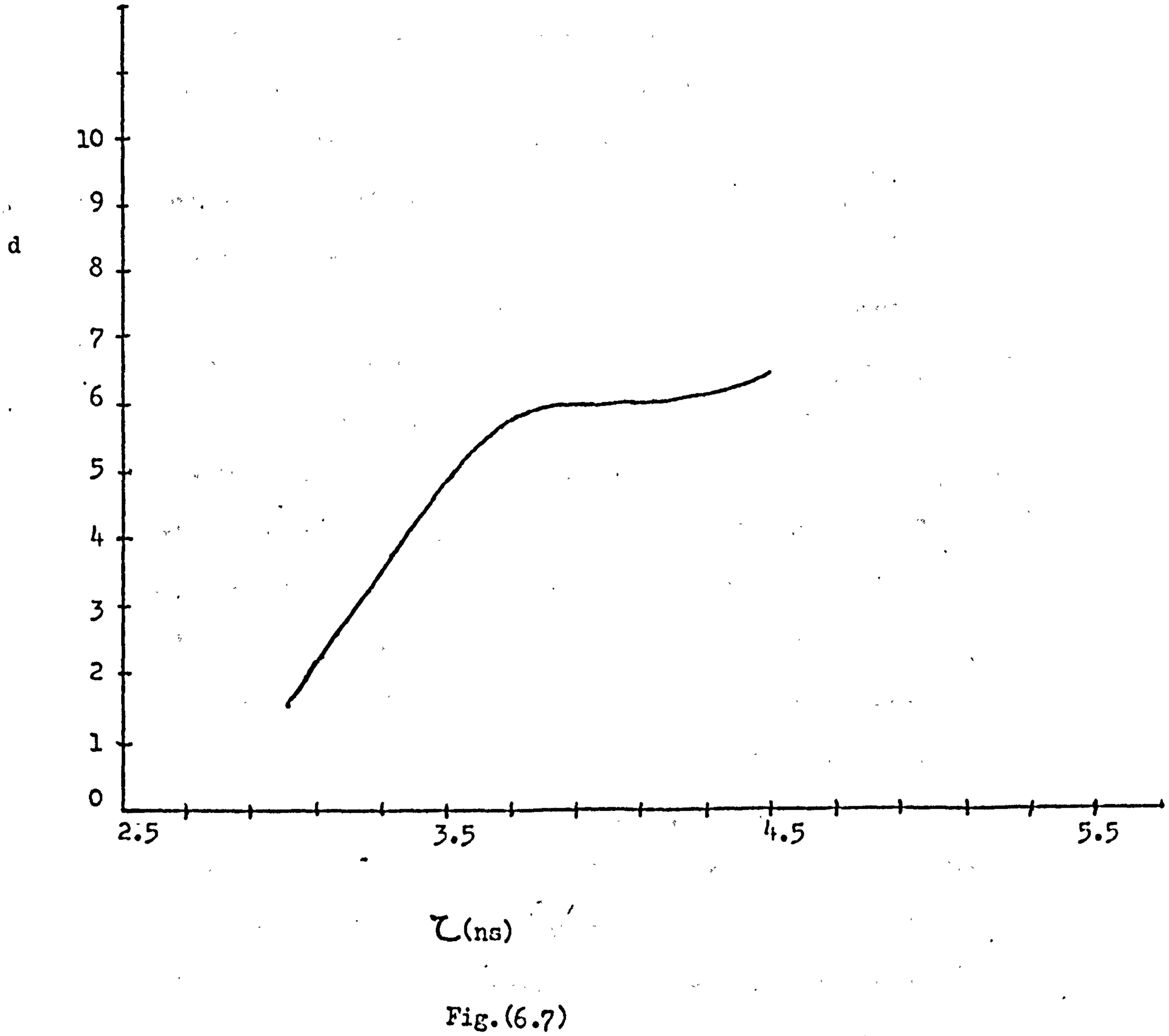

Fig.(6.7)

(6.2) Gas filled micro-balloons:

In this section we deal with a carbon micro-balloon filled with carbon at a density = 10 $kg/_{m}^{3}$. The inner radius of the micro-balloon is 35 μm while the wall thickness is 1 μm. The initial electron, ion and radiation temperatures are = 6×10^{4} K.

In the present work, our aim is to show the effect of the radiation on the compression of the target and not to simulate any particular experiment. It is therefore a reasonable approximation to consider a carbon micro-balloon filled with carbon at gas density. This approximation leads to computational simplifications.

We consider that the target is irradiated by a laser pulse which is Gaussian in time and has total energy 1.7 $J/_{steradian}$. The $\frac{1}{e}$ width of the pulse, τ = 60 ps while the maximum laser power is 1.62×10^{10} $W/_{steradian}$. For comparison, we simulate the compression of the target with and without the radiative transport. The implosion history of the target, in the two cases, is plotted in fig. (6.9) - (6.11), the shell region is cross-hatched. The graphs (a) correspond to the case when radiative transport is included while graphs (b) correspond to the case when radiative transport is omitted. Fig. (6.9a) shows that the radiation temperature, T_r, in the gas region has increased to 5.4×10^{5} K and that due to the electron-radiation interaction the electron temperature has gone up to 8×10^{4} K.

Fig. (6.10a) shows that the radiation temperature in the gas region becomes $\sim 8 \times 10^{5}$ K and the electron temperature is $\sim 1.4 \times 10^{5}$ K. In fig. (6.11a), the two temperatures have further increased to 10^{6} k and 2.4×10^{5} K respectively. This increase in the temperature of the uncompressed gas region causes the inner pressure to increase and therefore the final compression is reduced. In fig. (6.12) we plot the $\log T_{e_{10}}$ and $\log \rho_{10}$ for the two cases, at the time when the compression has achieved its maximum value. We see from

fig. (6.12b) that the maximum shell density is $\sim 10^5$ kg/$_m^3$ while the gas, on the average is compressed to a density $\sim 2.5 \times 10^4$ kg/$_m^3$. However, in fig. (6.12a) we find that the maximum shell density has dropped to 8×10^3 kg/$_m^3$ whereas the average compression in the gas region is $\sim 10^4$ kg/$_m^3$. We therefore see that as a result of radiative pre-heat, the gas compression is reduced by a factor of 2.5.

Micro-spheres vs Micro-balloons:

It is noticeable that in the case of a solid micro-sphere, the radiation energy diffuses more slowly in comparison with that in a thin micro-balloon. The reason for this is that the dimensions of the micro-balloon are comparable with the mean free path of the photons so that the photons penetrate straight into the centre of the micro-balloon, heating the gas almost uniformly. However, in the case of a micro-sphere, the photon mean free path << the dimensions of the target and the radiation diffuses in a manner similar to thermal electrons.

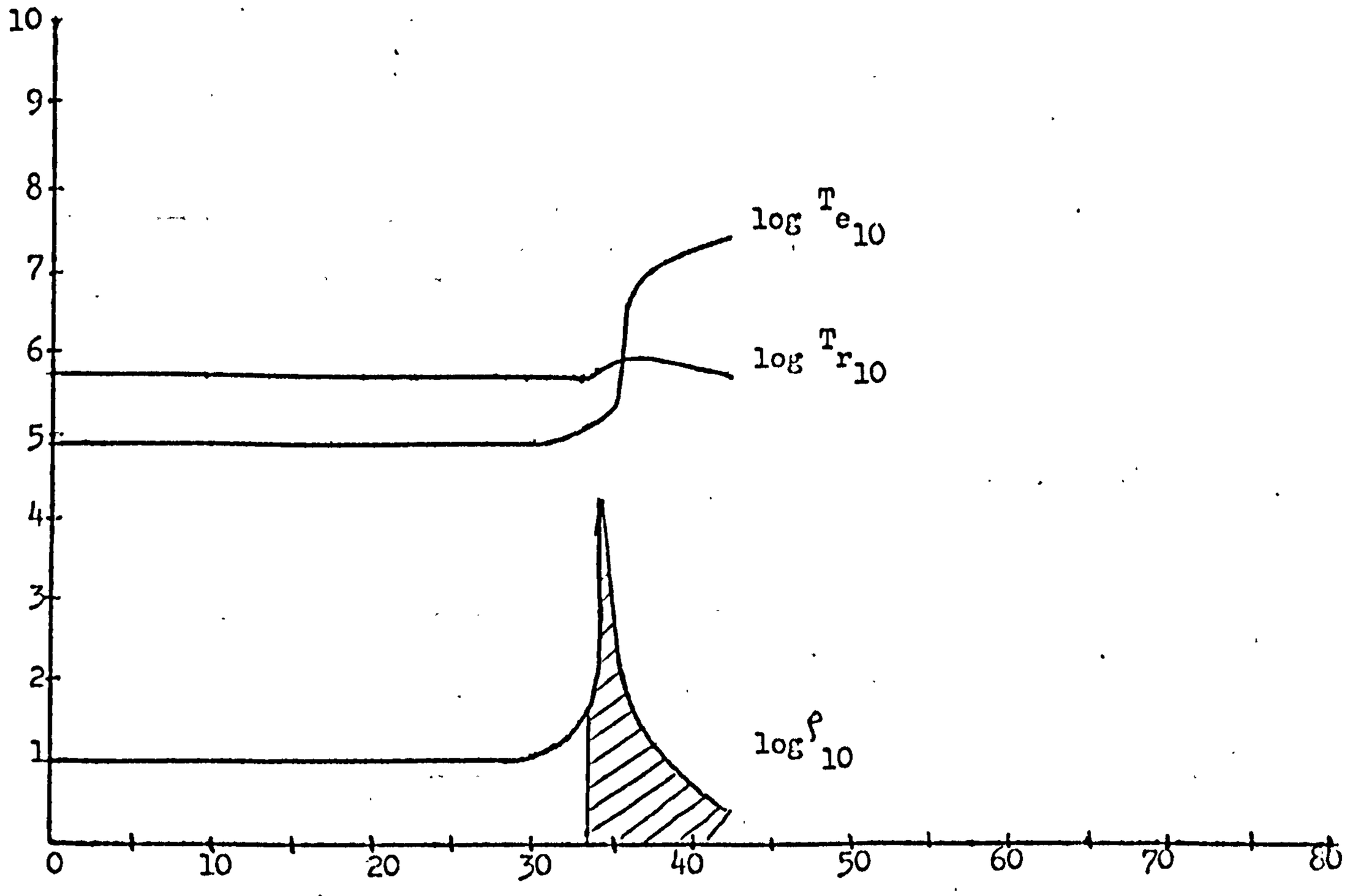

Fig. (6.8a)

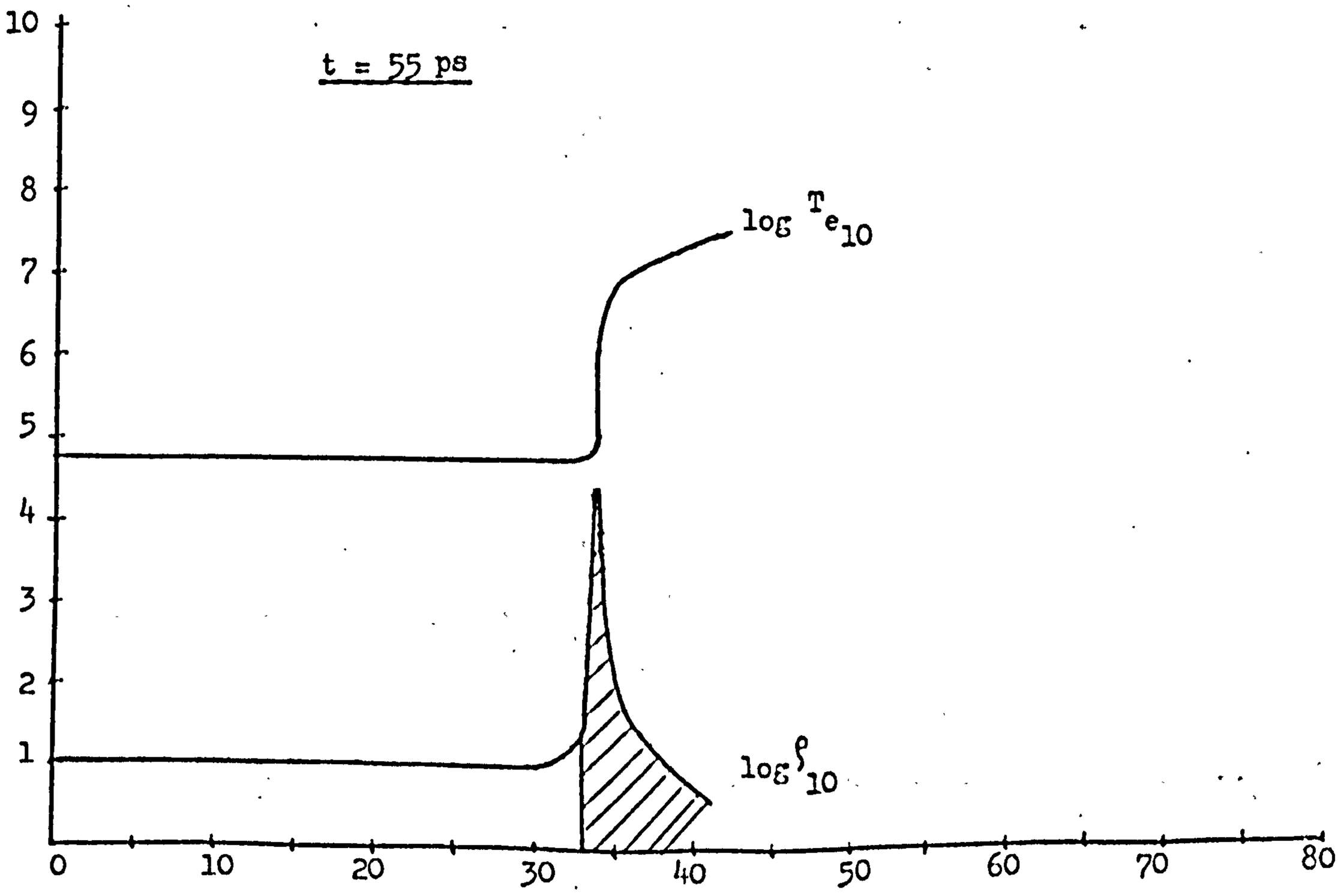

Fig. (6.8b)

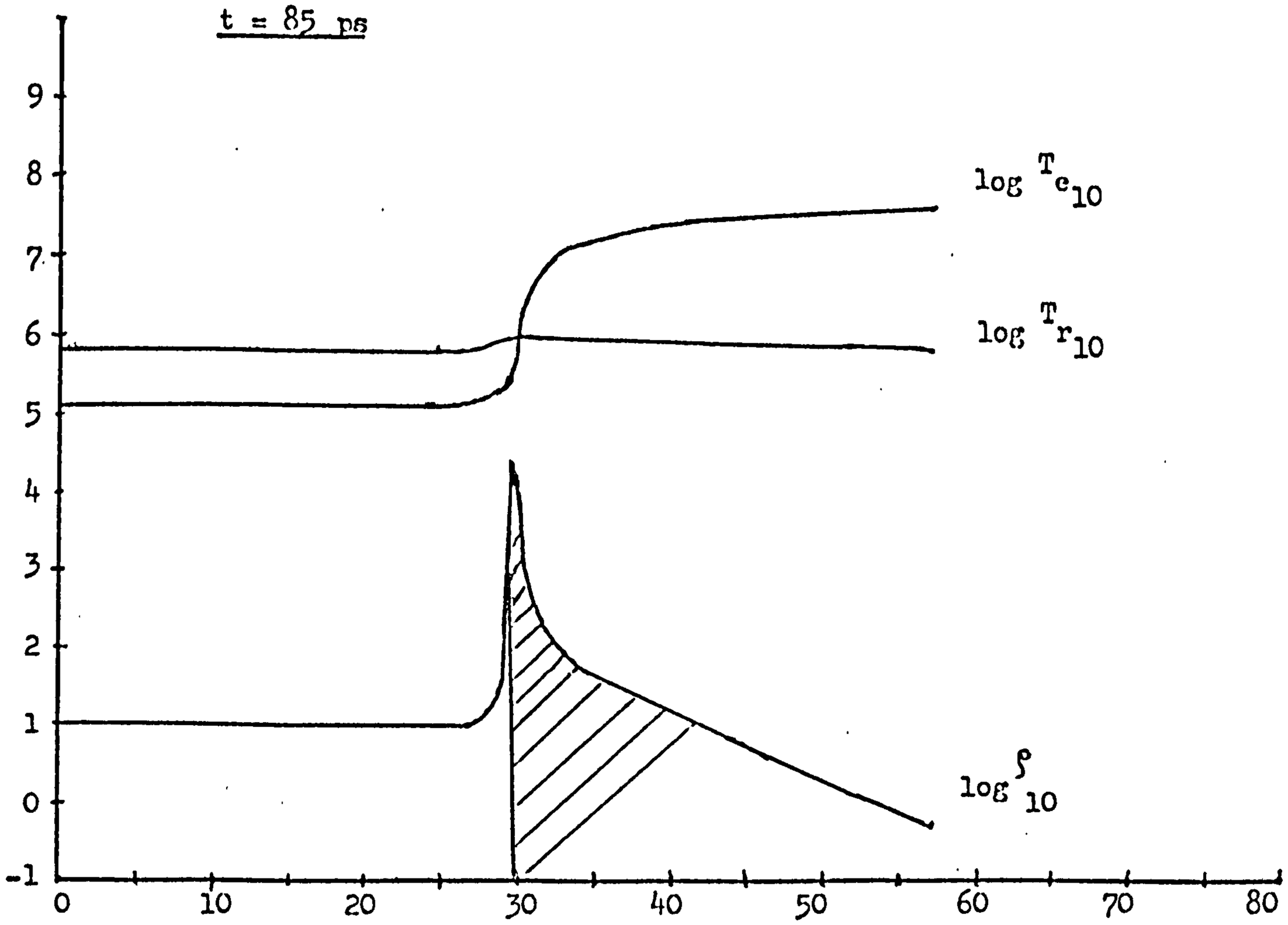

Fig. (6.9 a)

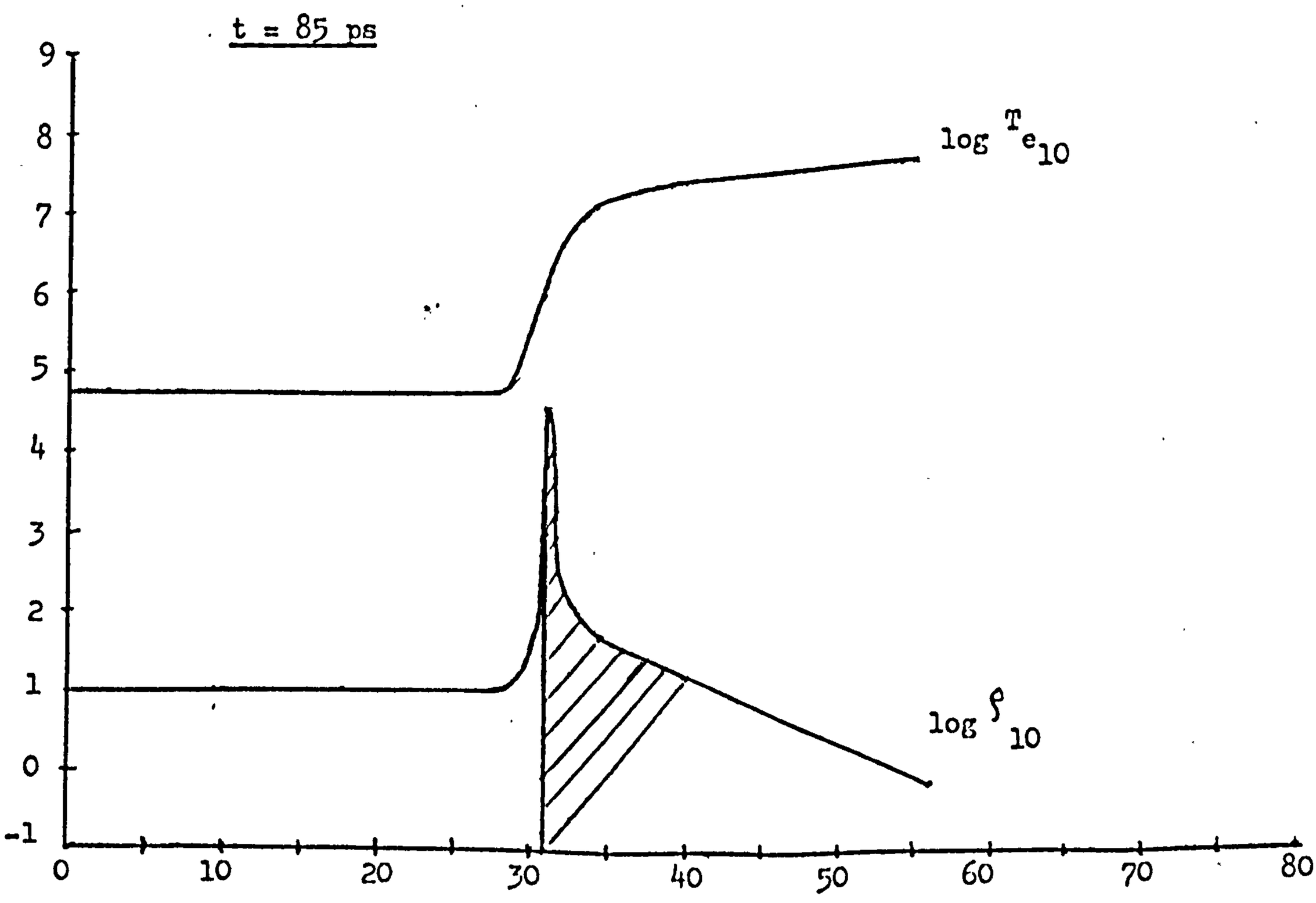

Fig. (6.9 b)

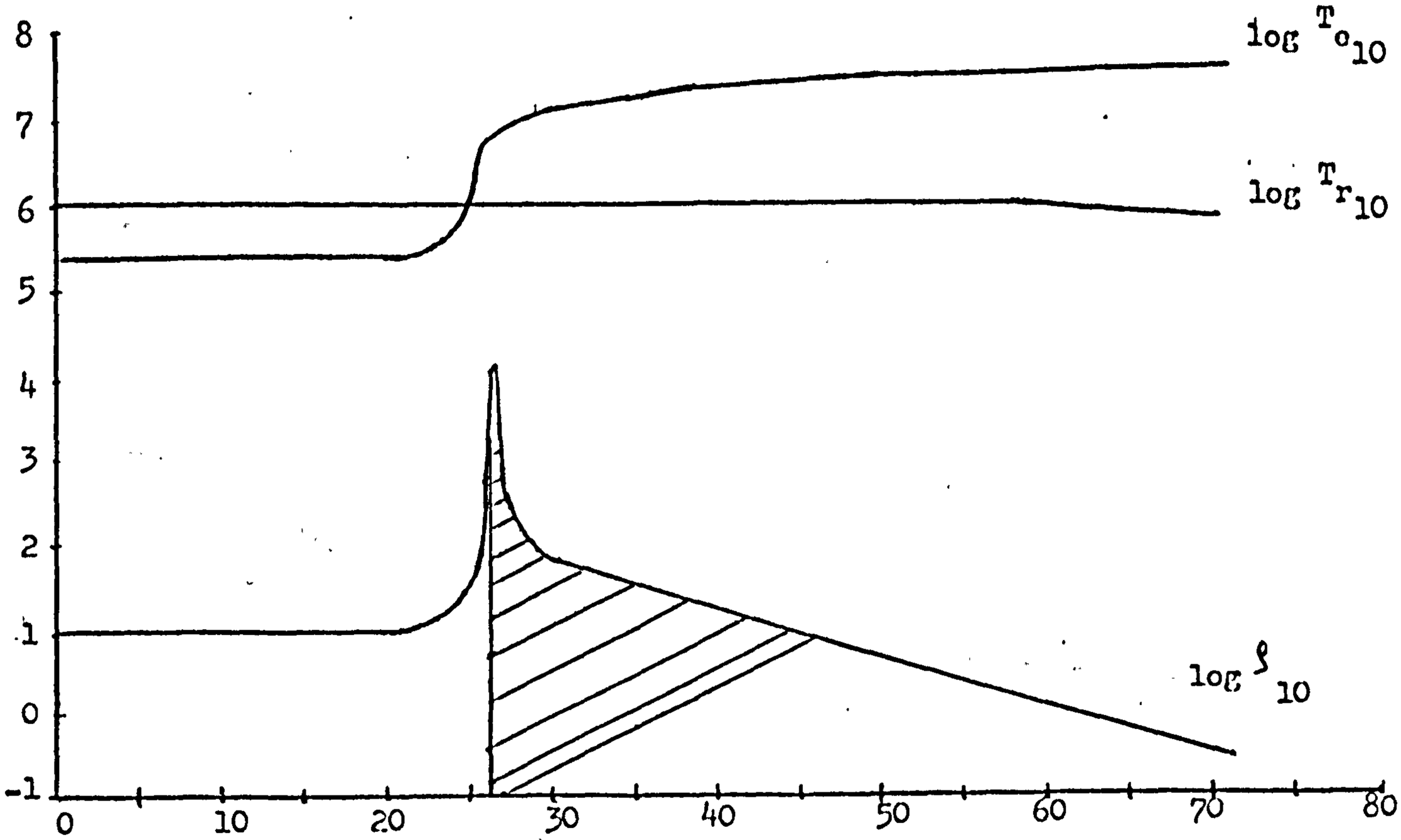

Fig. (6.10a)

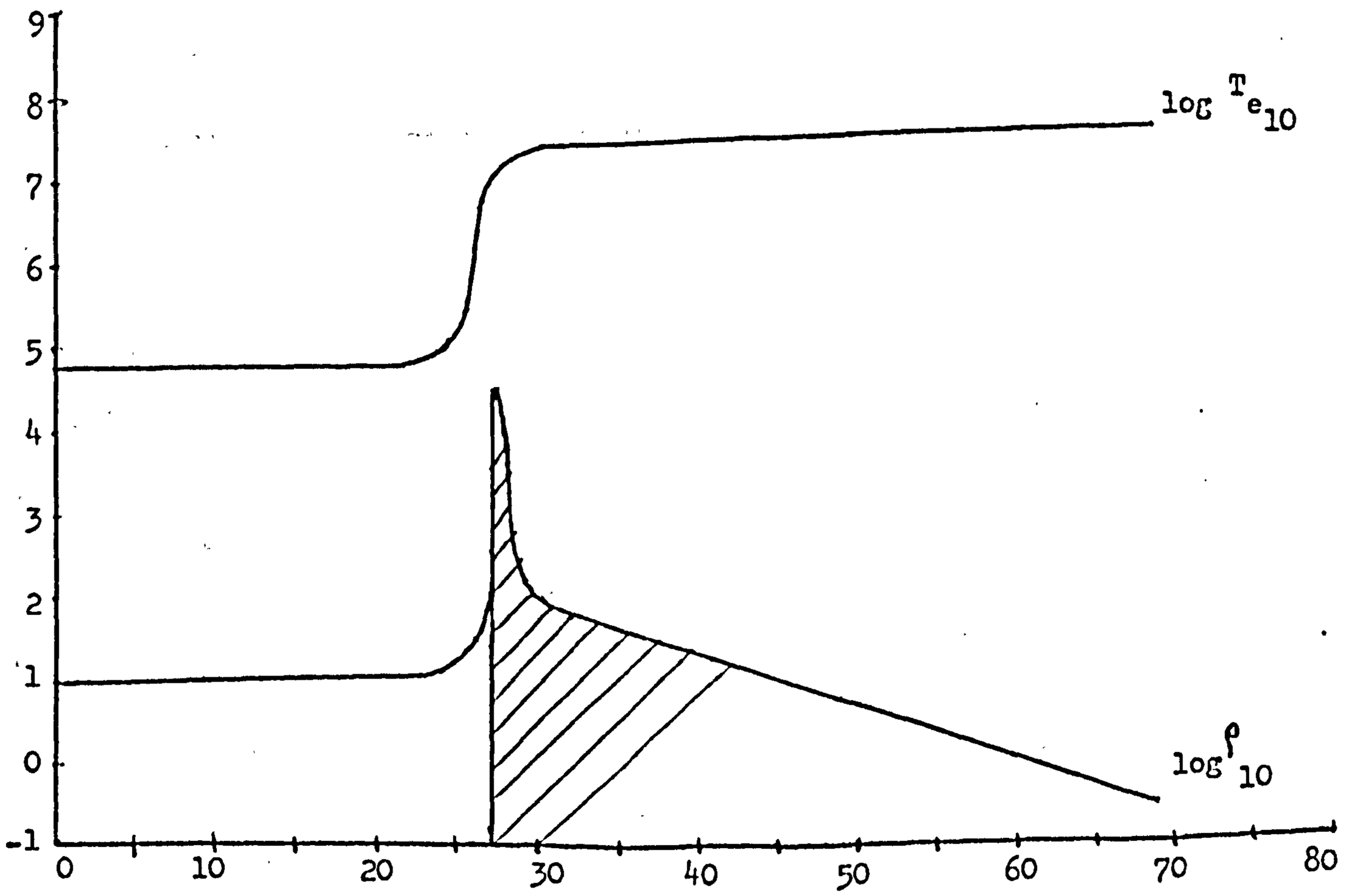

Fig. (6.10b)

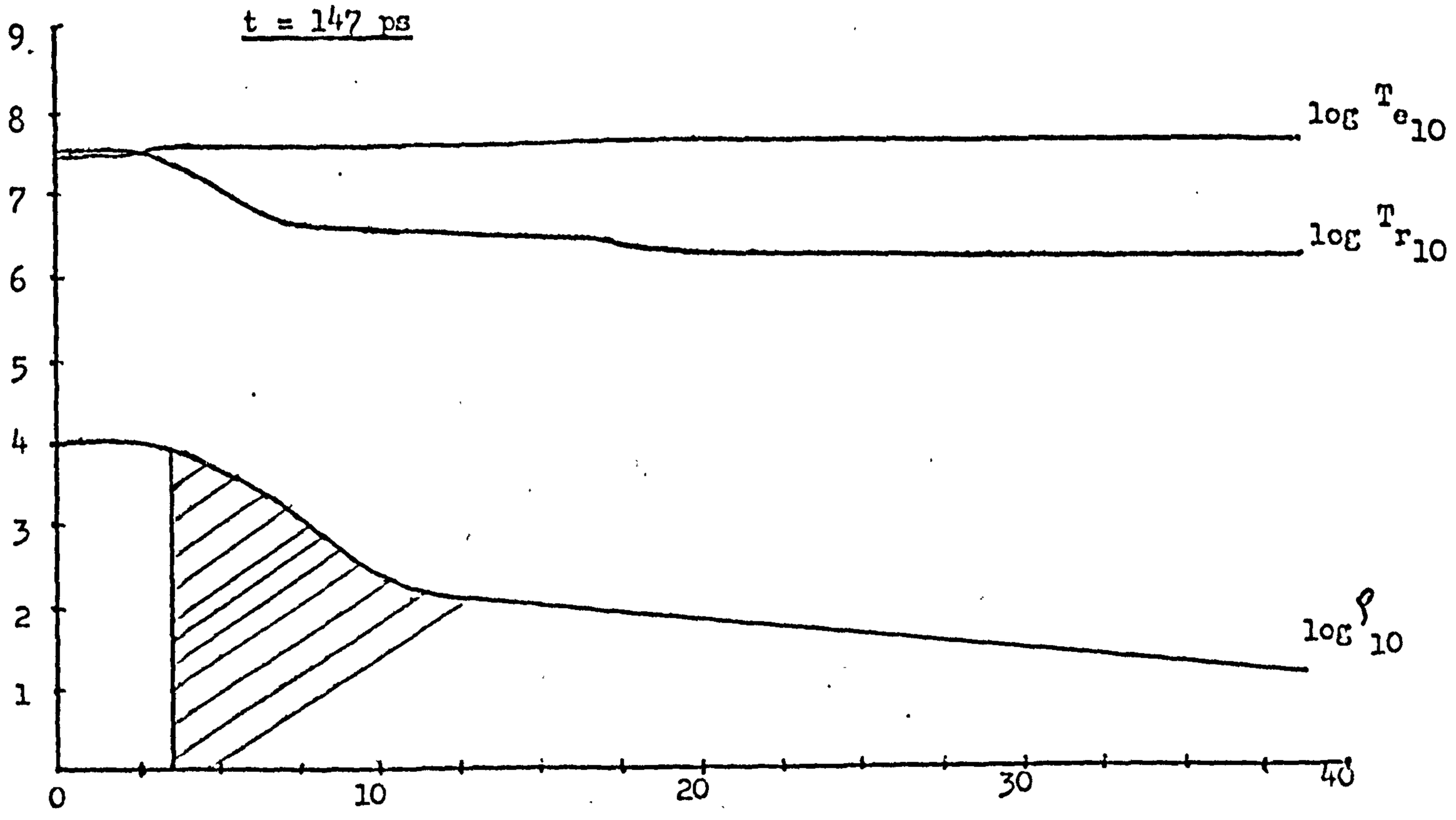

Fig. (6.11a)

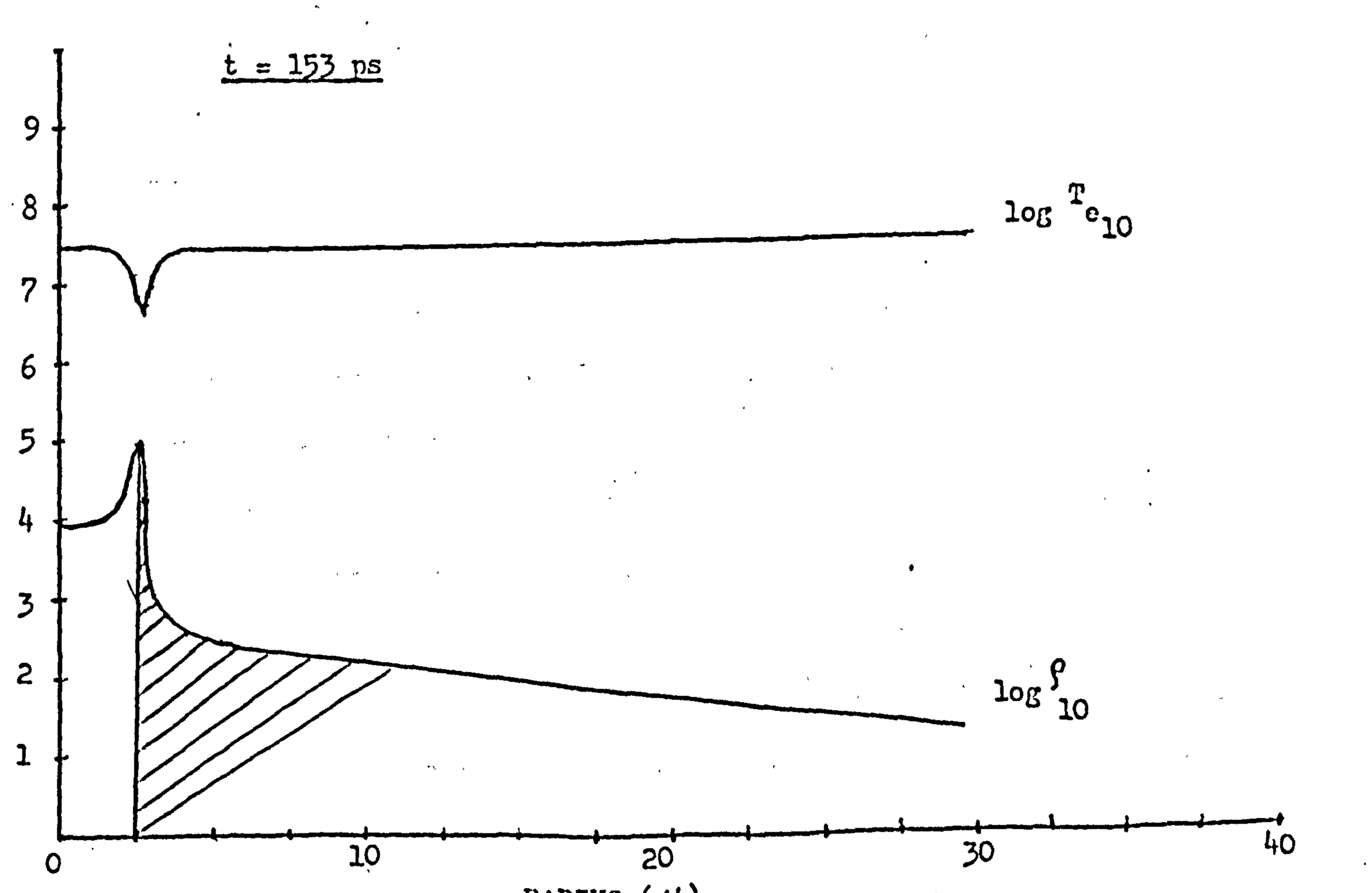

Fig. (6.11b)

(6.3) Conclusions:

The work presented in this thesis is mainly concerned with modifying MEDUSA to:

a) Handle gas filled micro-balloons and layered targets.

b) Incorporate some important physical effects, such as atomic physics processes and radiative transport.

It has been shown that the inclusion of an appropriate atomic physics model is necessary when considering compression of medium-z solid micro-spheres. In the case of thin micro-balloons with wall thickness $\sim$ 1-2 μm, however, the atomic physics processes can be neglected, because the target gets quickly ionized, and to a good approximation, can be treated as being fully ionized. In this approximation MEDUSA has been modified to handle a target with layers of different material, and was used to simulate compression of D-T filled glass micro-balloons to investigate the sensitivity of neutron yield to the target and pulse parameters. The results are summarized as follows:

The neutron yield is found to increase with shorter pulse lengths since these give rise to more shock heating, and as a result, the D-T is compressed to a relatively lower density but to a higher temperature. As the D-T reaction cross-section is very sensitive to the temperature in the range 5-100 Kev, the yield is increased.

When a small fraction (10-20%) of a medium-A impurity like Ne is added to the D-T mixture (A being the atomic weight), the shock heating rate in the ion energy equation, which is $\propto$ A, is increased. Consequently, the ion temperature increases, enhancing the neutron yield. If the percentage of the impurity is increased too much, the yield drops as a result of a decrease in the D-T mass available for reaction.

Keeping the pulse parameters and the inner radius of the micro-

balloon constant, we have studied the compression of micro-balloons of various thickness. It was observed that for thicker shells the compression is more ablative in type and that shock heating is minimized. As a result, the final temperature decreases, while the larger momentum of the shell compresses the gas to higher density.

We also found that if the outer surface of the micro-balloon is coated with a low-z material, such as Be, the thermal conduction rate, which is $\propto \frac{1}{z}$, increases, thereby improving the degree of compression and heating of the D-T.

MEDUSA has also been modified to include a diffusion treatment for the continuum radiation. This modified version has been used to investigate the effect of radiative pre-heat in the compression of solid micro-spheres and gas filled micro-balloons. It was shown that the micro-spheres are more sensitive to the radiative pre-heat as compared to thin micro-balloons.

(6.4) Future Work:

(i) In this work we have used a steady state model to evaluate the degree of ionization in the plasma. This is valid in the compressed core region and the denser part of the corona region, but not in the outermost tenous part of the corona. It is to be noted that the corona is the source of X-ray emission, the spectral distribution of which depends upon the ionizational state of the plasma. Thus for a comparison between the experimental and simulation results of the X-ray emission spectrum, the degree of ionization should be evaluated accurately. This can be achieved by using a time dependent atomic physics model to evaluate z.

(ii) The present modifications made in MEDUSA to handle micro-balloons and layered targets are based on the assumption that the atomic physics effects can be neglected. This assumption is valid for thin walled targets where the material is quickly ionized. However,

to study thick micro-shells the atomic physics effects must be included. This is computationally difficult. Nevertheless the problem can be overcome by using tabulated values for $\langle z \rangle$ and $\langle z^2 \rangle$.

(iii) The radiative transport model which has been incorporated into MEDUSA, assumes that the radiation is represented by a Planckian equilibrium, characterized by a radiation temperature T_r. The radiation mean free path is averaged over this distribution so that the model does not incorporate the effect of the high energy photons at the tail of the spectrum. Furthermore, the model does not treat the line radiation. One can include these two effects by using a multi-group diffusion treatment for radiation

(iv) Much interest has been shown recently, on bombardment of D-T targets by beams of energetic heavy ions. The present work can be extended to allow a computational study of such a process.

Appendix 1

γ For a Partially Ionized Gas In Coronal Equilibrium

From thermodynamic principles, for any system we have

$$C_p - C_v = T\left(\frac{\partial P}{\partial T}\right)_V \left(\frac{\partial V}{\partial T}\right)_P \qquad (A1.1)$$

where C_p and and C_v are the specific heats of the gas at constant pressure, P, and constant volume, V, respectively and T is the temperature.

The equation of state of the gas in coronal equilibrium can be written as:

$$PV = R(T)\, T \qquad (A1.2)$$

where $R(T) = (1+\langle z\rangle)\, R_o$, $\langle z\rangle = f(T)$ (A1.3)

and R_o is the universal gas constant.

From (A1.1) and (A1.2), we get

$$C_p - C_v = \frac{T}{PV}\left(R + T\,\frac{dR}{dT}\right)^2$$

$$\text{So} \qquad \gamma = 1 + \frac{R\left(1 + {}^{T}/_{R}\;\frac{dR}{dT}\right)^2}{C_v} \qquad (A1.4)$$

where $\gamma = {}^{C_p}/_{C_v}$

Now $C_v = \left(\frac{\partial U}{\partial T}\right)_v$ where U is the internal energy of the gas, given by,

$$U = \frac{3}{2}RT + N_i\langle E_z\rangle \qquad (A1.5)$$

where $\langle E_z\rangle$ is the average ionizational energy per atom such that $E_z = \sum_j^{j} X_j$, where X_j is the ionization potential of the atom to be ionized to state j.

$$\text{Thus} \quad C_v = \frac{3}{2}\left(R + T\,\frac{dR}{dT}\right) + N_i\,\frac{d\langle E_z\rangle}{dT} \qquad (A1.6)$$

From (A1.3), (A1.4) and (A1.6) we get

$$\gamma = 1 + \frac{\left[1 + \frac{T}{(1+\langle z\rangle)}\cdot\frac{d\langle z\rangle}{dT}\right]^2}{\frac{3}{2}\left[1 + \frac{T}{1+\langle z\rangle}\cdot\frac{d\langle z\rangle}{dT}\right] + \frac{1}{K(1+\langle z\rangle)}\cdot\frac{d\langle E_z\rangle}{dT}} \qquad (A1.7)$$

Appendix 2

Energy Equation

The internal energy of a gas can be written as:

$$U = U(\rho, t)$$

So that $$dU = \left(\frac{\partial U}{\partial T}\right)_{\rho} dT + \left(\frac{\partial U}{\partial \rho}\right)_{T} d\rho \quad \text{(A .1)}$$

From first law of thermodynamics

$$dU = dQ - P.dV \quad \text{(A .2)}$$

where dQ is the net energy flow into the system during the process and P.dv is the amount of work done by the system. From (A .1) and (A .2) we get

$$\left(\frac{\partial U}{\partial T}\right)_{\rho} dT + \left(\frac{\partial U}{\partial \rho}\right)_{T} d\rho + P\ dV = dQ$$

or $$C_v \frac{dT}{dt} + B_T \frac{d\rho}{dt} + P \frac{dV}{dt} = \mathcal{S} \quad \text{energy/unit mass. sec.}$$

where $$C_v = \left(\frac{\partial U}{\partial T}\right)_{\rho}$$

$$B_T = \left(\frac{\partial U}{\partial \rho}\right)_{T}$$

and $$\mathcal{S} = \frac{dQ}{dt}$$

Appendix 3

Source Terms In The Electron And Ion Energy Equations:

In this appendix we present the expression for the source terms in the electron and ion energy equations used in MEDUSA [11].

(A) Electron:

(A.1) Thermal Conductivity K_e:

$$K_e = 1.83 \times 10^{-10} \; T_e^{5/2} \; (\log\Lambda)^{-1} \bar{Z} (\bar{Z}^2)^{-1} \quad W/_m \; K$$

where coulomb logrithm, Λ, is given by

$$\Lambda = 1.24 \times 10^7 \; T_e^{3/2} \; n_e^{-\frac{1}{2}} \; /\bar{Z}$$

(A.2) Bremsstrahlung Radiation Loss J:

$$J = -8.5 \times 10^{-14} \, n_e \, \delta T_e^{1/2} \, \bar{Z}^2 \, \bar{M}^{-1} \qquad W/kg$$

where $$\delta T_e = T_e - \left(\frac{n_e}{n_e^o}\right)^{\gamma_e - 1} T_e^o$$

is the departure from the initial adiabat, T_e^o and n_e^o denote the initial temperature and density of the electrons.

(A.3) Laser-light Absorption X_L:

The intensity of the laser light at the plasma critical density surface is given by

$$P_L(r,t) = P_L(R_o,t) \; e^{-\alpha(R_o - r)}$$

where $P_{L(R_o,t)}$ is the intensity of the laser radiation at the plasma boundary, $r = R_o$. The inverse bremsstrahlung absorption coefficient, α is given by

$$\alpha = 13.51 \lambda^2 \beta^2 (1-\beta)^{-1/2} (5.05 + \log\lambda T_e) \bar{Z} \bar{T}_e^{-3/2} \bar{m}^{-1}$$

where λ is the wavelength of the laser radiation, $\beta = \rho/\rho_c$ and ρ_c is the critical mass density of the plasma, given by

$$\rho_c = \frac{\varepsilon_o M m_H m_e}{Z e^2} \omega_L^2$$

where the symbols have their usual meaning.

(B) Ions:

(B.1) Thermal Conductivity K_i:

$$K_i = 4.3 \times 10^{-12} T_i^{5/2} (\log\Lambda)^{-1} (\bar{Z}^2)^{-1} \overline{\bar{M}^{1/2} Z^2} \quad W/mK$$

(B.2) Viscous shock heating rate Q:

The viscous shock heating rate in finite difference form is given as

$$Q_\ell^{n-1/2} = -q_\ell^{n-1/2} \frac{V_\ell^n - V_\ell^{n-1}}{\Delta t^{n-1/2}}$$

where the viscous pressure q in cell ℓ is given by

$$q_\ell^{n-1/2} = b^2 \rho_\ell^{n-1/2} (u_{j+1}^{n-1/2} - u_j^{n-1/2})^2$$

and is only applied if $u_{j+1} < u_j$.

Appendix 4

In this appendix we discuss modifications made in the computer programme MEDUSA to be able to study the compression of gas-filled micro-balloons and layered targets. This modified version of the code can handle a target which is composed of three layers of different materials. The initial density profile for a solid micro-sphere is as follows:

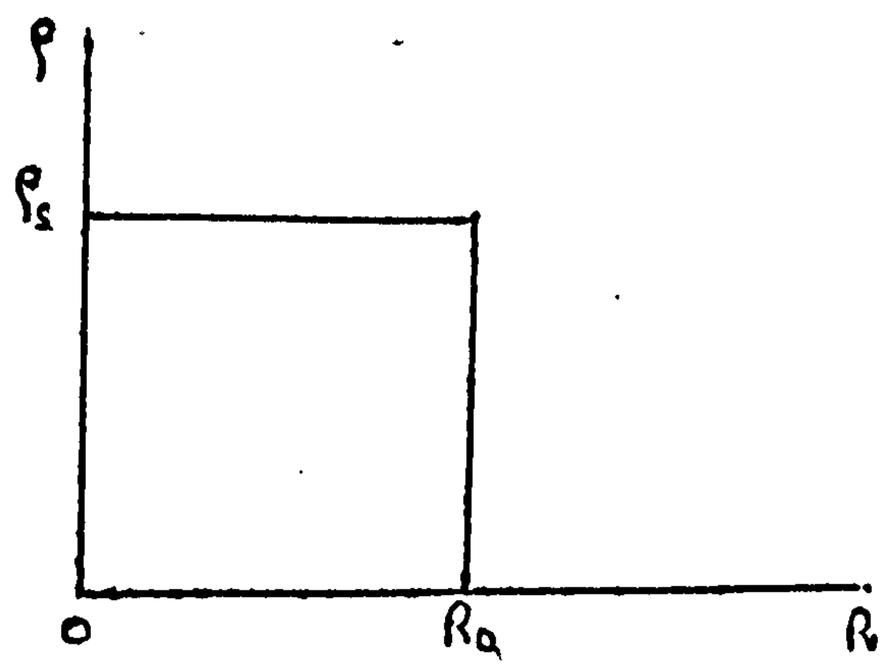

The target radius, R_o, in the code is replaced by a Lagrangian mesh of 40 cells, either of equal masses or of equal thicknesses. The cell boundaries are free to move, thereby changing the volume of the cell. In the case of a layered target, however, the initial density profile is different, as shown below.

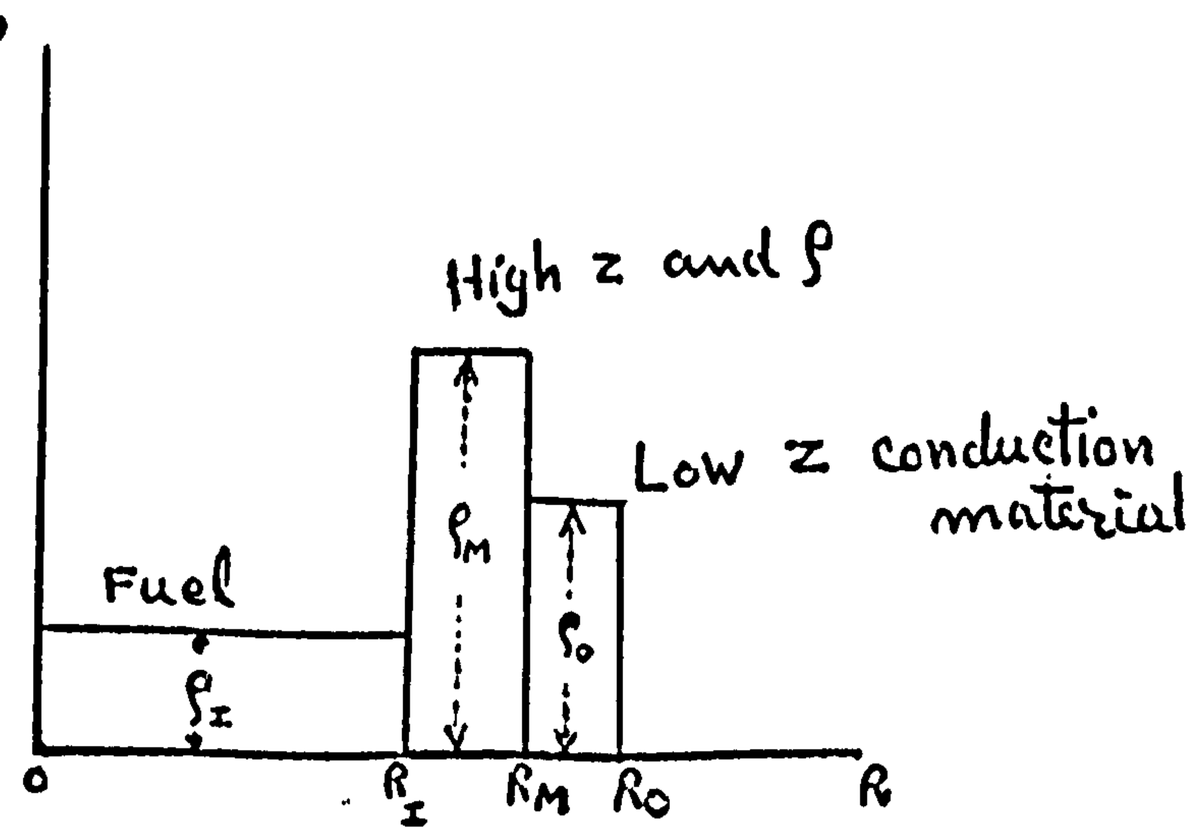

The radius of the pellet is split into three sections as shown in the above figure. The section R_I is divided into 20 cells while R_M and R_o are divided into 10 cells each. The initial density profile,

the effective z & A for each of the three layers is evaluated separately. The boundaries of the neighbouring cells can move freely, however, diffusion of the material is not allowed. It is also to be noted that in the physical model used by MEDUSA, the shell of solid material is replaced by a gas at solid density. Thus as soon as the system is released it starts relaxing to equalise the pressure. This problem can be overcome if the implosion is sufficiently efficient to catch up the relaxing material before it has moved apprcciably.

Appendix 5

Electron-radiation Collision frequency in a fully ionized gas

It has been shown [23] that the free-free absorption coefficient is given by

$$K_\nu = \frac{4}{3}\left(\frac{2\pi}{3mk}\right)^{1/2} \frac{e^6}{(4\pi\varepsilon_0)^{1/2}} \cdot \frac{1}{hcm}\left(\frac{\bar{Z}^2 \bar{Z} N_i}{T_e^{1/2} \nu^3}\right) \quad \text{(A4.1)}$$

where the symbols have their usual meaning. Substituting the values of the constants (in MKS units) in the above equation, we get

$$K_\nu = 3.69 \times 10^{-2} \left(\frac{\bar{Z}^2 \bar{Z} N_i^2}{T_e^{1/2} \nu^3}\right) \quad m^{-1} \quad \text{(A4.2)}$$

where N_i is in m^{-3} and T is in ^{o}K.

Now the R.H.S. of equation (4.22A) is,

$$K_{\nu e} = \frac{c}{\rho} \int_0^\infty K_\nu (U_{\nu\rho} - U_\nu)\, d\nu \quad \text{(A4.3)}$$

where the Planckian distributions $U_{\nu p}$ and U_ν are

$$U_{\nu\rho} = \frac{8\pi h\nu^3}{c^3} \frac{1}{e^{\frac{h\nu}{KT_e}} - 1} \quad \text{(A4.4)}$$

and

$$U_\nu = \frac{8\pi h\nu^3}{c^3} \frac{1}{e^{\frac{h\nu}{KT_r}} - 1} \quad \text{(A4.5)}$$

Let $X = \frac{h\nu}{KT_e}$, so that $d\nu = \frac{KT_e}{h}\, dx = 2.083 \times 10^{10}\, dx.$

Substituting the values of K_ν, $U_{\nu p}$, U_ν and $d\nu$ into equation (A4.3) and integrating w.r.t.x we get

$$K_{\nu e} = 8.5 \times 10^{-14} \left(\frac{\bar{Z}^2 \bar{Z} N_i}{M T_e^{1/2}}\right) T_e \int_0^\infty \left[\frac{1}{e^x - 1} \quad \frac{1}{e^{\xi x} - 1}\right] dx$$

where $\xi = \frac{T_e}{T_r}$

Multiplying and dividing the above equation by $(T_e - T_r)$ yields

$$K_{\nu e} = 8.5 \times 10^{-14} \left(\frac{\bar{Z}^2 \bar{Z} N_i}{M T_e^{1/2}}\right) (T_e - T_r) \left(\frac{T_e}{T_e - T_r}\right) \int_0^\infty \left[\frac{1}{e^x - 1} - \frac{1}{e^{\xi x} - 1}\right] c$$

Let

$$I_g = \frac{T_e}{T_e - T_r} \int_0^\infty \left[\frac{1}{e^x - 1} - \frac{1}{e^{\xi x} - 1} \right] dx = \int_0^\infty \frac{\xi (e^{\xi x} - e^x)\, dx}{(\xi - 1)(e^x - 1)(e^{\xi x} - 1)}$$

So that

$$K_{re} = 8.5 \times 10^{-14} \left(\frac{\bar{Z}^2 \bar{Z} N_i}{M T_e^{1/2}} \right) I_g (T_e - T_r) \qquad (A4.6)$$

Now assuming that

$$K_{re} = (C_v)_e \omega_{re} (T_e - T_r) \qquad (A4.7)$$

where ω_{re} is the electron-radiation collision frequency and $(Cv)_e$ is the specific heat of the electrons, comparing (A4.6) and (A4.7) gives

$$\omega_{re} = 8.5 \times 10^{-14} \left(\frac{\bar{Z}^2 \bar{Z} N_i}{(C_v)_e M T_e^{1/2}} \right) I_g \qquad (A4.8)$$

The integral Ig is solved numerically. The values of Ig for different values of ξ are given below.

	Ig
0.01	11.93
0.05	10.64
0.10	10.05
0.20	9.50
0.30	9.20
0.50	8.87
0.80	8.60
1.00	8.48
2.00	8.18
5.00	7.90
10.00	7.74
20.00	7.65
40.00	7.57
50.00	7.55
70.00	7.46

It is to be noted that the integrand is singular at $\xi = 1$ and is therefore evaluated by L' Hôpital's rule.

Appendix 6

Radiation Thermal conduction rate in a plasma

In this appendix we evaluate the radiative heat conduction rate. Consider three adjacent cells with centres marked by $\ell-1$, and $\ell+1$, as shown below:

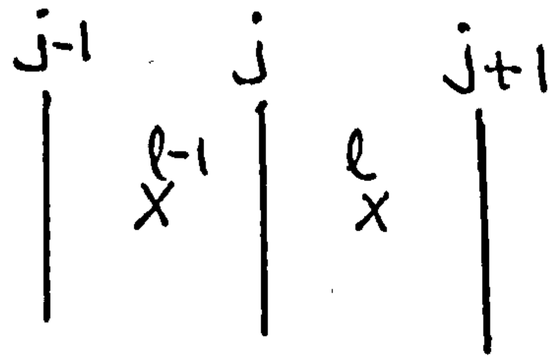

Now
$$H = \frac{1}{\rho}\nabla\cdot(D\nabla T) \qquad (A5.1)$$
for simplicity we drop the subscript r from the radiation thermal conductivity D_r and temperature T_r.

However, in spherical geometry, in one dimension one can write $\nabla\cdot\Psi = \frac{1}{R^2}\cdot\frac{d}{dR}\cdot(R^2\Psi)$, where Ψ is any scalar quantity.

Therefore $H = \frac{1}{\rho}\cdot\frac{1}{R^2}\cdot\frac{d}{dR}\cdot(R^2 D|\nabla T|)$

Let $F = R^2\cdot D|\nabla T|$

So
$$H = \frac{1}{\rho}\cdot\frac{1}{R^2}\cdot\frac{d}{dR}\ (F) \qquad (A5.2)$$

The amount of heat absorbed in cell ℓ due to radiation thermal conductivity is then,

$$H_\ell = \frac{1}{\rho_\ell}\cdot\frac{1}{R_j^2}\left[\frac{F_{j+1}-F_j}{R_{j+1}-R_j}\right] \qquad (A5.3)$$

But
$$\rho_\ell = \frac{dM_\ell}{dV_\ell} = \frac{dM_\ell}{4\pi R_j^2(R_{j+1}-R_j)}$$

Substituting ρ_e in equation (A5.3) we get

$$H_\ell = \frac{4\pi}{dM_\ell}\left[F_{j+1}-F_j\right]$$

However, in MEDUSA, we are interested in quantities per steradian.

Therefore the above equation is reduced to

$$H_\ell = \frac{1}{dM_\ell}\left[F_{j+1}-F_j\right]$$

Appendix 7

Energy Exchange Rates In a 3-Component Plasma

(Electrons, Ions and Radiation)

The ion, electron and radiation energy equations can be written as:

$$\frac{dT_i}{dt} = \frac{W_i}{(C_v)_i} - \frac{K_{ie}}{(C_v)_i} \qquad (A7.1)$$

$$\frac{dT_e}{dt} = \frac{W_e}{(C_v)_e} + \frac{K_{ie}}{(C_v)_e} - \frac{K_{re}}{(C_v)_e} \qquad (A7.2)$$

$$\frac{dT_r}{dt} = \frac{W_r}{(C_v)_r} + \frac{K_{re}}{(C_v)_r} \qquad (A7.3)$$

where W_i, W_e and W_r include the term $P\frac{dv}{dt}$, and the remaining source terms in the corresponding equations.

Also

$$K_{ie} = (C_v)_i \omega_{ie}(T_i - T_e) \qquad (A7.4)$$

and

$$K_{re} = (C_v)_e \omega_{re}(T_e - T_r) \qquad (A7.5)$$

where the symbols have their usual meaning.

Substracting equation (A7.2) from (A7.1) and equation (A7.3) from (A7.2), gives

$$\frac{d\xi_i}{dt} = \Phi_i - \beta_i \omega_{ie}\xi_i + \omega_{re}\xi_r \qquad (A7.6)$$

$$\frac{d\xi_r}{dt} = \Phi_r - \beta_r \omega_{re}\xi_r + G\omega_{ie}\xi_i \qquad (A7.7)$$

where $\xi_i = T_i - T_e$, $\xi_r = T_e - T_r$, $\Phi_i = \frac{W_i}{(C_v)_i} - \frac{W_e}{(C_v)_e}$, $\Phi_r = \frac{W_e}{(C_v)_e} - \frac{W_r}{(C_v)_r}$

$$\beta_i = 1 + \frac{(C_v)_i}{(C_v)_e}, \quad \beta_r = 1 + \frac{(C_v)_e}{(C_v)_r} \text{ and } \quad G = \frac{(C_v)_i}{(C_v)_e}.$$

Equations (A7.6) and (A7.7) are two first order, coupled differential

equations which can be decoupled by converting them to second order differential equations. This gives

$$\frac{d^2\xi_i}{dt^2} + \lambda \frac{d\xi_i}{dt} + \gamma \xi_i = \alpha_i \qquad (A7.8)$$

$$\frac{d^2\xi_r}{dt^2} + \lambda \frac{d\xi_r}{dt} + \gamma \xi_r = \alpha_r \qquad (A7.9)$$

where $$\lambda = \beta_i \omega_{ie} + \beta_r \omega_{re}$$

$$\gamma = (\beta_i \beta_r - G)\, \omega_{ie} \omega_{re}$$

$$\alpha_i = (\Phi_r + \beta_r \Phi_i)\, \omega_{re}$$

and $$\alpha_r = (\Phi_i G + \beta_i \Phi_r)\, \omega_{ie}$$

Solving equations (A7.8) and (A7.9) gives

$$\xi_i(t) = C_i\left[e^{Xt} - e^{Yt}\right] + \left(\xi_{io} - \frac{\alpha_i}{\gamma}\right) e^{Yt} + \frac{\alpha_i}{\gamma} \qquad (A7.10)$$

and $$\xi_r(t) = C_r\left[e^{Xt} - e^{Yt}\right] + \left(\xi_{ro} - \frac{\alpha_r}{\gamma}\right) e^{Yt} + \frac{\alpha_r}{\gamma} \qquad (A7.11)$$

where

$$X = -\lambda/2 + \frac{\sqrt{\lambda^2 - 4\gamma}}{2}$$

$$Y = -\lambda/2 - \frac{\sqrt{\lambda^2 - 4\gamma}}{2}$$

and the two integration constants, C_i and C_r, are given by

$$C_i = \frac{1}{\sqrt{\lambda^2 - 4\gamma}}\left[\Phi_i - \beta_i \omega_{ie} \xi_{io} + \omega_{re} \xi_{ro} + \lambda/2\left(\xi_{io} - \frac{\alpha_i}{\gamma}\right)\right] \qquad (A7.12)$$

$$+ \frac{1}{2}\left(\xi_{io} - \frac{\alpha_i}{\gamma}\right)$$

and $$C_r = \frac{1}{\sqrt{\lambda^2 - 4\gamma}}\left[\Phi_r - \beta_r \omega_{re} \xi_{ro} + \omega_{ie} G\, \xi_{io} + \lambda/2\left(\xi_{ro} - \frac{\alpha_r}{\gamma}\right)\right] \qquad (A7.13)$$

$$+ \frac{1}{2}\left(\xi_{ro} - \frac{\alpha_r}{\gamma}\right)$$

Averaging equations (A7.10) and (A7.11) over the time step $\Delta t^{n-\frac{1}{2}}$, gives

$$\xi_i^{n-1/2}(t) = C_i\left[\frac{1}{X \cdot \Delta t^{n-1/2}}\left(e^{X \cdot \Delta t^{n-1/2}} - 1\right) - \frac{1}{Y \cdot \Delta t^{n-1/2}}\left(e^{Y \cdot \Delta t^{n-1/2}} - 1\right)\right] \qquad (A7.14)$$

$$+ \left(\xi_{io} - \left(\frac{\alpha_i}{\gamma}\right)^{n-1/2}\right) \frac{1}{Y \cdot \Delta t^{n-1/2}}\left(e^{Y \cdot \Delta t^{n-1/2}} - 1\right) + \left(\frac{\alpha_i}{\gamma}\right)^{n-1/2}$$

and $$\xi_r(t) = C_r\left[\frac{1}{X\cdot\Delta t^{n-1/2}}\left(e^{X\cdot\Delta t^{n-1/2}}-1\right)-\frac{1}{Y\cdot\Delta t^{n-1/2}}\left(e^{Y\cdot\Delta t^{n-1/2}}-1\right)\right] \quad (A7.15)$$
$$+\left(\xi_{r_0}-\left(\frac{\alpha_r}{\gamma}\right)^{n-1/2}\right)\frac{1}{Y\cdot\Delta t^{n-1/2}}\left(e^{Y\cdot\Delta t^{n-1/2}}-1\right)+\left(\frac{\alpha}{\gamma}\right)^{n-1/2}$$

The quantities Φ_i and Φ_r, required for the calculation of C_i and C_r in the equations (A7.12) and (A7.13), are evaluated from equations (A7.6) and (A7.7) as

$$\Phi_i = \frac{\xi_i^n - \xi_i^{n-1}}{\Delta t^{n-1/2}} + \beta_i\omega_{ie}\xi_i - \omega_{re}\xi_r$$

and $$\Phi_r = \frac{\xi_r^n - \xi_r^{n-1}}{\Delta t^{n-1/2}} + \beta_r\omega_{re}\xi_r - G\,\omega_{ie}\xi_i$$

The energy exchange rates can then be evaluated as:

$$K_{ie}^{n-1/2} = (C_v)_i\,\omega_{ie}^{n-1/2}\,\xi_i^{n-1/2} \quad (A7.16)$$

$$K_{re}^{n-1/2} = (C_v)_e\,\omega_{re}^{n-1/2}\,\xi_i^{n-1/2} \quad (A7.17)$$

Special Cases

(1) $\beta_i\omega_{ie}\Delta t^{n-\frac{1}{2}} \gg \beta_r\omega_{re}\cdot\Delta t^{n-\frac{1}{2}}$

i.e. the electron-ion energy exchange dominates. In such a case, the two integration constants C_i and C_r become

$$C_i = \frac{\Phi_i}{\beta_i\omega_{ie}} - \frac{\alpha_i}{\gamma}$$

and $$C_r = \left(\frac{\Phi_r}{\beta_i\omega_{ie}} + \frac{G}{\beta_i}\xi_{i0}\right) + \left(\xi_{r_0} - \frac{\alpha_r}{\gamma}\right)$$

Thus $$\xi_i^{n-1/2}(t) = \frac{1}{\beta_i\omega_{ie}\Delta t^{n-1/2}}\left(\frac{\Phi_i^{n-1/2}}{\beta_i\omega_{ie}^{n-1/2}} - \xi_i^{n-1}\right)\cdot$$
$$\left(e^{-\beta_i\omega_{ie}^{n-1/2}\cdot\Delta t^{n-1/2}} - 1\right) + \left(\frac{\alpha_i}{\gamma}\right)^{n-1/2}$$

and $$\xi_r^{n-1/2}(t) = \frac{1}{\beta_i\omega_{ie}\Delta t^{n-1/2}}\left(\frac{\Phi_r^{n-1/2}}{\beta_i\omega_{ie}} + \frac{G}{\beta_i}\xi_i^{n-1}\right)\cdot$$
$$\left(e^{-\beta_i\omega_{ie}\Delta t^{n-1/2}} - 1\right) + \left(\frac{\alpha_r}{\gamma}\right)^{n-1/2}$$

(2) $\underline{\beta_r \omega_{re} \Delta t^{n-\frac{1}{2}} \gg \beta_i \omega_{ie} \Delta t^{n-\frac{1}{2}}}$

i.e. the electron-radiation energy exchange rate dominates. The integration constants then reduce to,

$$C_i = \left(\frac{\Phi_i}{\beta_r \omega_{re}} + \frac{1}{\beta_r}\xi_{ro}\right) + \left(\xi_{io} - \frac{\alpha_i}{\gamma}\right)$$

and $$C_r = \frac{\Phi_r}{\beta_r \omega_{re}} - \frac{\alpha_r}{\gamma}$$

The two equations (A7.14) and (A7.15) can then be simplified to

$$\xi_{i(t)}^{n-\frac{1}{2}} = \left(\frac{\Phi_i}{\beta_r \omega_{re}} + \frac{1}{\beta_r}\xi_r^{n-1}\right)\frac{1}{\beta_r \omega_{re}\Delta t^{n-\frac{1}{2}}}\left(e^{-\beta_r \omega_{re}\Delta t^{n-\frac{1}{2}}} - 1\right) + \left(\frac{\alpha_i}{\gamma}\right)^{n-\frac{1}{2}}$$

and $$\xi_r^{n-\frac{1}{2}}(t) = \left(\frac{\Phi_r}{\beta_r \omega_{re}} - \xi_r^{n-1}\right)\frac{1}{\beta_r \omega_{re}\Delta t^{n-\frac{1}{2}}}\left(e^{-\beta_r \omega_{re}\Delta t^{n-\frac{1}{2}}} - 1\right) + \left(\frac{\alpha_r}{\gamma}\right)^{n-\frac{1}{2}}$$

(3) $\underline{\beta_i \omega_{ie} \Delta t^{n-\frac{1}{2}} \ll 1 \text{ and } \beta_r \omega_{re} \Delta t^{n-\frac{1}{2}} \ll 1}$

i.e. when both the energy exchange rates are very slow. In such a case, however, we get

$$\xi_{i(t)}^{n-\frac{1}{2}} = \xi_i^{n-1}$$

and

$$\xi_{r(t)}^{n-\frac{1}{2}} = \xi_r^{n-1}$$

Appendix 8

Coefficients A, B, C, D, G of Equation (4.78)

The radiation energy equation in finite difference form can be written as

$$(C_v)_\ell^{n-1/2}\left(\frac{T_\ell^n - T_\ell^{n-1}}{\Delta t^{n-1/2}}\right) + 4P_\ell^{n-1/2}\left(\frac{V_\ell^n - V_\ell^{n-1}}{\Delta t^{n-1/2}}\right) = H_\ell^{n-1/2} + K_{r_2 e}^{n-1/2} \quad (A8.1)$$

where $(C_v)_\ell^{n-1/2} = 0.5\left[(C_v)_\ell^n + (C_v)_\ell^{n-1}\right]$, $P_\ell^{n-1/2} = 0.5\left[P_\ell^n + P_\ell^{n-1}\right]$

$$H_\ell^{n-1/2} = 0.5\left[H_\ell^n + H_\ell^{n-1}\right] \text{ and } \quad H_\ell^n = \frac{1}{dM_\ell}\left[F_{j+1}^n - F_j^n\right]$$

Also $$F_j^n = \frac{(R_i^n)^2 D_i^n (T_\ell^n - T_{\ell-1}^n)}{R_\ell^n - R_{\ell-1}^n} = \frac{2(R_j^n)^2 D_j^n (T_\ell^n - T_{\ell-1}^n)}{R_{j+1}^n - R_{j-1}^n}$$

Hence $$H_\ell^n = \frac{1}{dM_\ell}\left[\frac{2 R_{j+1}^{n\,2} D_{j+1}^n (T_{\ell+1}^n - T_\ell^n)}{R_{j+2}^n - R_j^n} - \frac{2 R_j^{n\,2} D_i^n (T_\ell^n - T_{\ell-1}^n)}{R_{j+1}^n - R_{j-1}^n}\right]$$

Substituting $H_\ell^{n-\frac{1}{2}}$ in equation (A8.1) we get

$$0.5\left[(C_v)_\ell^{n-1} + (C_v)_\ell^n\right]\left[T_\ell^n - T_\ell^{n-1}\right] + 2\left(P_\ell^n + P_\ell^{n-1}\right)\left(V_\ell^n - V_\ell^{n-1}\right)$$
$$= -C_\ell^n (T_{\ell+1}^n - T_\ell^n) + A_\ell^n (T_\ell^n - T_{\ell-1}^n) - C_\ell^{n-1}(T_{\ell+1}^{n-1} - T_\ell^{n-1})$$
$$+ A_\ell^{n-1}(T_\ell^{n-1} - T_{\ell-1}^{n-1}) + K_{r_2 e}^{n-1/2} \cdot \Delta t^{n-1/2} \quad (A8.2)$$

where $$A_\ell^n = -\frac{(R_j^n)^2 D_j^n \Delta t^{n-1/2}}{dM_\ell (R_{j+1}^n - R_{j-1}^n)}$$

and $$C_\ell^n = -\frac{(R_{j+1}^n)^2 D_{j+1}^n \Delta t^{n-1/2}}{dM_\ell (R_{j+2}^n - R_j^n)}$$

One can rearrange the coefficients of $T_{\ell-1}^n$, T_ℓ^n and $T_{\ell+1}^n$ such that

$$A_\ell^n T_{\ell-1}^n + B_\ell^n T_\ell^n + C_\ell^n T_{\ell+1}^n = G_\ell^{n-1} + D_\ell^n \quad (A8.3)$$

where $$B_\ell^n = 0.5\left[(C_v)_\ell^n + (C_v)_\ell^{n-1}\right] - C_\ell^n - A_\ell^n$$

$$D_\ell^n = 0.5 \left[T_\ell^{n-1} \left((C_v)_\ell^n + (C_v)_\ell^{n-1} \right) - 4 \left(P_\ell^n + P_\ell^{n-1} \right) \left(V_\ell^n - V_\ell^{n-1} \right) + 2 K_{2e}^{n-1/2} \cdot \Delta t^{n-1/2} \right]$$

$$G_\ell^{n-1} = A_\ell^{n-1} \left(T_\ell^{n-1} - T_{\ell-1}^{n-1} \right) + C_\ell^{n-1} \left(T_{\ell+1}^{n} - T_\ell^{n} \right)$$

REFERENCES

1 A. Simon, An introduction to thermonuclear research, International series of monographs on nuclear energy.

2 J. Lawson, Proc Phys. Soc. B70, 6 (1957).

3 J. Nuckolls, L. Wood, A. Thiessen and G. Zimmerman, Nature 239, 139 (1972).

4 J.S. Clarke, H.N. Fisher and R.J. Mason, Phys. Rev. letters, 30, 89 (1973).

5 K.A. Brueckner and S. Jorona, Reviews of Modern Physics 46, 325 (1974).

6 P.K. Kaw and J.M. Dawson, Phys. Fluids, 12, 2586 (1969).

7 J.P. Freidberg, R.W. Mitchell, R.L. Morse and L.I. Rudrinske, Resonance Absorption of Laser light by Plasma Targets, Phys. Rev. Letters, 28, 13, 795 (1972).

8 R.L. Morse and C.W. Nielson, Phys. Fluids, 16, 909 (1973).

9 L. Spitzer, Physics of fully ionized gases, John Wiley and Sons, London.

10 D.E.T.F. Ashby and J.P. Christiansen, The effect of the electron free-streaming limit on laser compression, 6th European conference on Controlled Fusion and Plasma Physics, Moscow, P.431 (1973).

11 J.P. Christiansen, D.E.T.F. Ashby and K.V. Roberts, MEDUSA, A one-dimensional laser fusion code, CLM - P.374 (1973).

12 R.C. Malone, R.L. McCrory and R.L. Morse, Indications of strongly limited electron thermal conduction in laser-target experiments, Phys. Rev. Letters 34, 721 (1975).

13 R.J. Bickerton, Thermal conduction limitations in laser fusion, Nuclear Fusion, 13, 457 (1973).

14 G.S. Fraley, W.P. Gula, D.B. Henderson, R.L. McCrory, R.C. Malone, R.J. Mason and R.L. Morse, Implosion, Stability and Burn of multi-shell Fusion targets, Fifth I.A.E.A. conference on Plasma Physics and Controlled Nuclear Fusion Research, Tokyo, Japan (1974).

15 G.S. Fraley and R.J. Mason, Pre-heat Effects on Micro-balloon Laser-Fusion Implosion, Physical Review Letters, 35, 520 (1975).

16 D. Mosher, The Coronal Equilibrium of High Atomic Number Plasmas, NRL Memorandum Report 2563 (1973).

17 J.P. Christiansen and K.V. Roberts, Numerical treatment of Rapid Equipartition Rates, Journal of Computational Physics, Vol.17, No.3, March 1975.

18 F. Frontini, L. Garifo, M.A. Khan and A.M. Malvezzi, A numerical code for describing the time-dependent ionization, recombination and lazer produced plasma, CISE-N-183, Segrate (Milano), May 1977.

19 R.W.P. McWhirter and T.F. Stratton, Plasma Diagnostic Techniques (R.H. Huddelestone and S.L. Leonard, Eds), Academic Press, New York, 1965.

20 H.A. Hyman, Degree of ionization of a high-temperature Plasma, Applied Physics Letters, Vol.25, No.10 (1974).

21 J. Magill, TRIP 1: A Time dependent Recombination and Ionization Package, Department of Natural Philosophy, Glasgow University.

22 J. Magill, E.W. Laing and N.A. Tahir, A general approach to solving the rate equations for ionization recombination processes in a plasma, paper presented at Second European conference on Computational Physics, Garching (1976).

23 Zel'dovich and Raizer, Physics of Shock Waves and High-temperature Hydrodynamic Phenomena, Vol.I, Academic Press,

New York and London.

24. R.D. Richtmeyer and K.W. Morton, Difference methods for initial value problems, 2nd Ed. Interscience Publishers (1967).

25 A.F. Argo and W.F. Huebner, Group Mean Emissivities and Opacities of High-temperature S_i O_2, J. Quantum Spectroscopy and Radiative transfer, Vol. 16, p.1090 (1976).